Alma Mater Studiorum – Università di Bologna

DOTTORATO DI RICERCA IN CHIMICA

Ciclo XXXIV

Settore Concorsuale: 03/A1 – CHIMICA ANALITICA
Settore Scientifico Disciplinare: CHIM/01 – CHIMICA ANALITICA

Smartphone-based analytical devices with optical detection for on-site biosensing: environmental, food and forensic applications

Presentata da: Laura Montali

Coordinatore Dottorato:
Prof.ssa Domenica Tonelli

Supervisore:
Prof.ssa Elisa Michelini

Co-Supervisore:
Dott.ssa Maria Maddalena Calabretta

Esame finale anno 2022

To my family, my strength.

Contents

Abstract

The routine health monitoring of living organisms and environment using biosensors has recently attracted much public interest. There has been an increasing demand for fast and easy monitoring technologies and paper based optical biosensors, designed to respond to different analytes or classes of analytes, and these biosensors have been successfully implemented in portable and cost-effective analytical devices. The standard analytical techniques generally offer accurate and precise results; however, they require clean samples, sophisticated equipment and skilled personnel. For these reasons, they are not suitable for on site, real-time, cost-effective routine monitoring. To this end, biosensors represent suitable analytical alternative tools. Biosensors are analytical devices integrating a biological recognition element (i.e. antibody, receptor, cell) and a transducer element able to convert the biological response into an easily measurable analytical signal. These tools can easily quantify an analyte or a class of analytes of interest even in a complex matrix, like clinical or environmental samples, thanks to the specificity of the biological components. The activity carried out during my PhD was mainly focused on the development of different type of portable paper-based biosensors for multianalyte detection and their implementation into portable analytical devices for point-of-care and point-of-need applications. In particular, enzymes and cells (bacteria and mammalian cell lines) have been exploited as biorecognition elements, in some cases even by coupling different elements in the same biosensor to increase its robustness. The final goal of biosensors developed during these years was the application in the environmental and forensic fields, since the target analytes are organophosphorus pesticides (OPs), heavy metals, such as mercury (Hg^{2+}), present in liquid samples and molecules with androgenic activity, including new drugs or endocrine disrupting chemicals. Moreover, different optical detection principles (chemiluminescence, bioluminescence, colorimetry) have been exploited and coupled to create an orthogonal detection, which provides more accurate results by reducing false positive results and increases the selectivity of the biosensor. The assays were validated and characterized in terms of analytical performance and applied to different fields, from environmental monitoring to clinical diagnostics. Different portable detectors, such as coupled-charged device, smartphone cameras and silicon photomultiplier, and also benchtop laboratory instruments have been used to validate and support the developed biosensors. Several paper-based platforms have been designed and implemented with adaptors and devices fabricated using a dual-extrusion 3D printer to better adapt to the type of assay, reagents, samples and detection method.

1

Introduction

1.1 Biosensors

The on-site monitoring of analytes of environmental, clinical, and forensic interest still represents a challenge and most of analysis are performed with sophisticated equipment and highly trained personnel, which renders real-time, cost-effective routine monitoring cumbersome, time-consuming and costly. Cutting-edge research of the last decade has provided excellent concepts and new molecular tools to obtain sensitive biosensors for rapid on site-analysis. Biosensors, defined as "devices that use specific biochemical reactions mediated by isolated enzymes, immuno-systems, tissues, organelles or whole cells to detect chemical compounds usually by electrical, thermal or optical signals" according to the IUPAC definition provide an unbeatable arsenal of front-line tools for point-of-care and point-of-need analytical devices (McNaught and Wilkinson, 1997).

The signal transducing element (electrode, optical detector, piezo crystal and others) converts the biochemical response into optic and electric signals which are amplified, measured and decoded by an appropriate electronic unit. The choice of a biological element for assembling a biosensor depends on the biological targeting of toxic species and specificity of detection of their specific interactions. A biosensor can produce either individual or successive digital signals that are equivalent to the concentration of a single analyte or a group of analytes being monitored.

In the last two decades research in the field of biosensor has increased significantly thanks to the need for cheap, fast, simple and sensitive analytical tools able to provide real-time information about the sample composition.

Ideally, a biosensor has to:

- be small, with reduced weigh and autonomous electrical power in order to be portable;
- offer qualitative or quantitative results, as required, by treating the primary measurement output provided by the detection system;
- be robust in different environmental applications;
- have short response times;
- be user-friendly in order to be used by non-skilled personnel outside well-equipped laboratories;
- have a low-cost production.

Furthermore, an ideal device should be based on low cost and disposable elements and it should ensure stability for long-term storage (Aguilera-Herrador et al., 2010).

A schematic representation of a biosensor is shown in Figure 1.1:
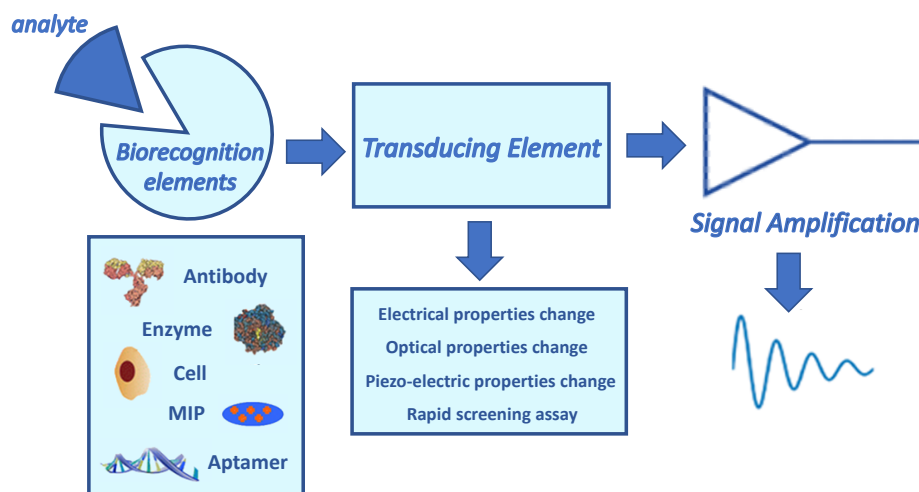
Fig. 1.1: *Schematic representation of biosensors with different biorecognition elements and transducing elements.*

Biological recognition elements can selectivity recognize the analyte from similar molecules and interferents as they are the results of naturally selective evolution processes. Despite this, some recognition elements are preferred over others depending on the application (Riglar et al., 2017; Morales and Halpern, 2018).

Some types of biosensors use antibody as biological recognition elements and are called immunosensors. Thanks to their sensitivity, these biosensors are suitable for detecting ultra-low concentrations of target analyte. Indeed, the high specificity and sensitivity of the interaction between antigen and antibody is the main advantage of this class. They are ideal for point-of-care and point-of-need identification of HIV, hepatitis, cardiovascular diseases and cancers biomarkers because of their low concentration in clinical samples. Furthermore, they are widely used for detecting toxins, explosives, pesticides' residues and other low concentrated pollutants in environmental and food samples. A variety of signal transduction, both optical and electrochemical, have been coupled with immunosensors, but colorimetric and chemiluminescent based detection are until now the most used.

In the last few years, a new class of biosensors is becoming more popular especially for the identification of small molecules, the aptamer-based biosensors. Aptamers are short, 3D-folded single strand nucleic acids (i.e. DNA, RNA and PNA) that are able to recognize an antigen by their conformation. Thanks to their self-annealing properties, they are more stable

than antibodies. Aptamer specific toward an analyte is obtained by an in vitro artificial selection process called SELEX (Systematic Evolution of Ligands by Exponential enrichment) leading to a potentially unlimited range of applications. Although, they can't be used for the identification of low concentrated molecules as their specificity and selectivity for the analyte are still not competitive with those obtained with antigen-antibody interaction (Luzi et al., 2003; Minunni et al., 2004; Pfeiffer and Mayer, 2016). Furthermore, aptamers can be used for the identification of an analyte not only by their three-dimensional structure, but by their primary sequence. In particular, aptamer-based biosensors are the most promising biosensors for the identification of specific DNA/RNA sequence. These biosensors have great potential applications for sensitive early detection of several pathologies like cancer and genetic related diseases, for example those related with mutation in small non-coding miRNA and mRNA (Pfeiffer and Mayer, 2016).

The challenge of on-site analysis, irrespective of whether the application is environmental, food, or clinical, necessarily requires biosensors with high sensitivity, selectivity, robustness, rapidity (possibly approaching real time analysis), ease of operation, possibility of direct analysis of sample in complex matrices without preliminary sample treatment, and cost effectiveness (Mirasoli et al., 2014).

1.1.1 Enzymatic biosensors

Enzyme-based biosensors represent the most popular analytical tools, providing a viable and potentially portable alternative. These biosensors are usually easy to be produced, low-cost and sensitive. Enzymes are widely used as biological elements in biosensors due to their specificity to bind with substrates. Typically, enzymes are highly selective, bind to the substrate very easily and have catalytic activity, thus improving the assay sensitivity. In addition, they can be easily immobilized to the transducer surface with high stability (Pessela, et al., 2003; Cracknell et al., 2008). In particular, in enzymatic biosensors, the biorecognition element can react selectively with its substrate (target analyte), for measuring the catalysis or the inhibition of enzymes by the target analyte. The enzyme can metabolize the analyte and its concentration is determined through the measurement of the catalytic transformation of the analyte in the product by the enzyme. On the other hand, the enzyme can be inhibited by the analyte and its concentration is associated with a decrease in formation of the product. Enzymatic biosensors can, therefore, detect the produced or the

consumed species, respectively. The inhibition can be reversible when the enzyme can recover its biological activity, in this case the type of inhibitor can be (Engelking et al., 2015):

- competitive inhibitor;
- non-competitive inhibitor;
- uncompetitive.

In a non-competitive inhibition, the inhibitor reversibly binds at a different site from the active site of the enzyme. The active site changes conformation but can still receive the substrate; the ESI (enzyme-substrate-inhibitor) complex is formed. The turnover number goes down and the maximum speed of the enzymatic reaction decreases, while the Km remains unchanged. Instead, the uncompetitive inhibitor binds to the already formed enzyme-substrate complex and this significantly reduces the possibility for the enzyme to get rid of the product: it decreases the affinity for the substrate and the maximum speed of the enzymatic reaction.

(a) Reaction
substrate
active site
enzyme
Substrate molecule binds with active site of enzyme molecule
Reaction occurs and product molecules are generated

(b) Inhibition
inhibitor
active site
enzyme
Inhibitor molecule binds with the active site of enzyme molecule
Inhibitor molecule prevents the binding of substrate molecule
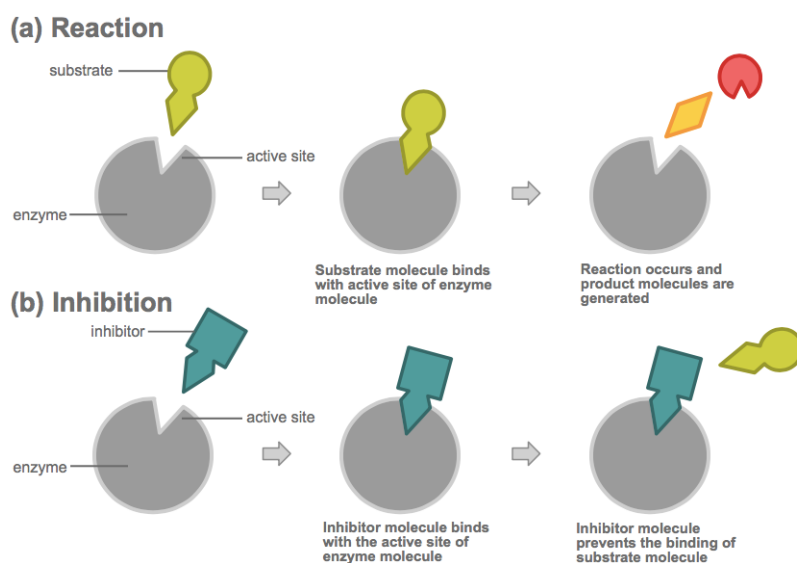
Fig. 1.2: *(a)Schematic view of enzymatic reaction.*
(b) Inhibited enzymatic reaction, competitive inhibitor competes with the substrate.

On the other hand, in a competitive inhibition (Fig. 1.2), the inhibitor reversibly binds to the active site of the enzyme. The competition for the active site of the enzyme depends on the concentration of the two contenders.

The affinity for the substrate (Km) tends to apparently increase when increasing concentrations of inhibitor are present. The maximum speed of the enzymatic reaction does not change while the number of turnovers can rapidly drop to zero (Bhagavan et al., 2011).

When the inhibition is irreversible, enzymatic activity is lost due to the covalent binding between the inhibitor molecule and the active site, irreversibly modifying the active site shape and conformation of the enzyme. Usually, only one enzyme is employed in enzymatic biosensors but the progress in this field involves combining enzymes to obtain coupled enzymatic reactions. These biosensors can be also coupled with different transducers, as they are able to produce a variety of different quantitative dose-dependent signal like light, heat, electrons or protons. In particular, enzyme-based biosensors for glucose and urease detection are largely used, due to the need for glucose/urea monitoring for medical and environmental applications (Chambers et al., 2008; Barhoumi et al., 2006). Several glucose biosensors have been developed over the years and nowadays they cover the majority of the biosensors' world market. Few modifications have been made from the first prototype with the possibility to develop implantable biosensors for non-invasive and continuous monitoring of glucose level in the blood of diabetic patients (https://www.fda.gov/news-events/press-announcements/fda-approves-first-continuous-glucose-monitoring-system-fully-implantable-glucose-sensor-and). Most glucose biosensors use as recognition element the glucose oxidase, that catalyzes the oxidation of glucose to gluconolactone with the production of H_2O_2. Also, artificial mediators have been explored for glucose biosensors. For example, Prussian blue and inorganic redox couples are the most commonly used electrochemical mediator for H_2O_2 detection (Fig. 1.3) (Chambers et al., 2017).
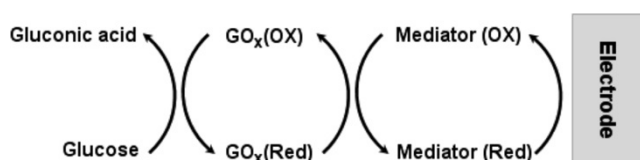
Fig. 1.3: *Example of the enzymatic reaction of glucose oxidase and the electrochemical mediator. Reprinted with permission from Wang, J. (2008). Electrochemical glucose biosensors. Chemical reviews, 108(2), 814-825. Copyright © 2008, American Chemical Society.*

Cholinesterase (ChE) biosensors represent another class of enzymatic biosensors widely used to detect pesticides in water, food and other environmental matrices (Pundir et al.,2012; Andreescu et al., 2006). ChEs are enzymes present in vertebrates and insects, which hydrolyze the neurotransmitter acetylcholine (ACh) in the nervous system. In the body, ChE is responsible for transmission of nerve impulses to the cholinergic synapses and is connected with human memory and Alzheimer's disease. Acetylcholinesterase (AChE) and butyrylcholinesterase (BChE) are the two types of cholinesterase enzymes and they

have been widely used as bioreceptors for the development of biosensors (Arduini et al., 2015; Scordo et al., 2018; Guardigli et al, 2005, Pundir et al, 2012, Andreescu et al., 2006). ChEs are inhibited by several compounds including organophosphate and carbamate pesticides, nerve agents, natural toxins, heavy metals and some drugs (Songa et al., 2016). Chemiluminescent assays based on coupled enzymatic reactions have been also developed for AChE detection and for the evaluation of AChE inhibitors (Guardigli et al, 2005; Pasini et al., 1998). These assays are very rapid and can be applied for the screening of inhibitors drugs including butyryl cholinesterase and oxidases enzymes. In particular, Guardigli et al. (Guardigli et al, 2005) described the development of a chemiluminescent enzymatic biosensors for high throughput screening of new potential inhibitor drugs. The chemiluminescent detection of AChE activity was based on coupled enzymatic reactions involving choline oxidase and horseradish peroxidase (HRP) as the enzymes leading to light emission and using luminol solution to the detect the formation of H_2O_2 (Pasini et al., 1998; Roda et al., 2000). At the end, another widely used enzyme in the field of biosensing is β-galactosidase (β-gal). This enzyme hydrolyzes D-galactosyl residues like lactose or β-galactose comprising chromogenic or fluorogenic substrates from oligosaccharides and polymers (Ghéczyet al., 2016). β-galactosidase has been employed in many food industries to hydrolyze lactose, enhance digestibility, sweetness, solubility and flavor of dairy products and several biosensors for lactose quantification have been developed over the years. (Grosova et al., 2008; Sharma et al., 2016). β-galactosidase has been exploited as a marker to fabricate a quick detection chemiluminescent porous silicon-based biosensor for diagnosis of *Escherichia Coli* (Mathew and Alocilja, 2005). Another accessible, sensitive and simple biosensor based on β-galactosidase activity has been developed for determination of toxoflavin, a toxic component of various plants, fungi, animals, and bacteria (Choi et al., 2013). Bazin et al., in 2017, reported the monitoring of water samples with a bioluminescent biosensor based on bacterial endocrine disruption via β-galactosidase activity in recombinant yeast combined with yeast estrogen screening assays (Bazin et al., 2017). As last example, Yang et al. produced a wireless biosensor co-immobilizing β-galactosidase, glucose oxidase, and catalase onto a magnetoelastic ribbon-like sensor which was pre-plastered with a layer of pH-sensitive polymer to analyze lactose in milk samples. (Yang et al., 2007). Examples shown prove that β-galactosidase is exploited individually or coupled with other enzymes, is integrated with different transduction elements, and used for different applications. Despite this, biosensors based on this enzyme have the same components, summarized schematically in Fig. 1.4:
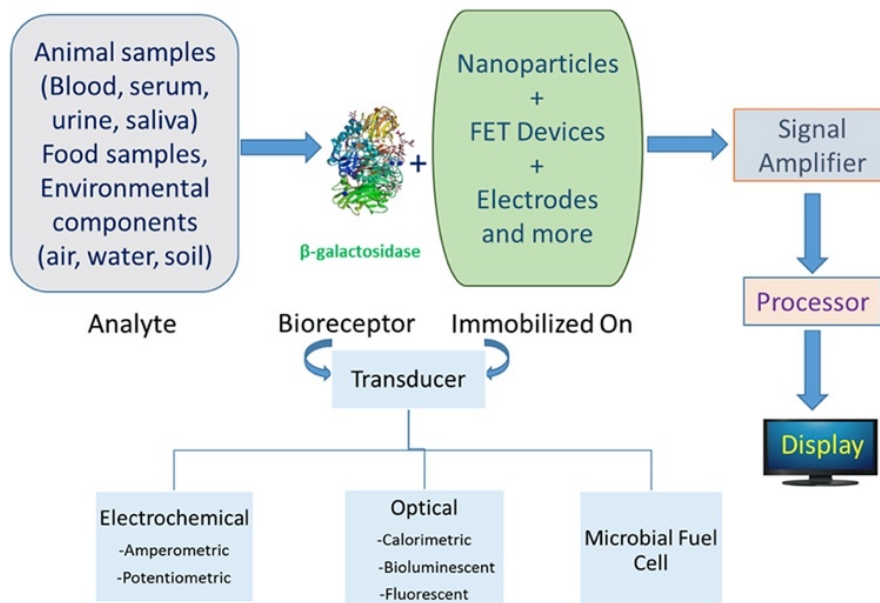
Fig. 1.4: *Components of β-galactosidase biosensors schematically summarized. Reprinted with permission from Sharma, S.K., Leblanc, R.M., 2017. Anal. Biochem. 535: 1-11. License number: 5176410121971, Oct 26, 2021, © 2017 Eselvier L.C. All rights reserved.*

1.1.2 Whole-cell based biosensors

Whole-cell biosensors, exploit living whole-cells as sensing elements and present unique advantages compared to other type of biosensors (Durand et al., 2015; Gui et al., 2017). Living whole cells used as sensing systems have proved to be valuable for prediction of the physiological response to drugs, chemicals, and samples in complex matrices, whose toxic effects and specific biological activity can be evaluated in an easy and straightforward manner. Some of the main advantages of the whole-cell-based biosensors are:

- Versatility (cells can be engineered to express biorecognition element for several classes of analytes, even more than one at the same time);
- measure the bioavailable fraction (the fraction of analyte able to enter into live cells and activate specific signalling pathways);
- provide information about general toxicity;
- provide synergic effects (nonlinear cumulative effects of two or more analytes able to interact with the same cell pathway, or converging pathways, leading to an increased biological outcome);
- provide comprehensive functional information (i.e. pharmacology, toxicology, physiology);

15

- High sensitivity due to intracellular transcriptional and translational cascade mechanism;
- Higher predictivity of human effects.

Many cell-based assays have been reported over the years, but few of them can be considered as true biosensors according to the IUPAC definition because sometimes they are not stand-alone integrated receptor-transducer devices due to the need for cell growth control, sterility and the need for particular storage conditions. In the past, several comparisons between the performance of whole-cell biosensors and standard analytical techniques have been made. In many cases, some divergences have been found between the response of the different analytical methods. Bacteria, yeast and mammalian cell lines have been widely used for whole-cell biosensors applications. Each cell line shows its own advantages and disadvantages.

The first reported whole-cell biosensors were naturally bioluminescent microorganisms called *Aliivibrio fischeri*, thanks to their easy cultivation and integration with a transducer. Yeast based biosensors offer the same advantages of bacterial biosensors but with increased predictivity; due to the higher degree of conservation of cellular processes and molecular pathways with human cells. While, when predictive information about bioactivity or toxicity to humans is required mammalian cell lines are highly valuable.

Compared with yeast and bacterial cells, implementation of mammalian cells in biosensors is less common because of several disadvantages, such as slow growth of cells, cell culture facilities requirement and cell viability highly affected by external factors. For these reasons, microbial cells are exploited when specificity and robustness are required, while mammalian cells biosensors are used when more predictive results are needed (Cevenini et al., 2016a).

Recently, thanks to genetic engineering and reporter gene technologies, whole cells biosensors can be modified to detect a several type of analytes for medical and environmental applications (Fig. 1.5). Many whole-cell-biosensors able to detect heavy metals, organic xenobiotic, toxins and other biomarker have been developed thanks to these approaches (Guedri and Durrieu, 2008; Ivask et al., 2007; Kumar et al., 2006; Silva et al., 2009; Valdman and Gutz, 2008; Kwok et al., 2005; Dhall et al., 2008; Chee et al., 2000; Tag et al., 2007; Stolper et al., 2008; Fujimoto et al., 2006; Reshetilov et al., 1997; Nomura et al., 1998; Petänen and Romantschuk, 2002; Arora et al., 2010; Saini et al., 2019; Alpat et al., 2008).
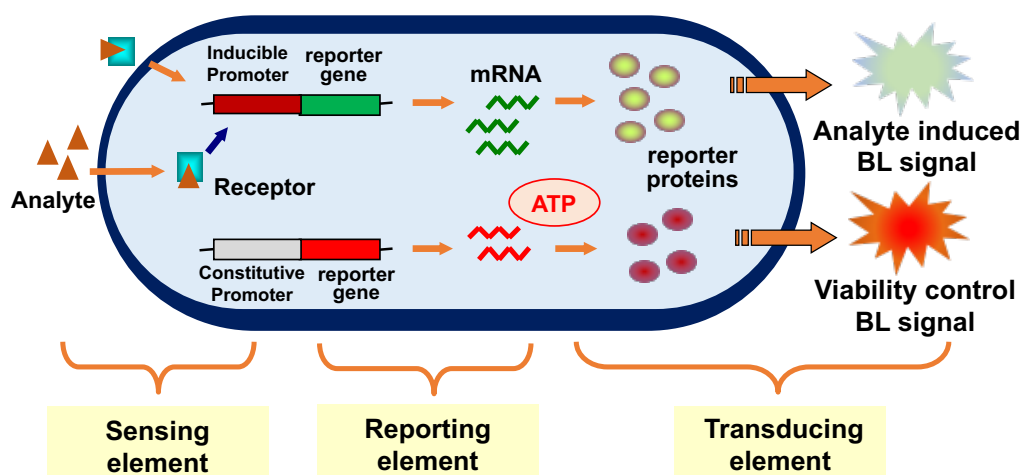
Fig. 1.5: *Schematic representation of a whole cell bioreporter for simultaneous monitoring of different biological pathway into the same cell.*

The well-known disadvantages of whole-cell biosensors are related to their limited portability and shelf-life due to the difficulties of keeping cells alive and responsive for long periods. Obtaining cells in a ready-to-use format is the final goal in this research field. In particular, the possibility of store cells for a long period of time (at least months) under controlled conditions and activate them at the desired time (i.e. by a defined temperature change or addition of nutrients) keeping a constant and reproducible number of viable cells to be revitalized are important issues to be studied in the near future (Michelini and Roda, 2012).

In recent years, 3D cell culture-based biosensors have found great success due to the possibility of their exploitation for biomedical and bioanalytical applications (Wang et al., 2012a), from early detection of illness (Ngoepe et al., 2013) to environmental monitoring (Souiri et al., 2012). 3D culture systems represent great promise for applications in drug discovery, pharmacological studies, cancer cell biology and tissue engineering, and they should be considered the obligatory step between the traditional 2D monolayer cell culture and animal models. Two-dimensional (2D) cell-based assays provides simple, fast and cost-effective tool to avoid large-scale and cost-intensive animal testing. For these reasons they are one of the most appealing bioanalytical tools for the drug discovery process. Due to their altered response to drugs due to different morphology and functionality, 2D cell assays can provide non-predictive and misleading data for in vivo response and they must necessarily be supported by more predictive tests on animals (Birgersdotter et al., 2005; Weaver et al.,

17

1997; Bhadriaraju and Chen, 2002). On the other hand, thanks to hierarchical structure and cellular heterogeneity, 3D cell models can closely mimic in vivo tissue physiology, generating the extracellular matrix and diffusion barriers and restoring cell-to-cell communication. 3D cells cultures better replicate intrinsic physiological conditions and in vivo cellular responses to external stimuli (Bahrvand et al., 2006; Benya and Shaffer, 1982; Nelson and Bissell, 2005).

The generation of 3D structured spheroids are based on the basic principle of self-assembly (Whitesides and Grzybowski, 2002) and exhibit improved cell viability and stable morphology, increasing physiological metabolic function (Antoni et a., 2015). In order to obtain different 3D cell structures, natural or synthetic hydrogels are used for 3D cell-based biosensors. The selection of the suitable matrix for each cell line is of crucial important for biosensor applications (Fig. 1.6).
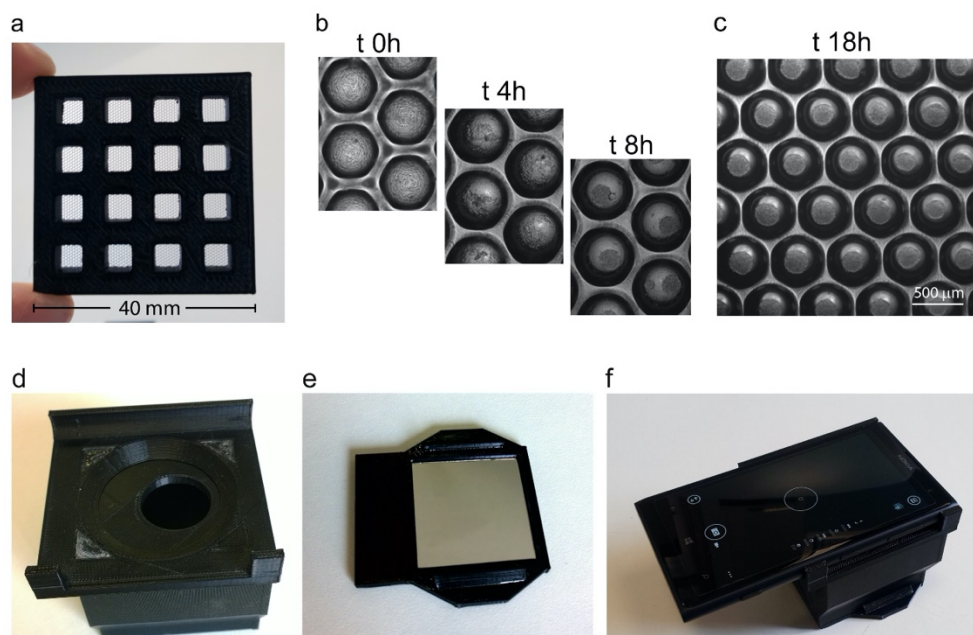
Fig. 1.6: *3D-printed smartphone accessories and spheroid formation.*
a) Picture of the 3D printed cartridge made of PLA printed over a microspace bottom sheet; (b) HekHEK293 cells seeded into the cell cartridge and imaged at time 0 or after 4 h, 8 h, and 18 h overnight incubation (c); (d) Smartphone black-box accessory; (e) 3D printed cartridge holder comprising a mirror; (f) assembled smartphone-based device. Reprinted with permission from Michelini, E., Calabretta, M. M., Cevenini, L., Lopreside, A., Southworth, T., Fontaine, D. M., Simoni, P., Branchini, B.R., Roda, A., 2019. Biosens. Bioelectron. 123: 269-277. License number: 5177011363355, Oct 27, 2021, © 2018 Eselvier L.C. All rights reserved.

1.2 Optical detection principles

Optical detection proved to be a highly sensitive detection principle, with the possibility of implementation into low-cost and miniaturized analytical devices, with several successful examples, mostly relying on fluorescence (FL) and colorimetric detection. Due to size constraints of such devices, also the amounts of sample and reagents are reduced, thus decreasing the analytical signal generated by the biorecognition event. This requires additional efforts to improve the sensitivity. The recent technical advancement in instrumentation and miniaturization allows to obtain analysis of small-volume samples, which ultimately leads to the development of miniaturized and high- throughput assays. Ultrasensitive bioassays have been reported, including whole-cell biosensors and miniaturized devices for high-throughput screening (HTS), with applications ranging from clinical diagnostics to environmental monitoring and drug screening (Roda et al., 2011a).

1.2.1 Chemiluminescent detection

Chemiluminescence consists in the production of light via a chemical reaction. Two reagents, usually a substrate and an oxidant in the presence of some cofactors, react to form a product or an intermediate, sometimes in the presence of a catalyst. Then some fraction of the product or intermediate will be formed in an electronically excited state, which can subsequently relax to the ground state with emission of a photon. (Roda et al., 2012). To obtain light from a chemical reaction, some essential requirements should be met (Roda et al., 2011b):

- To populate an electronically excited (singlet) state the reaction has to be sufficiently exergonic. The free energy requirement can be calculated using:

$$-\Delta G \geq \frac{hc}{\lambda_{ex}} = \frac{28600}{\lambda_{ex}}$$

Therefore, chemiluminescence reactions producing photons in the visible (400–750 nm) range require around 40-70 kcal mol^{-1}.

- This electronically excited state has to be accessible on the reaction coordinate.
- Photon emission from the excited state has to be a favorable energy release route.

This means that either the product of the reaction has to be fluorescent or – if energy transfer is involved in the process – an excited state can be populated (this energy transfer can occur intra- or intermolecularly).

The chemical luminescence quantum yield, defined as the number of photons emitted per reacting molecule, can be expressed as:

$$\phi_{CL} = \phi_R \phi_{ES} \phi_F$$

where ϕ_R reflects the chemical yield of the reaction, ϕ_{ES} is the fraction of the product entering the excited state and ϕ_F is the fluorescent quantum yield.

The oxidation of luminol is one of the oldest CL reactions used. Luminol can be considered a diprotic acid with pK_A of 6 and 13, respectively. During the CL reaction under basic conditions in presence of H_2O_2, luminol is oxidized to luminol radical anion in its excited state, which releases a photon while decaying to the ground state (Fig. 1.7). The light is emitted at 428 nm (blue light emission) with a relatively low quantum yield of 1% (Créton et al, 2001).
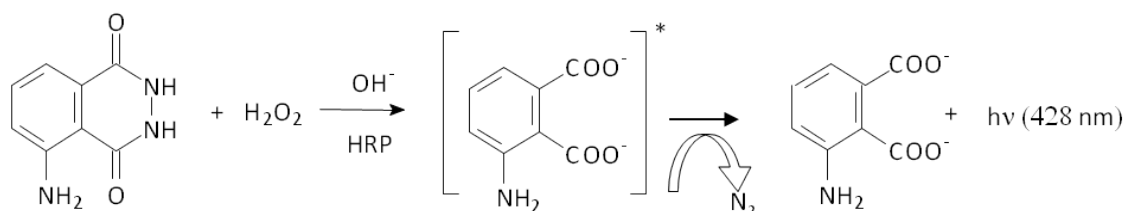
Fig. 1.7: *Reaction of luminol with horseradish peroxidase with light emission at 428 nm.*

The reaction of luminol can be catalyzed by horseradish peroxidase (HRP) that is commonly used as label in binding assays thanks to its signal amplification capability (Roda et al., 2012).

In the presence of certain chemicals and/or buffers and at suitable pH conditions the light emitted could be enhanced up to 1000-fold, so the light is detected easily, and the sensitivity of the reaction is increased.

HRP is an enzyme used extensively in biochemistry applications that is found in the roots of horseradish. It is a metalloenzyme with many isoforms, it catalyzes the oxidation of various organic substrates by hydrogen peroxide.

Numerous substrates for HRP have been described and commercialized, some of these are chromogenic substrates (3,3',5,5'-Tetramethylbenzidine or TMB, 3,3'-diaminobenzidine or DAB, 2,2'-azino-di-(3-ethylben thiazoline sulfonic acid or ABTS) and are converted by HRP into colored products, others instead are chemiluminescent substrates and produce light (luminol).

HRP is an ideal enzyme because it is stable, small and is cheaper than other commercial alternatives. Thanks to the high turnover rate it allows generation of strong signals in a relatively short time span.

To avoid enzyme activity disruption by certain experimental conditions is important to pay attention when enzyme labels are employed. Since the enzyme activity depends on temperature, a thermo-stated read-out cell should be used. The possibility to exploit an enzyme like HRP or alkaline phosphatase (AP) as label allows to amplify the CL signal because many product molecules are generated from one enzyme molecule in the presence of an excess of CL substrate (Roda et al., 2000).

Since the steady-state light intensity is directly related to the enzyme activity, the quantitation of the labeled probe under investigation is allowed. Moreover, the achievement of a steady state of the CL emission allows the standardization of the experimental conditions.

Chemiluminescence detection techniques gain analytical interest mainly due to their ability to produce photons without the need for photoexcitation, as occurs in fluorescence detection. This avoids problems deriving from light scattering, background fluorescence or instability of the light source. Since no external excitation light source is required, the instrumentation for chemiluminescence measurements is in principle very simple. In addition, when chemical luminescence detection is employed in conjunction with imaging detection systems, such as charge coupled devices (CCDs), flexible configurations of the reading cell (e.g., microarray spots distributed on a functionalized surface) are possible, provided that crosstalk phenomena are controlled.

At the end, the analysis of samples with very different analyte concentrations is facilitated thanks to the wide dynamic ranges of chemical luminescence detection. Unfortunately, one of the main disadvantages of these detection techniques is the potential effect of the constituent elements of the sample matrix on the chemical reaction, as light production can be increased or inhibited (Wolter et al., 2007). These unpredictable effects can lead to artifacts or spurious results. It is also important to take into account also the photon emission kinetics since it varies according to the chemistry exploited (ranging from flash type to glow type). Another aspect to consider is the phenomenon of diffusion in solution, which causes loss of resolution, to which long-lived light-emitting species are subject (Cheek et al., 2001). Analytical chemiluminescence is a versatile and ultra-sensitive tool with a wide range of applications in different fields such as biotechnology, pharmacology, clinical and environmental chemistry. Enzyme activities, enzyme substrates and inhibitors can be

efficiently determined when directly involved in luminescent reactions, and also when they take part in a reaction suitable for coupling to a final light-emitting reaction.

1.2.2 Bioluminescent detection

Bioluminescence (BL) is one of the most spectacular phenomena that naturally occurs in several living organisms, from fireflies to bacteria, abyss species, and mushrooms (Fig. 1.8). Light emission derives from different chemical reactions that involve a luciferase, an enzyme that catalyzes the oxidation by molecular oxygen of a substrate, luciferin, and its conversion to an excited state of the oxyluciferin molecule, emits visible light that then returns to the ground state (Sadik et al., 2004).
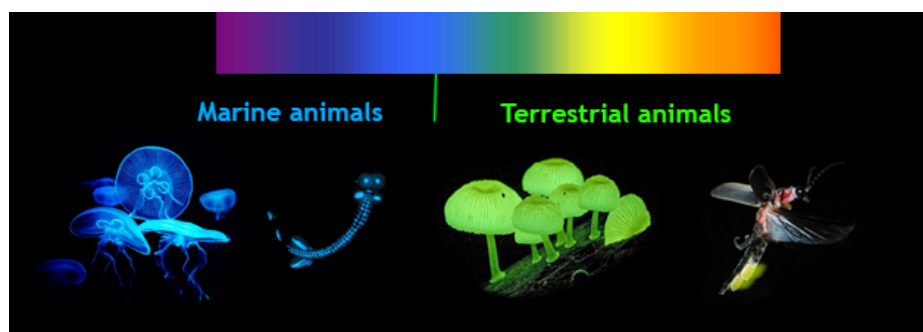
Fig. 1.8: *Examples of naturally bioluminescent emitting organisms. From left to right: Aequorea victoria, Bathophilus digitatus, Agaricus gardneri and Photinus pyralis.*

The BL emission intensity depends on the overall quantum yield of the reaction (ϕ_{BL}) and can be defined by following the equation:

$$\phi_{BL} = \phi_C \phi_{EX} \phi_F$$

where ϕ_C reflects the chemical yield of the reaction, ϕ_{EX} is the excited state production and ϕ_F is the emission quantum yield of the excited state.

Compared to conventional CL systems, the peculiar photo- physical property of BL reaction is that the light emission process derives from an enzyme-singlet excited state product complex.

Due to the simple chemistry of BL reactions (Chau et al., 2018), the non-toxicity of luciferin, the high detectability and the remarkable high quantum yield, which is about one order of magnitude higher than that of CL reactions, many in vitro and in vivo analytical methods with

BL detection have been developed, including gene expression assays, immunoassays, and non-invasive in vivo and in vitro imaging techniques.

BL-based methods are sensitive and provide good spatial resolution, a wide dynamic range and simple quantitative signal assessment. Indeed, in contrast with fluorescence technique, BL does not require an external excitation light source and in the experimental measurements there are no interference from light scattering and background fluorescence. Thanks to the possibility of exploiting signal amplification due to the turnover of the luciferase enzymatic reaction, BL systems represent a suitable detection principle for analytical applications where high sensitivity is required for example for detection of low concentrations of target analyte or small sample size (Yagur-Kroll et al., 2015).

More than 30 different BL systems have been elucidated to date (Chau et al., 2018), however only 9 natural luciferin structures have been identified. *Photinus pyralis* (PpyLuc), is the most studied BL protein, with an emission in the yellow-green light (λ_{em} = 557 nm at pH 7.8), a glow-type kinetic and a broad emission band. PpyLuc is a 61 kDa monomeric protein that does not require any post-translational modifications. It is suitable for heterologous expression in both prokaryotic and eukaryotic systems since PpyLuc does not show any toxicity to cells even at high concentrations. PpyLuc bioluminescence shows a remarkable red shift at lower pH and higher temperatures.

The luciferase-catalyzed oxidation of luciferin involves the presence of adenosine-5'-triphosphate (ATP) and Mg^{2+} as co-factors. As shown in Figure 1.9, in the first step, D-luciferin in the presence of ATP, is converted into luciferyl adenylate, the central intermediate in the BL reaction. Thanks to the presence of molecular oxygen, around 80% of adenylate is oxidized via a single electron-transfer mechanism (Date et al., 2007) into peroxide whose ultimately leads to production of oxyluciferin and emission of a light quantum. Different tautomeric forms of the oxyluciferin in its excited state are possible, but it is thought that the actual emitters inside the luciferase pocket are keto-(-1) or enol-(-1') forms.

As ATP molecules are found in every living organism, the D-luciferin-luciferase reaction is widely employed for ATP detection to identify microbial contaminations and for analysis of seawater and water treatment plants, hygiene monitors in hospitals and cell viability studies (Yagur-Kroll et al., 2014).
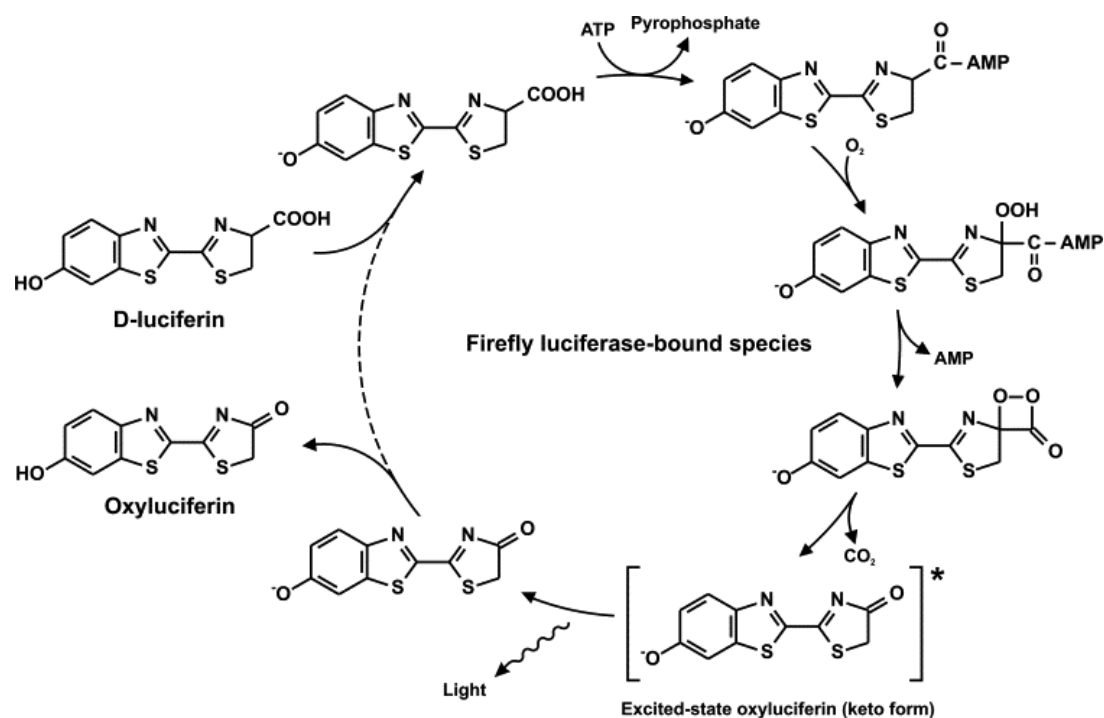
Fig. 1.9: *Luciferase-catalyzed oxidation of D-luciferin. Reproduced from Rowe L, Dikici E, Daunert S. Engineering bioluminescent proteins: expanding their analytical potential. 2009; 8662-8.*

Following *P. pyralis* luciferase, beetle luciferases derived from *Pyrophorus plagiophthalamus* are the second most popular choice (Shin H.J., 2011) thanks to the availability in nature in a wide range colors, from green to red. The possibility to have a wide range of natural and mutant BL reporters with different well-separated emission spectra and improved properties (e.g. thermal stability) is essential for the development of dual-color and multicolor assays (Esteban et al., 2014). We have also recently developed a dual-luciferase gametocyte assay with immature and mature *Plasmodium falciparum* gametocyte stages expressing red and green-emitting luciferases for anti-malarial drug screening (Cevenini et al., 2014).

In particular, this dual color assay was allowed to quantitatively and simultaneously measure stage-specific drug effects on parasites at different developmental stages with significant reduction of assay time and cost in comparison to state-of-the-art analogous assays. New luciferases obtained from other species have been recently commercialized showing a good potential; for instance, a synthetic NanoLuc® luciferase designed on the small *Oplophorus* luciferase domain was developed by Hall and colleagues in 2012 (Hall et al., 2021). NanoLuc is a 19.1 kDa luciferase enzyme that utilizes a synthetic furimazine substrate (a coelenterazine analogue) to produce high intensity and glow-type luminescence, providing a sensitivity superior than other luciferases (Fig. 1.10). The BL

signal intensity is increased by 2.5 million times with respect to the parent luciferase. Thanks to its small size and brightness, NanoLuc has been employed for several applications, for exploring gene regulation and cell signalling, for monitoring protein stability, for the development of novel based BL biosensors and BL imaging.
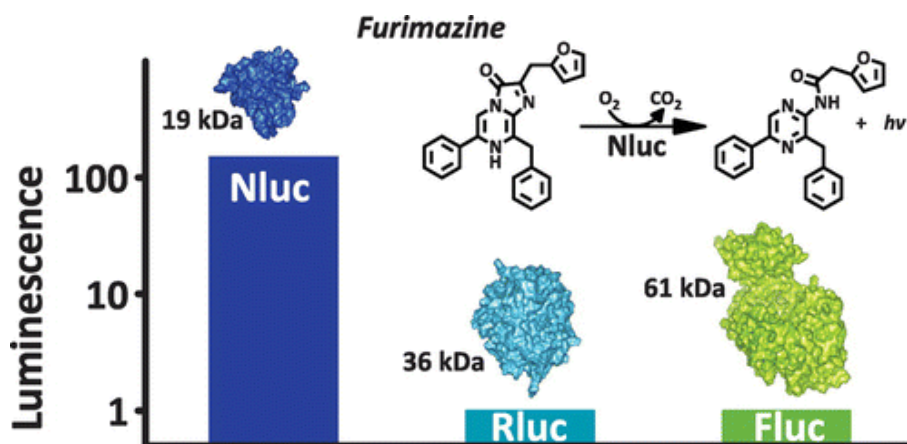
Fig. 1.10: *Comparison between NanoLuc, Renilla and Firefly luciferase. Reproduced by permission from Hall, M.P., Unch, J., Binkowski, B.F., Valley, M.P., Butler, B.L., Wood, M.G., ... & Wood, K.V., 2012. ACS Chem. Biol. 7(11): 1848-1857 (https://pubs.acs.org/doi/10.1021/cb3002478). Copyright © 2012, American Chemical Society.*

From an analytical point of view, the light emission produced by a chemical reaction allows quantitative analysis in which, under certain experimental conditions, the light intensity is closely related to the concentration of analyte. In comparison to all methods based on the interaction of the light with the matter (absorption spectroscopy and fluorimetry), BL has appealing features since the detection of the signal is not influenced either by the drift of the light source and the detector or by interferences due to the light diffusion. For this reason, BL is a suitable method for the detection of analyte molecules in a complex biological matrix. Different molecular biology tools based on BL reactions have been developed, being suitable for both *in vitro* assays, with purified proteins and cells, and *in vivo* methods, i.e. small animals. The investigation of protein–protein interactions, protein conformational changes, protein phosphorylation, second-messengers expression, and, in general, the study of gene expression and gene regulation *in vitro* and *in vivo* (Yagur-Kroll et al., 2014; Shin H.J., 2011; Esteban et al., 2014; Wanekaya et al., 2008; Hall et al., 2012; Rantala et al., 2011) are the typical bioanalytical applications of the BL. Since the luminescence

reaction is quantitative, and has an extremely low background, *in vitro* BL imaging is particularly useful for longitudinal studies and quantitative imaging (Martín-Betancor et al., 2015). One of the most frequently used applications of *in vivo* bioluminescence imaging is cell tracking (Roda et al., 2013). In this application, luciferase-expressing cancer cells, immune cells, stem cells, or other types of cells can be imaged repeatedly in animal models, providing information about the number and spatial distribution of the cells.
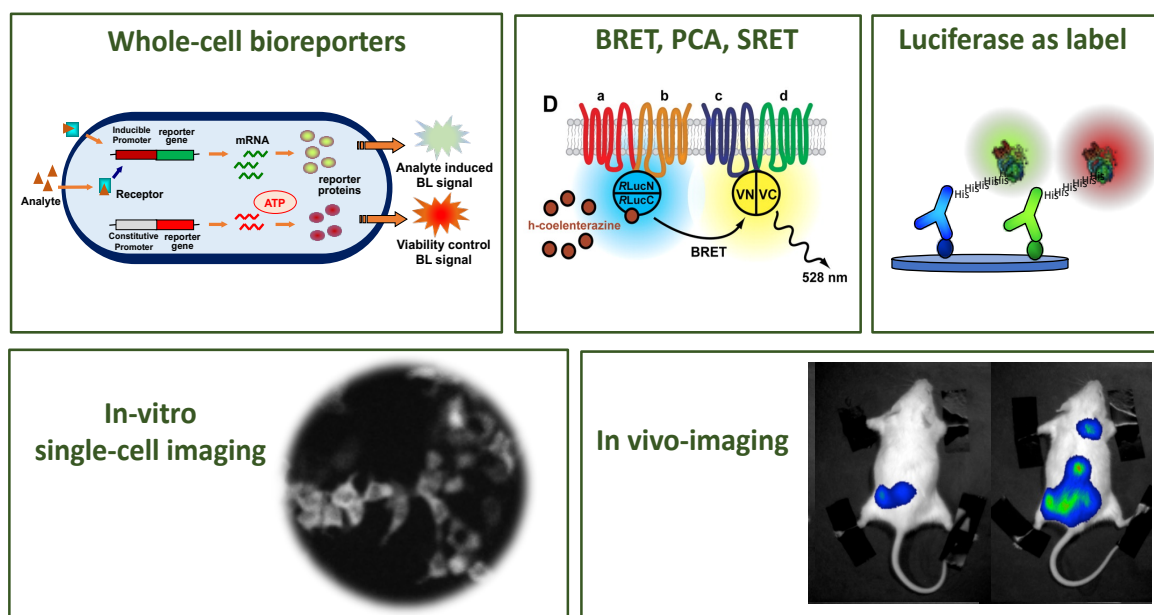
Fig. 1.11: *Bioanalytical applications of luciferases to in vitro and in vivo monitor activation of molecular pathways, protein-protein interactions and to quantify target analytes.*

BL proteins can be detected down to very low levels and for this reason they allow an ultrasensitive detection of the target analytes and monitoring of the physiological phenomena under investigation. Thanks to recent advances in genetic engineering and in silico study, directed evolution of new luciferases have been made leading to improvement of analytical performance, thermostability, spectral diversity and quantum yield emission (Nakatsu T., 2006; Branchini et al., 2005; Rowe et al., 2009). For example, mutants emitting in orange/red-colored light have been obtained changing the size and hydrophobicity of the amino acid I288 from Isoleucine (nonpolar and neutral, MW= 131) to valine (nonpolar and neutral, MW= 117) and alanine (nonpolar and neutral, MW= 89) respectively. Because of this improvement, the luciferase reporter gene can be used for new applications, such as biosensors with multiplex capability, that allow to simultaneously measure more than one analyte (Nakatsu T., 2006). Also multiplex detection can be performed, by exploiting spatial, temporal, spectral resolution or by selecting luciferases such us firefly and NanoLuc luciferase that require different substrates (Cevenini et al., 2015).

1.2.3 Colorimetric detection

Colorimetry is one of the most suitable readouts are the most common method of detection in these microfluidic devices due to its simplicity and compatibility with inexpensive portable detectors, such as smartphones (Martinez et al., 2008) and scanners (Martinez et al., 2007). In 2000's, the pioneer work on digital imaging for analytical purposes by Byrne et al. (Byrne et al., 2000) prompt the use of digital tools for qualitative, semi-quantitative and fully quantitative analysis of multiple analytes using colorimetric reactions. Since then, the area of qualitative and quantitative analysis using colorimetric readouts has experienced a huge development (Cate et al., 2015). There is a multitude of ways to obtain a colorimetric output for biosensing, including nanoparticles, dyes, redox and pH indicators, and each has unique drawbacks and benefits. There are also multiple variables that impact the analysis of colorimetric biosensors including color homogeneity, image capture methods, and the data handling itself (Morbioli et al., 2017)**.**

Products of enzymatic reactions are not typically chromophores; it is therefore often necessary to couple these reactions with a colorimetric reporting system. Redox indicators should be colorless in the reduced form (or the color must change between the reduced and oxidized form), should have an intense color in the oxidized form, a color stability to complete the analysis and ideally should have low or no toxicity. Is really difficult to obtain al these characteristics in real systems, the final coloration is influenced by the contrast between oxidized/reduced form, the support material (i.e. paper), the color of enzymes and the color of the sample itself (Morbioli et al., 2017).

Nanoparticles (NPs) are another sensing method for colorimetric detection in the field of biosensors. Thanks to the possibility to label NPs with antibodies, antigens or oligonucleotides and thanks to the possibility of naked-eye observation are widely used for biomolecule detection (R. Wilson, 2008). Metal nanoparticles (i.e. AuNPs, AgNPs) shows optical properties due to the surface plasmon resonance effect (SPR) (P. Mulvaney, 1996), which gives rise to a well-defined absorption band in the UV-vis spectrum (Kelly et al., 2003). Nanoparticles can also be prepared from non-metallic sources, including polymeric latex or carbon dots. Other approaches to generate color are pH indicators, weak acid or bases that present a color change (Lopez-Ruiz et al., 2014), light-induced polymerization amplification, when monomers are irradiated where the photo initiator molecules are located (bonded with the analyte of interest), inducing a color change in the region (Badu-Tawiah et al., 2015), metallic complexes formation or destruction causing a color change in the system (Hossain

and Brennan, 2011; Mentele et al., 2012) and chemo responsive dyes, which change color depending on the chemical environment in which are exposed (Janzen et al., 2006).

1.3 Portable detectors

1.3.1 Light detectors

To implement luminescent-based assays into portable formats and turn them into real biosensors with adequate analytical performance the selection of miniaturized light detectors is crucial. The selection of a detector to measure photons produced by bio and chemiluminescent reactions requires some considerations related to the intensity of the emitted light, the kinetics of photon emission, the presence of diffusion phenomena, and the emission wavelength, the latter also connected to multiplexing possibility. In addition, the choice could be also related to the necessity of obtaining spatial information, and in this case imaging systems are required, or only collect as much light as possible, and light-collecting systems are thus employed. As concerns imaging systems, additional constraints are present involving more complex optics to avoid distortions and loss of light collection efficiency. Several portable light detectors were explored spanning from photomultiplier tubes (PMT), charge-coupled devices (CCD), complementary metal oxide semiconductors (CMOS), single photon avalanche diodes (SPADs), silicon photomultipliers (SiPMs), and smartphone-integrated CMOS.

Thanks to their high sensitivity to low-light levels and high stability, PMTs are generally the first choice. PMTs, composed of a photocathode and an electron multiplier, rely on the external photoelectric effect, i.e., when photons hit a metal or semiconductor in vacuum, electrons are produced from its surface. After the photon hits the photocathode, an electron is emitted and accelerated by electric fields into a dynode, the collision generates new electrons which are in turn accelerated into other dynodes, with an electron gain of about 106. Since PMTs are characterized by a rapid response to a wide range of wavelengths, filters or monochromators are generally required to improve the sensitivity at specific wavelengths. PMTs are still the optimal choice for laboratory-based applications, however significant drawbacks limit their implementation into portable instruments, including the requirement for high voltages (higher than 1000 Volt) and intrinsic fragility (necessity for sealed vacuum tube).

Photodiodes are solid-state detectors composed of silicon p-n junctions that create a depletion region lacking mobile charge carriers. Once a photon is absorbed an electron lone pair is generated; by applying a reverse bias an electric field is produced across the depletion region causing the charge carriers to move towards the cathode (electrons) or the anode (holes). Thus, in a reverse-biased photodiode the absorption of a photon will generate a flow of current (Tavernier and Steyaert, 2011). A similar architecture is present in p-i-n photodiodes which are characterized by improved collection efficiency due to a lightly doped region at the pn-junction. Thanks to their low cost, easy miniaturization and possibility of implementation in arrays, photodiodes are very appealing for on-site bioanalytical applications. Nevertheless, they lack an inherent gain mechanism, and therefore they are not as sensitive as PMTs or SiPMs; this is not an issue for most biological applications, but they are generally a non-viable option for BL typical low light intensities (Yotter and Wilson, 2003). The use of photodiodes to detect low-light emissions was explored with a-Si:H photodiodes by Caputo and others who reported a remarkable detection of horseradish peroxidase with the luminol/peroxide/enhancer system at the attomole level (Caputo et al., 2013).

SiPM, thanks to its small size, negligible sensitivity to magnetic fields, low operating voltage (25-70 Volt), fast response time, and good Photon Detection Efficiency (PDE), represents a feasible alternative to conventional PMT (Bondarenko et al., 2000; Buzhan et al., 2003).

After the pioneering work of Daniel et al. who reported the use of a single photon avalanche photodiode (SPAD) working in the Geiger mode to detect BL-based SOS toxin response of *Escherichia coli* bacteria, SiPMs have been proposed as sensitive light detectors for BL (Daniel et al., 2008; Li et al., 2021; Jia and Ionescu, 2015).

SiPMs are arrays of avalanche photodetectors connected in parallel in which each pixel operates in limited Geiger mode, under bias voltage of 10-20% higher than breakdown voltage (Dolgoshein et al., 2006).

Combining the robustness of avalanche photodiodes and unmatched photon number resolution capability with high quantum efficiency and wide sensitive areas, SiPMs replaced PMTs in a high number of applications (Lomazzi et al., 2020; Santangelo et al., 2018; Sciuto et al., 2021). Thanks to a very high gain (106 vs 100-200 of avalanche photodiodes) SiPM have a very low electronic noise. The main source of noise is the dark noise which is due to the thermal generation of carriers and to the effects of high electric fields. A reduction of the SiPM dark rate occurs decreasing the temperature; therefore, in particular for large

photosensitive areas (1 cm^2) the performance of SiPM is affected when measuring low-light levels (Vincent et al., 1979)

One of the first comparisons of PMT vs SiPM for BL detection was performed by Li et al. who reported that PMT provided the lowest limit of detection, while cooled SiPM exhibited a wider linear range using genetically engineered BL *Pseudomonas fluorescens* bioreporters (Li et al., 2012).

Very recently these solid-state sensors were also exploited in a low-cost customized set up for performing aequorin-based intracellular Ca^{2+} measurements (Ruffinatti et al., 2020). This system showed performance similar to that obtained by a custom-designed PMT tube-based assay, thus supporting the potential use of SiPM devices for low-level BL detection for point-of-need applications. Recently, Jung et al compared the performance of a field deployable SiPM device with smartphones in detecting pathogens via BL phage reporters. Their result showed that SiPM provided better performance than smartphones in terms of time to detection and signal-to-noise ratio (Jung et al., 2020).

Charge-coupled devices (CCD) and complementary metal oxide semiconductors (CMOS), have a great potential like alternative light sensors due to their compact size and their ability to image and quantify multiple spots simultaneously on the detections area of the sensor (Lengger et al., 2014; Zangheri et al., 2015; Zhou et al., 2014). Modern cooled back-illuminated CCDs create high-quality, low-noise images reaching a quantum efficiency (QE) of up to 90%, read-out noise of <5 e$^-$, dark count rates of 0.001 e$^-$/s, and formats as large as 4096 x 4096 pixels with size down to 4 x 4 μm (Roda et al., 2016). In order to obtain a thermal insulation between the bioassay components and the cooled CCD sensor, and a coherent photon transfer between the two surfaces, a fiber optic mosaic faceplate or tape was used for contact imaging. Exploiting a thermoelectrically cooled (double Peltier) CCD camera in contact imaging configuration, Roda et al. developed an ultrasensitive portable device for point-of-need CL bioassays (Roda et al., 2011b). Thanks to this device, Mirasoli et al. developed a miniaturized multiplex biosensor for detecting parvovirus B19 DNA in serum samples (Mirasoli et al., 2013), showing competitive analytical performance respect to conventional ELISA assay.

The smartphone ubiquitous distribution and connectivity around the world is changing the concept of mobile health with the potential to reshape the biosensor market landscape (Wei et al., 2014; Roda et al., 2017). Smartphones, thanks to their integrated camera, multifunction and geotagging capabilities, and computing power are a sort of evolution of point-of-care devices, providing the possibility to perform tests without any additional

equipment, even in remote areas and low resource settings. For these reasons, CMOS sensors represent an interesting alternative, thanks to their small and compact size, low power consumption, camera-on-a-chip integration and lower fabrication costs (Singh et al., 2011; Rodrigues et al., 2010). In comparison to the first generations of CMOS where the majority of the pixel area was dedicated to the support transistors, with a limited photon-sensing area (fill factor), modern back-illuminated CMOS uses the entire area of each pixel for photon capture. In this configuration CMOS shows higher sensitivity, thus ensuring high signal-to-noise even in low-light conditions. To use smartphone-integrated CMOS as CL-BL detectors the first requirement is a mini dark box to shield from environmental light and the fabrication of a smartphone accessory to integrate cartridges or sensing papers hosting the bio-specific reactions. In most of the applications, this has been performed exploiting low-cost three-dimensional (3D) printing technology. For example, we recently reported a yeast estrogenic assay based on newly developed yeast biosensors expressing NanoLuc as reporter protein immobilized onto a 3D printed minicartridge and an adaptor to fit the smartphone. This biosensor was used to analyze water samples and complex samples showing limits of detection comparable to those obtained with standard yeast estrogenic bioassays (Fig. 1.12) (Lopreside et al., 2019). It must be pointed out that most of the reported smartphone-based biosensors are not fully optimized, especially regarding the design of the optical system and the use of smartphone with small lens apertures (Li et al., 2020). Smartphone-integrated CMOSs are specifically designed for taking photographs and have autofocus mechanisms that do not work perfectly in low-light conditions. "Tricks" such as the use of chambers and cartridges with reflection materials and plano-convex lenses for efficiently capturing and focusing light emission are required. The identification of best conditions permits to improve the limit of detection of the method and increase the dynamic range. The most important parameters that should be optimized in smartphone-based sensing platforms are ISO and exposure time, both can be controlled in most recent operating systems. As with all other detectors, a preliminary investigation of the CL-BL system emission kinetics is mandatory before identifying the optimal measurement window. As a general rule, at a fixed exposure time, the increase of ISO permits to decrease the limit of detection, however aberrant images can be obtained at high concentrations of the target analyte, as exemplified in a recent work based on a paper sensor for ATP exploiting the luciferin-luciferase system (Calabretta et al., 2020).
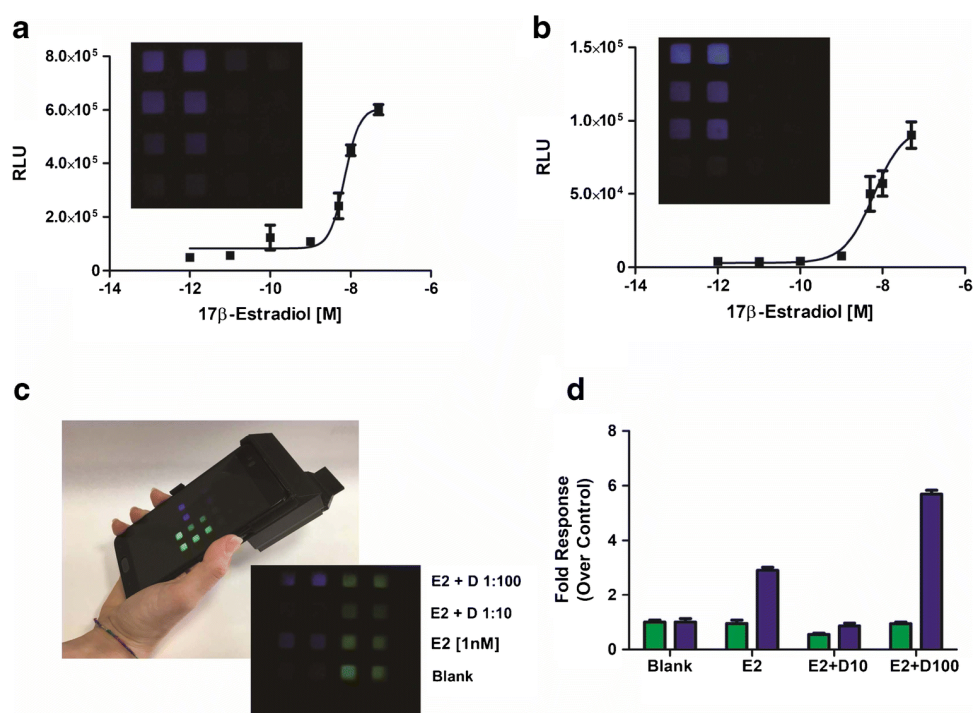
Fig. 1.12: *Newly developed yeast biosensors smartphone based expressing NanoLuc as reporter protein immobilized onto a 3D printed minicartridge. Analysis of water samples and complex samples showing limits of detection comparable to those obtained with standard yeast estrogenic bioassays. Reprinted with permission from Lopreside, A., Calabretta, M.M., Montali, L., Ferri, M., Tassoni, A., Branchini, B.R., Southworth, T., D'Elia, M., Roda, A., Michelini, E., 2019. Anal. Bioanal. Chem. 411: 4937-4949. License number: 5176410925241, Oct 26, 2021, © 2019 Springer Nature. All rights reserved.*

1.3.2 Reporting systems for colorimetry

Once the colorimetric assay has been performed, it is necessary to read off the information and this is a crucial step for the quantitative readouts. The information obtained can be performed by a standard analytical instrumental technique, such as diffuse reflectance spectroscopy, or by information technology communication equipment, such as scanners and smartphone cameras (Quesada-González and Merkoçi, 2016).

Gotardo et al. (Gotardo et al., 2004) affirmed that the use of diffuse reflectance spectroscopy was not originally considered for quantitative analysis in the past (~1970s) due to low resolution and poor relative accuracy. Thanks to recent instrumentation development, including optical fibers and reflectance spheres, diffuse reflectance spectroscopy gain attraction for colorimetry readouts. This method is not the most suitable choice in comparison with a smartphone camera or a flatbed scanner for on-site analysis because is expensive and requires skilled personnel. Grudpan et al. (Grudpan, et al., 2015) reports that

the use of information technology (IT) communication equipment (i.e. scanners, smartphone cameras and webcams) have helped analytical and clinical chemistry in the last years, improving the development of low-cost tools for point-of-care testing (POCT) and on-site biosensing applications (Yang et al., 2016). Several studies show that in 2019 half of the population has internet access (Statistics, Int. Telecommun. Union (2019) http://www.itu.int/en/ITU-D/Statistics/Pages/stat/default.aspx) and 90% of people own a mobile phone today (https://www.bankmycell.com/blog/how-many-phones-are-in-the-world), this shows how widespread and accessible IT communications are. Two-dimensional optical scanners work with the same principle of diffuse reflectance spectroscopy but uses filters for binning light into 3 or 4 wavelength ranges prior to detection by CCDs instead of separating light with a prism or diffraction grating based monochromator (Poce-Fatou et al., 2011).

Smartphone cameras are lightweight, portable, inexpensive, does not require skilled personnel and have the possibility of transmitting data. Besides scanners, presents minor disadvantages due to the possibility of varying lighting conditions, angle of imaging, shadows, and focal distance, which contribute to the variability intra and inter-assays. Researchers have worked to improve these issues using several hardware strategies O. (Mudanyali et al., 2012; Oncescu et al., 2013). Data obtained whit scanners and smartphone cameras are preprocessed by device software, for this reason there are some device-dependent differences in the colorimetric read-outs (Göröcs and Ozcan, 2014). Obtaining the raw bit data from the device can alleviate this issue, as can the use of an external scanning calibration.

1.4 Immobilization methods

In the field of enzymatic biosensors there is great interest in understanding effects of solution conditions on enzyme stability, as well as in developing strategies to improve enzyme stability in desired reaction media. Recent methods include novel chemical modifications of protein, lyophilization in the presence of additives, and physical immobilization on novel supports. One main disadvantage of enzymes is that have evolved to work in the cellular environment and, therefore, are not usually tolerant to the presence of organic solvents, extremes pH or high temperatures (Polizzi et al., 2017). In the past years, one of the tools available to improve enzyme stability was the chemical modification of residues. Covalent modifications of enzymes and crosslinking with chemicals such as glutaraldehyde had been

used through the years. Later, new modifications with several polyethylene glycol derivatives and other polymers was demonstrated (DeSantis and Jones, 1999).

Freeze drying technology (lyophilization) it is one of the most used processes to preserve and immobilize enzymes on a surface. Is possible to add protectants directly to the reaction medium and lyophilization in the presence of additives can enhance stability and activity.

Another way to improve stability of enzyme is immobilization on a solid support. There are many types of immobilization strategies, such as covalent attachment of physical adsorption, entrapment in a matrix or cross-linking of enzyme crystals. These techniques are not generalizable because type of immobilization and matrix that preserve enzyme stability and activity often change from protein to protein (Bornscheuer, 2003).

Talking about whole-cell biosensing, maintenance of cells viability and physiological activity are very important issues. For this reason, cell immobilizations strategies have been studied over the years to obtain a portfolio of different approaches, each one having advantages and limitations. Depending on final application of the immobilization and on the type of cell, both microbial and mammalian cells, were successfully immobilized on surfaces or entrapped into suitable matrixes. In the field of whole-cell biosensors, is necessary to take into account several factors to choose an appropriate immobilization method, for example, opacity of some matrices, like PVA, could be an interference for an optical signal unlike for an electric signal (Houbertz et al., 2003; Charrier et al., 2011). Some optimal requirements for cell immobilization support and matrices for cell biosensing are retention of immobilized cell viability, maintenance of biological and metabolic activity, controlled cell growth and oxygenation, accessibility of nutrients, mechanical and chemical stability, ease to scale-up and handling and low cost of chemicals. The most promising and widely exploited methodologies in cell preservation are nature inspired. Three groups of matrices for cell biosensor's immobilization can be selected: ionic hydrogels, thermogels and synthetic polymers.

The first one, hydrogels entrapment, i.e. using agarose or sodium alginate, is one of the easiest, inexpensive and most used approach for cell immobilization (Barin et al., 2009; Ruan et al., 2018; Mbeunkui et al., 2002; Borin et al., 2018).

Several work report bacteria and yeast entrapped into alginate beads or slices and implemented into portable biosensing devices for remote areas monitoring. It is possible to observe long-term storage, low toxicity and good reproducibility (Jouanneau et al., 2016; Belkin et al., 2017; Cevenini et al., 2018).

Thanks to the capability to survive to extreme conditions (freezing temperatures, desiccation, dry and wet heat) some spore-forming bacteria *Bacillus subtilis* and *Bacillus megaterium* for arsenic and zinc detection achieved one of the longest storage times for this kind of cells (up to 8 months). Recently, spores were also exposed to extreme conditions, such us simulate Mars surface conditions, showing good survival rates (Cortesão et al., 2019; Date et al., 2007). Recently, to reduce matrix effect and increase analytical performance, researchers are focused to achieve fine control over cells, to enable their manipulation, providing new strategies to concentrate cells and separate them from media before the analysis (Ranmadugala et al., 2018).

The choice of a suitable support for integrating living cells is important to provide the cells a protection from external agents and to create an optimal micro-environment (Table 1.1). Indeed, local concentration of cytokines and other soluble factors for paracrine signaling improves cell-to-cell communication and survival.

Inorganic	Organic	Biological	Nanomaterials
Aluminium oxide	Polyethylene	Cellulose	Gold nanoparticles
Nickel oxide	Polystyrene	Dextran	Quantum dots
Stainless steel	Polyacrylate	Agarose	Liponanoparticles
Porous glass	Nylon	Starch	Nanofibres
Porous silica	Polyacrylamide	Alginate	Nanoporous silica
Fused silica	Polymethacrylate	Carrageenan	Nanotubes
Diatomaceous earth	Polypyrrole	Chitin	Nanoparticles
Iron oxide	Polyaniline	Chitosan	
Titanium oxide	Polyphenol	Collagen, gelatin	
Pumice stone	Polyester		
Zirconium oxide	Poly(vinyl alcohol)		
Silicon dioxide			
Activated carbon			

Table 1.1: *Suitable material and supports for cells immobilization. Reprinted with permission from Lopreside, A., Calabretta, M.M., Montali, L., Roda, A., Michelini, E., (2022) Live Cell Immobilization. In: Thouand G. (eds) Handbook of Cell Biosensors. Springer, Cham. License number: 5176411476927, Oct 26, 2021, © 2022 Springer Nature. All rights reserved.*

Several materials have been exploited as matrices for mammalian cells immobilization. Among others, agarose, naturals and synthetic hydrogels and gelatin are the most promising. Nevertheless, the lack of optimal culture conditions during storage (i.e. temperature, humidity and CO_2) negatively affect cell metabolism and responsiveness leading to a rapid loss of their function. Nowadays, storage times (in air, at room

temperature) of 6-weeks were achieved (Linet al., 2011; Cevenini et al., 2016b; Xu et al., 2015; Michelini et al., 2019; Baraniak et al., 2012; Cruz-Acuña et al., 2018).
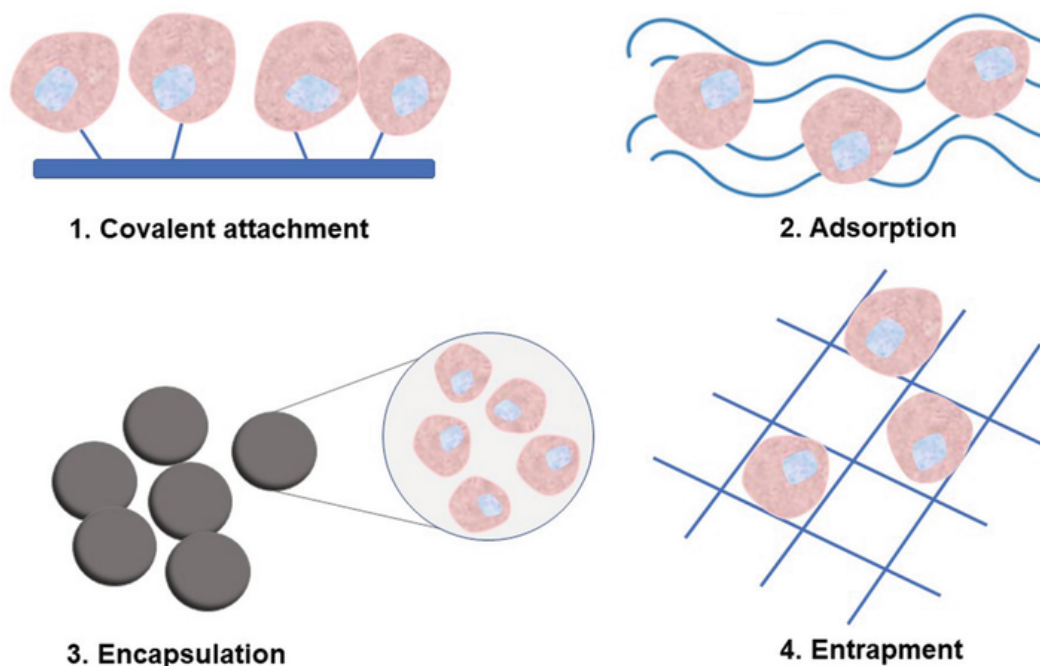
Fig. 1.13: *Different immobilization techniques methods categories for whole-cell immobilization approaches for biosensing. Reprinted with permission from Lopreside, A., Calabretta, M.M., Montali, L., Roda, A., Michelini, E., 2022. Live Cell Immobilization. In: Thouand G. (eds) Handbook of Cell Biosensors. Springer, Cham. License number: 5176411476927, Oct 26, 2021, © 2022 Springer Nature. All rights reserved.*

1.5 Paper based platforms

Paper-based analytical devices (PADs) represent a new alternative technology for fabricating simple, low-cost, portable and disposable biosensors for many application areas including clinical diagnosis, food quality control and environmental monitoring (López-Marzo et al., 2016).

Paper is abundant, available in a wide range of format, thicknesses, and porosity grade, is lightweight and has "green" properties such as biodegradability and recyclability (Hu et al., 2014; Martinez et al, 2010; Bruzewicz et al., 2008, Wang et al.; 2014). Indeed, thanks to the hydrophilicity and porosity properties, paper provides a natural platform for fabricating microfluidic channels that can be operated without an external power source (Cate et al, 2015; Bruzewicz et al, 2008; Lu et al., 2009; Carrilho et al., 2009). It can be easily printed, coated and impregnated with chemical/biochemical reagents representing an ideal sensing platform for developing low-cost and portable diagnostic devices (Xia et al., 2016; He et al.,

2015; Eltzov et al., 2015). Currently, quantitative analytic methods used for PADs have been developed exploiting colorimetric (Tang et al., 2009; Nath et al, 2015; Wang et al., 2012b), electrochemical (Sun et al., 2015; Cunningham et al., 2015), fluorescence (FL) (Velu et al., 2015), photoluminescence (PL) (Morales-Narváez et al.,2015), chemiluminescence (CL) (Zangheri et al., 2015; Roda et al., 2016; Mirasoli et al., 2014; Zhou et al. 2014), electrochemiluminescence (ECL) (Delaney et al.; 2011) detections. In addition, in the last years with the improvement of the detection technologies, several paper-based devices are implemented and integrated with objects of common use such as smartphones (Zangheri et al., 2015), wearable technology, or other imaging devices, scanners, optical drives/disc players, and strip readers for creating new innovative devices with higher analytical performance. Moreover, these devices require only small volumes of reagents and samples, provide rapid analysis, and are portable and disposable.

Fabrication of this paper-based devices is really simple. A pattern of wells or microfluidics channels (according to the final application) is designed using software, such as PowerPoint (Microsoft) or Adobe Illustrator, and printed onto the chosen paper (i.e. filter paper, office paper) using an office wax printer. After printing, the waxed pattern is cured for 1 min at 100°C to allow wax to diffuse in the paper thickness, producing a hydrophobic region, which defines the hydrophilic zone. Reagents (i.e. enzymes, substrates, samples) are then loaded in the biosensor by dispensing appropriate volumes of solutions. Finally, the biosensor was let drying for 30 min at 37°C (Arduini et al., 2019). These paper-based devices represent an interesting way to create reagent-free biosensors, once all necessary regents have been absorbed and/or immobilized on the paper. Cinti et al. reported the first example of a fully integrated paper-based electrochemical biosensor able to detect nerve agents exploiting screen-printing technology to print the electrochemical cell on paper as well as wax printing for paper-based microfluidics (Fig. 1.14) (Cinti et al., 2017).
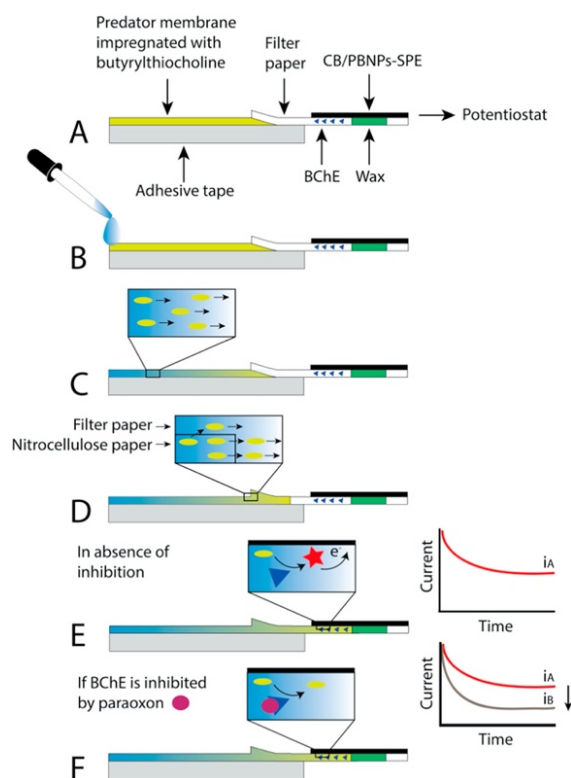
Fig. 1.14: *First example of a fully integrated paper-based electrochemical biosensor able to detect nerve agents exploiting screen-printing technology to print the electrochemical cell on paper as well as wax printing for paper-based microfluidics. Reprinted with permission from Cinti, S., Minotti, C., Moscone, D., Palleschi, G., Arduini, F., 2017. Biosens. Bioelectron. 93: 46-51. License number: 5176420236187, Oct 26, 2021, © 2017 Elsevier B.V. All rights reserved.*

Enzyme solutions are easily inactivated and need storage conditions between +4 and +8°C. Immobilization of reagents (both enzyme and substrate) on a solid support (such as paper) is suitable to improve the long-term stability of enzymes without special storage conditions (Kratasyuk and Esimbekova, 2003; Esimbekova et al., 2007). To provide a user-friendly platform Calabretta et al. developed a new lyophilization strategy (Calabretta et al., 2020) that enable to immobilize luciferase and reagents required for bioluminescent reaction directly on paper with higher reproducibility and enzyme stability than previously reported methods (Yousefi-Nejad et al., 2007; Wang et al., 2015). A wax printed nitrocellulose paper biosensor was developed exploiting paper as support and using smartphone camera as light detector (Fig. 1.15)
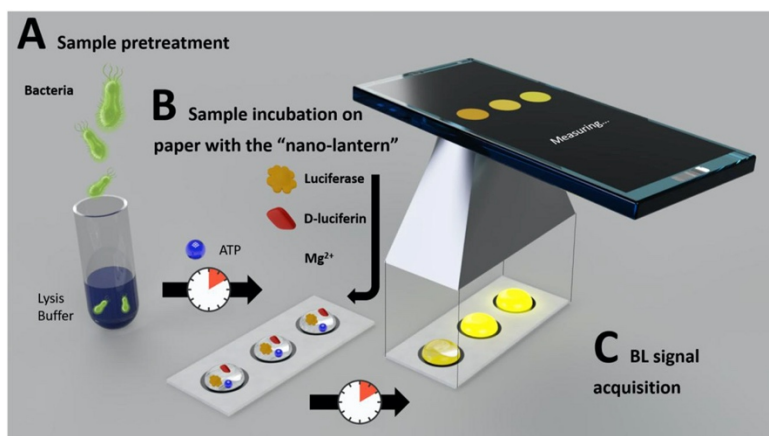
Fig. 1.15: *Schematic representation of the optimized ATP sensing paper assay with immobilized luciferase and reagents required for bioluminescent reaction directly on paper. Reprinted with permission from Calabretta, M.M., Álvarez-Diduk, R., Michelini, E., Roda, A., Merkoçi, A. 2020. Biosens. Bioelectron. 150: 111902. License number: 5176420589453, Oct 26, 2021, © 2019 Elsevier B.V. All rights reserved.*

1.5.1 Origami 3D paper-based biosensors

In order to create a 3D device, 2D devices can be stacked together using alternating layers of patterned paper and double-sided tape. 3D paper devices were further developed with only a single sheet of patterned paper and folded based on the origami principle. Origami, the art and science of paper folding, is a technique in which elegant and complex 3D objects are produced from planar paper (Liu et al. 2011).

In 2012, Ge et al. developed a sandwich-type chemiluminescence immunoassay based on 3D origami device for the detection tumor markers. This 3D origami-based immunodevice has the capability to separate the operational procedures into several steps including (i) folding pads above/below and (ii) addition of reagent/buffer under a specific sequence, showing excellent analytical performance for the simultaneous detection of four tumor markers. This paper-based microfluidic origami CL detection system provides a new strategy for a low-cost, sensitive, simultaneous multiplex immunoassay and point-of-care diagnostics (Ge et al., 2012).

Recently, Arduini et al. proposed the first three-dimensional origami paper-based device for the detection of several classes of pesticides by combining different enzyme-inhibition biosensors. This device was developed by integrating two different office paper-based screen-printed electrodes and multiple filter paper-based pads to load enzymes and enzymatic substrates. The versatile analysis of different pesticides was carried by folding

and unfolding the filter paper-based structure, without any addition of reagents and any sample treatment (i.e. dilution, filtration, pH adjustment) (Fig. 1.16) (Arduini et al., 2019).
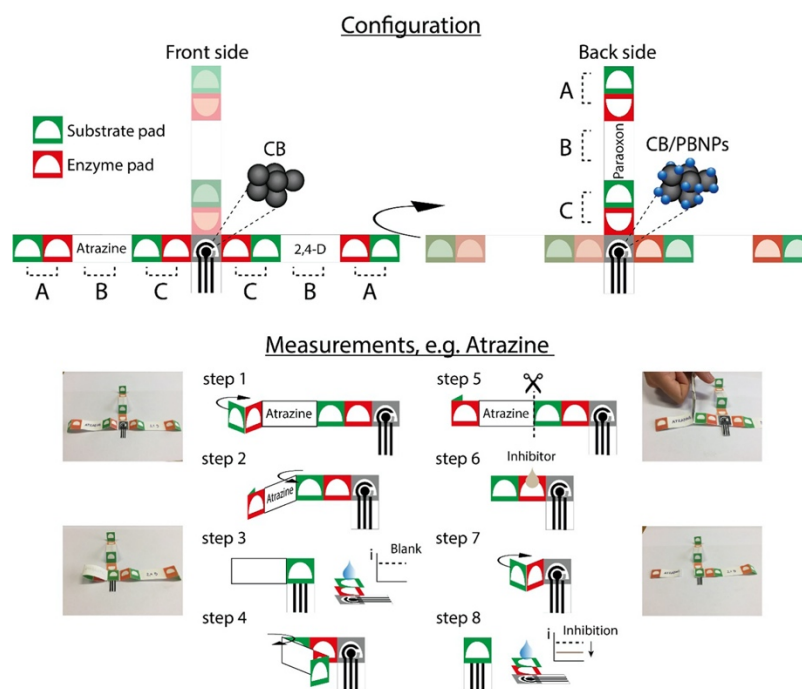
Fig. 1.16: *First three-dimensional origami paper-based device for the detection of several classes of pesticides by combining different enzyme-inhibition biosensors. Reprinted with permission from Arduini, F., Cinti, S., Caratelli, V., Amendola, L., Palleschi, G., Moscone, D., 2019. Biosens. Bioelectron. 126: 346-354. License number: 5176541429808, Oct 26, 2021, © 2019 Elsevier B.V. All rights reserved.*

1.6 3D-printing technologies

Three-dimensional (3D) printing is a process that enables the rapid production of 3D solid object using the technology of making layer-upon-layer from a computer-aided design (CAD). Thanks to this technology, combined with additive and affordable micro/nano-fabrication technologies, is possible to produce complex and well characterized prototypes with several materials, spanning from polymers to metals (Bishop et al., 2016; Sharafeldin et al., 2018) and several functional devices (Marks et al., 2011), like tissue grown scaffolds (Shepherd et al., 2011), microfluidics (Therriault et al., 2003), electronics (Ahn et al., 2009), which can be used as new tools for point-of-need biosensing applications. Around the year 200, in China, there was an example of the first printing technique of this type obtained with a woodblock. In order to obtain a prototype to be used to repeatedly form an imprint on a substrate, a block of wood was carved. After that, the printing technologies have evolved from the printing press, lithography, xerography, laser printing to finally reach modern 3D printing in which a physical pattern is printed using a print head, nozzle, or other

mechanisms and by converting it from a 3D computer design (Gross et al., 2014; Shallan et al., 2014; Knowlton et al., 2015). Depending on the mechanism by which materials are bonded together and the type of materials different types of 3D printing are classified. Fused deposition modelling, photopolymer jetting and material jetting are the most used types for biosensing applications (Palenzuela and Pumera, 2018). Fused deposition modelling (FDM), introduced for the first time by Scott Crump (Crump SS (1992) Google Patents. US Patent No. 5,121,32) is one of the first technology used for on-site biosensing application, related to the development of customized adaptor for biosensors integration into portable device. FDM 3D printers use thermoplastic materials that are fused and extruded trough a nozzle. In order to obtain a 3D structure, FDM 3D printers use thermoplastic material that are fused and extruded trough a nozzle and deposited layer by layer on the build platform that then cools down and solidifies (Waldbaur et al., 2011; Pham and Gault, 1998; Sood et al., 2009). Melted thermoplastic polymers such as acrylonitrile butadiene styrene (ABS), polylactic acid (PLA, a biodegradable polymer), polycarbonate, polyamide and polystyrene are used for FDM because are cheap, durable (Au et al., 2016), biocompatible and represents an interesting option for obtaining portable devices (Cevenini et al., 2016a; Cevenini et al., 2016b). FDM can be also used for printing several liquid materials, such as hydrogels, metallic solutions, and cell-based solutions, through the possibility of using the printer without heating.
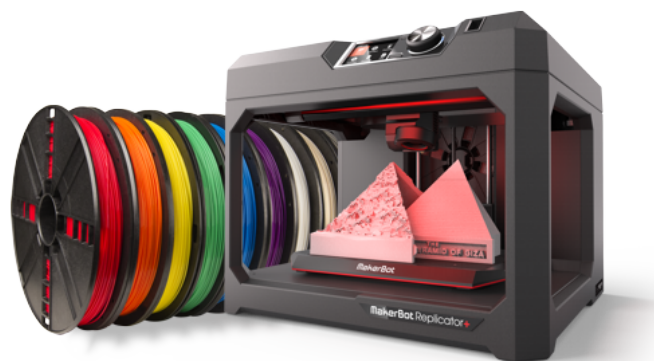
Fig. 1.17: *3D printer MakerBot Replicator.*

In the last few years, material jetting technology is gaining interest in the field of biosensing, with this technology is possible to print polymers, ceramics, metal and biomaterials (Calvert, 2001). These wax-like materials are melted and printed using an inkjet print head onto a mobile build platform. The material, deposited layer by layer, cools and forma solid 3D

structure. It allows to print different materials at the same time, obtaining unique prototypes with particular properties in the final 3D-printed object. In this case final product is not only an inert scaffold but also a functional material with several advanced properties. For this reason, also mammalian cells can be successfully directly printed onto a scaffold (Xu et al., 2005; Wüst et al., 2011). To obtain "living materials", increased storage, in vivo implants and differentiation process have been also exploited. (Liu et al., 2018). Another technology widely used in the field of biosensors for microfluidics devices fabrication, is photopolymer jetting, introduced by Hanan Gothait (Gothait H Apparatus and method for three-dimensional model printing (2001) Google Patents) for printing support liquid photopolymers onto a mobile build platform. Materials are cured and solidified though UV light, allowing layer-by-layer fabrication. (Erkal et al., 2014; Begolo et al., 2014; Causier et al., 2015; Bonyár et al., 2010; Anderson et al., 2013). Is used for any material in powder form and is a fast, simple and inexpensive process since powder particles are glued together to produce a solid structure and, repeating the process, a 3D structure is built up in the powder bed. For plastic powdered materials, is used laser sintering, another process that not require support structures and in which laser source and scanning mirrors sinter layer-by-layer the powder. A similar process is used by laser melting 3D printers, but in this case metal powders are used, and a support structure is required. Lastly, metal powders can also be printed with an electron beam melting. In this process an electron beam is used to melt metal powders.

1.7 References

Aguilera-Herrador, E., Cruz-Vera, M., Valcarel, M., 2010. Analyst. 135: 2220-2232.

Ahn, B.Y., Duoss, E.B., Motala, M.J., Guo, X., Park, S.I., Xiong, Y., Yoon, J., Nuzzo, R.G., Rogers, J.A., Lewis, J.A., 2009. Science. 323: 1590–1593.

Alpat, Ş., Alpat, S.K., Çadirci, B.H., Yaşa, İ, Telefoncu, A., 2008. Sens. Act. B. Chem. 134(1): 175-81.

Anderson, K.B., Lockwood, S.Y., Martin, R.S., Spence, D.M., 2013. Anal. Chem. 85: 5622–6.

Andreescu, S., Marty, J.L., 2006. Biomol. Engineer. 23: 1-15.

Antoni, D., Burckel, H., Josset, E., Noel, G., 2015. Int. J. Mol. Sci. 16(3): 5517-5527.

Arduini, F., Cinti, S., Caratelli, V., Amendola, L., Palleschi, G., Moscone, D., 2019. Biosens. Bioelectron.126: 346-354.

Arduini, F., Forchielli, M., Amine, A., Neagu, D., Cacciotti, I., Nanni, F., Moscone, D., Palleschi, G., 2015. Microchim. Acta 182(3): 643-651.

Arora, S., Pastorella, G., Byrne, B., Marsili, E., O'Kennedy, R., 2010. Rev. Pharm. Biom. Anal. 63-75

Au, A.K., Huynh, W., Horowitz, L.F., Folch, A., 2016. Angew. Chem. Int. Ed. Engl. 55: 2- 22.

Badu-Tawiah, A.K., Lathwal, S., Kaastrup, K., Al-Sayah, M., Christodouleas, D.C., Smith, B.S., Whitesides, G.M., Sikes, H.D., 2015. Lab. Chip, 15: 655-659.

Bahrvand, H., Hashemi, S.M., Kazemi Ashtini, S., Farrokhi, A., 2006. Int. J. Dev. Biol. 50: 645-652.

Baraniak, P.R., Cooke, M.T., Saeed, R., Kinney, M.A., Fridley, K.M., McDevitta, T.C., 2012. Journ. Mec. Behav. Biom. Mat. 11:63-71.

Barhoumi, A.H., Maaref, A., Rammah, M., Martelet, C., Jaffrezic, N., Mousty, C., Vial, S., Forano, C., 2006. Mat. Sci. Eng. C. 26: 328–33.

Barin, M., Otadi, M., Khorasheh, F., Kheirolomoom, A., 2009. Sci. Iran. Trans. C. Chem. Chem. Eng.

Bazin, I., Seo, H.B., Suehs, C.M., Ramuz, M., De Waard, M., Gu M.B., 2017. Environ. Sci. Pollut. Res. Int. 24: 33-41.

Begolo, S., Zhukov, D., Selck, D.A., Li, L., Ismagilov, R.F., 2014. Lab. Chip. 14: 4616–28.

Belkin, S., Yagur-Kroll, S., Kabessa, Y., Korouma, V., Septon, T., Anati, Y., Zohar-Perez, C., Rabinovitz, Z., Nussinovitch, A., Agranat, A.J., 2017. Nat. Biotec. 35:308.

Benya, P.D., Shaffer, J.D., 1982. Cell. 30: 215-224.

Bhadriaraju, K., Chen, C.S. 2002. Drug. Discov. Today 7: 612-620.

Bhagavan, N.V., Ha, C.E., 2011. Essentials of Medical Biochemistry. 6: 47-58.

Birgersdotter, A., Sandberg, R., Ernberg, I., 2005. Semin. Cancer Biol. 15: 405-412.

Bishop, G.W., Satterwhite-Warden, J.E., Kadimisetty, K., Rusling, J.F., 2016. Nanotec. 27: e284002.

Bondarenko, G., Buzhan, P., Dolgoshein, B., Golovin, V., Guschin, E., Ilyin, A., Kaplin, V., Karakash, A., Klanner, R., Pokachalov, V., Popova, E., Smirnov, K., 2000 Nucl. Instrum. Methods. 442: 187-192.

Bonyár, A., Sántha, H., Ring, B., Verga, M., Kovacs, J.G., Harsányi, G., 2010. Procedia Eng. 5; 291–4.

Borin, G.P., de Melo, R.R., Crespim, E., Sato, H.H., Contesini, F.J., 2018. In Polymer Gels. Springer.

Bornscheuer, U.T., 2003. Angew. Chem. Int. Ed. Engl. 42: 3336-3337.

Branchini, B.R., Southworth, T.L., Khattak, N.F., Michelini, E., Roda, A., 2005. Anal. Biochem. 345(1): 140-8.

Bruzewicz, D. A., Reches, M., Whitesides, G. M., 2008. Anal. Chem. 80: 3387–3392.

Buzhan, P., Dolgoshein, B., Filatov, L., Ilyin, A., Kantzerov, V., Kaplin, V., Karakash, A., Kayumov, F., Klemin, S., Popova, E., Smirnov, S., 2003. Nucl. Instrum. Methods. 504: 48–52.

Byrne, L., Barker, J., Pennarun-Thomas, G., Diamond, D., Edwards, S., 2000. Trac. Trends Anal. Chem. 19: 517-522.

Calabretta, M.M., Álvarez-Diduk, R., Michelini, E., Roda, A., Merkoçi, A., 2020. Biosens. Bioelectron. 150: 111902.

Calvert, P., 2001. Chem. Mater. 13: 3299-305.

Caputo, D., De Cesare, G., Dolci, L.S., Mirasoli, M., Nascetti, A., Roda, A., Scipinotti, R., 2013. IEEE Sens. J. 13: 2595 – 2602.

Carrilho, E., Martinez, A. W., Whitesides, G. M., 2009. Anal. Chem. 81: 7091–7095.

Cate, D.M., Adkins, J.A., Mettakoonpitak, J., C.S. Henry, 2015. Anal. Chem. 87: 19-41.

Causier, A., Carret, G., Boutin, C., Berthelot, T., Berthault, P., 2015. Lab. Chip. 15: 2049–54.

Cevenini, L., Calabretta, M.M., Calabria, D., Roda, A., Michelini, E., 2015. Biol: Fund. Appl. 3:3-17.

Cevenini, L., Calabretta, M.M., Lopreside, A., Tarantino, G., Tassoni, A., Ferri, M., Roda, A., Michelini, E., 2016a. Anal. Bioanal. Chem. 408 (30): 8859-8868.

Cevenini, L., Calabretta, M.M., Tarantino, G., Michelini, E., Roda, A., 2016b. Sens. Actuat. B. Chem. 225: 249-257.

Cevenini, L., Camarda, G., Michelini, E., Siciliano, G., Calabretta, M. M., Bona, R., Kumar, T.R.S., Cara, A., Branchini, B.R., Fidock, D.A., Roda, A., Alano, P., 2014. Anal. Chem. 86(17): 8814-8821.

Cevenini, L., Lopreside, A., Calabretta, M.M., D'Elia, M., Simoni, P., Michelini, E., Roda, A., 2018. Anal. Bioanal. Chem. 410:1237-46.

Chambers, J.P., Arulanandam, B.P., Matta, L.L., Weis, A., Valdes, J.J., 2008. Biosensor recognition elements. Texas Univ San Ant Dept Biology.

Charrier, T., Durand, M.J., Jouanneau, S., Dion, M., Pernetti, M., Poncelet, D., Thouand, G., 2011. Anal. Bioanal. Chem. 400(4):1051-60.

Chau, H.T., Kadokami, K., Duong, H.T., Kong, L., Nguyen, T.T., Nguyen, T.Q., Ito, Y., 2018. Environ. Sci. Pollut. Res. Int. doi:10. 1007/s11356-015-5060-z

Chee, G.J., Nomura, Y., Ikebukuro, K., Karube, I., 2000. Biosens. Bioelectron. 15(7): 371-6.

Cheek, B.J., Steel, A.B., Torres, M.P., Yu, Y.Y., Yang, H., 2001. Anal. Chem. 73: 5777-5783.

Choi, O., Lee, Y., Han, I., Kim, H., Goo, E., Kim, J., Hwang, I., 2013. Biosens. Bioelectron., 50: 256-261.

Cinti, S., Minotti, C., Moscone, D., Palleschi, G., Arduini, F., 2017. Biosens. Bioelectron. 93: 46-51.

Cortesão, M., Fuchs, F.M., Commichau, F.M., Eichenberger, P., Schuerger, A.C., Nicholson, W.L., Setlow, P., Moeller, R., 2019. Front Microbiol. 10:333.

Cracknell, J.A., Vincent, K.A., Armstrong, F.A., 2008. Chem. Rev. 108: 2439-2461.

Créton, R., Jaffe, L.F., 1992. BioTechniques. 31: 1098-1105.

Crump, S.S., (1992) Google Patents. US Patent No. 5,121,32

Cruz-Acuña, R., Quirós, M., Huang, S., Siuda, D., Spence, J.R., Nusrat, A., García, A.J., 2018. Nat. Protoc. 13(9):2102.

Cunningham, J.C., Scida, K., Kogan, M.R., Wang, B., Ellington, A.D., Crooks, R.M., 2015. Lab. Chip. 15: 3707–3715.

Daniel, R., Almog, R., Ron, A., Belkin, S., Diamand, Y.S., 2008. Biosens. Bioelectron. 24: 882–887.

Date, A., Pasini, P., & Daunert, S., 2007. Anal. Chem., 79(24): 9391-9397.

Delaney, J.L., Hogan, C.F., Tian, J., Shen, W., 2011. Anal. Chem. 83: 1300–1306.

DeSantis, G., Jones, J. B., 1999. Current Opinion Biotechnol. 10: 324-330.

Dhall, P., Kumar, A., Joshi, A., Saxsena, T.K., Manoharan, A., Makhijani, S.D., Kumar, R., 2008. Sens. Act. B. Chem. 133(2): 478–83.

Dolgoshein, B., Balagura, V., Buzhan, P., Danilov, M., Filatov, L., Garutti, E., Groll, M., Ilyin, A., Kantserov, V., Kaplin, V., Karakash, A., Kayumov, F., Klemin, S., Korbel, V., Meyer, H., Mizuk, R., Morgunov, V., Novikov, E., Tikhomirov, I., 2006. Nucl. Instrum. Methods. 563: 368-376.

Durand, M.J., Hua, A., Jouanneau, S., Cregut, M., Thouand, G., 2015. Adv. Bioc. Eng. Biotec. 3: 77-99.

Eltzov, E., Cohen, A., Marks, R.S., 2015. Anal. Chem. 87: 3655-3661.

Engelking, L.R., 2015. Textbook of Veterinary Physiological Chemistry. 6: 32-38.

Erkal, J.L., Selimovic, A., Gross, B.C., Lockwood, S.Y., Walton, E.L., McNamara, S., Martin, R.S., Spence, D.M., 2014. Lab. Chip. 14: 2023–32.

Esimbekova, E.N., Torgashina, I.G., Kratasyuk, V.A., 2007. Biochemistry (Mosc.), 74: 695-700.

Esteban, S., Gorga, M., Petrovic, M., González-Alonso, S., Barceló, D., Valcárcel, Y., 2014. Sci. Total Environ. 466-467: 939-951.

Fujimoto, H., Wakabayashi, M., Yamashiro, H., Maeda, I., Isoda, K., Kondoh, M., Kawase, M., Miyasaka, H., Yagi, K., 2006. Appl. Microbiol. Biotechnol. 73(2): 332–338.

Ge, L., Wang, S., Song, X., Ge, S., Yu, J., 2012. Lab. Chip. 12: 3150-3158.

Ghéczy, N., Küchler, A., Walde, P., 2016. Anal. Biochem., 513: 54-60.

Göröcs, Z., Ozcan A., 2014. Lab. Chip. pp. 3248-3257.

Gotardo, M.A., Gigante, A.C., Pezza, L., Pezza, H.R., 2004. Talanta. 64: 361-365.

Gothait, H., Apparatus and method for three-dimensional model printing (2001) Google Patents

Grosova, Z., Rosenberg, M., Rebros, M., 2008. Czech J. Food Sci. 26: 1-14.

Gross, B.C., Erkal, J.L., Lockwood, S.Y., Chen, C., Spence, D.M., 2014. Anal. Chem. 86: 3240–53.

Grudpan, K., Kolev, S.D., Lapanantnopakhun, S., McKelvie, I.D., Wongwilai, W., 2015. Talanta. 136: 84-94.

Guardigli, M., Pasini, P., Mirasoli, M., Leoini, A., Andreani, A., Roda, A., 2005. Anal. Chim. Acta. 535: 139-144.

Guedri, H., Durrieu, C., 2008. Microchim. Act. 163(3): 179-84.

Gui, Q., Lawson, T., Shan S., Yan, L., Liu, Y., 2017. Sensors. 17(7): 1623.

Hall, M.P., Unch, J., Binkowski, B.F., Valley, M.P., Butler, B.L., Wood, M.G., ... & Wood, K.V., 2012. ACS Chem. Biol. 7(11): 1848-1857.

Hanson Shepherd, J.N., Parker, S.T., Shepherd, R.F., Gillette, M.U., Lewis, J.A., Nuzzo, R.G., 2011. Adv. Funct. Mater. 21: 47–54.

He, Y., Wu, Y., Fu, J.-Z., Wu, W.-B., 2015. RSC Adv. 5: 78109–78127.

Hossain, S.M.Z., Brennan, J.D., 2011. Anal. Chem. 83: 8772-8778.

Houbertz, R., Domann, G., Cronauer, C., Schmitt, A., Martin, H., Park, J-U., Fröhlich, L., Buestrich, R., Popall, M., Streppel, U., Dannberg, P., Wächter, C., Bräuer, A., 2003. Thin Solid Films. 442: 194–200.

https://www.bankmycell.com/blog/how-many-phones-are-in-the-world

Hu, J., Wang, S.Q., Wang, L., Li, F., Pingguan-Murphy, B., Lu, T.J., Xu, F., 2014. Biosens. Bioelectron. 54: 585–597.

Ivask, A., Green, T., Polyak, B., Mor, A., Kahru, A., Virta, M., Marks, R., 2007. Biosens Bioelectron. 22(7): 1396-402.

Janzen, M.C., Ponder, J.B., Bailey, D.P., Ingison, C.K., Suslick, K.S., 2006. Anal. Chem., 78: 3591-3600.

Jia, K., Ionescu, R.E., Measurement of bacterial bioluminescence intensity and spectrum: current physical techniques and principles, In: Thouand G., Marks R. (eds) Bioluminescence: Fundamentals and Applications in Biotechnology - Volume 3. Advances in Biochemical Engineering/Biotechnology, vol 154. Springer, Cham, 2015, pp. 19-45.

Jouanneau, S., Durand-Thouand, M.J., Thouand, G., 2016. Env. Sci. Pol. Res. 23(5): 4340-5.

Jung, Y., Coronel-Aguilera, C., Doh, I-J., Min, H.J., Lim, T., Applegate, B.M., Bae, E., 2020. Appl. Optics. 59: 801-810.

Kelly, K.L., Coronado, E., Zhao, L.L., Schatz, G.C., 2003. J. Phys. Chem. B, 107: 668.

Knowlton, S., Onal, S., Yu, C.H., Zhao, J.J., Tasoglu, S., 2015. Trends Biotechnol. 33: 504–13.

Kratasyuk, V.A., Esimbekova, E.N., 2003. Polymer immobilized bioluminescent systems for biosensors and bioinvestigations R. Arshady (Ed.), Polymeric Biomaterials, the PBM Series (Introduction to Polymeric Biomaterials), vol. 1, pp. 301-343 London.

Kumar, J., Jha, S.K., D'Souza, S.F., 2006. Biosens. Bioelectron. 21(11): 2100-5.

Kwok, N.Y., Dong, S., Lo, W., Wong, K.Y., 2005. Sens. Act. B. Chem. 110 (2): 289–98.

Lengger, S., Otto, J., Elsasser, D., Shneider, O., Tiehm, A., Fleischer, J., Niessner, R., Seidel, M., 2014. Anal. Bioanal. Chem. 406: 3323-3334.

Li, H., Lopes, N., Moser, S., Sayler, G., Ripp, S., 2012. Biosens. Bioelectron. 33.

Li, J., Ye, D., Fu, K., Wang, L., Piao, J., Wang, Y., 2021. Optics Exp. 29: 25922-25944.

Li, Y., Ma, X., Wang, W., Yan, S., Liu, F., Chu, K., Xu, G., Smith, Z.J., 2020. J. Biophoton. 13: e201900241.

Lin, C.C., Anseth, K.S., 2011. Proc Nat. Ac. Sci. 108(16):6380-5.

Liu, H., Crooks, R.M., 2011. J. of the American Chem. Soc. 133(44): 17564-17566.

Liu, Y., Li, T., Ma, H., Zhai, D., Deng, C., Wang, J., Zhuo, S., Chang, J., Wu, C., 2018. Act. Biomater. 73: 531-46.

Lomazzi, S., Caccia, M., Distasi, C., Dionisi, M., Lim, D., Martemiyanov, A., Nardo, L., Ruffinatti, F.A., Santoro, R., 2020. Nucl. Instrum. Methods. 979: 164493.

López-Marzo, A.M., Merkoçi, A., 2016. Lab. Chip. 16: 3150-3170.

Lopez-Ruiz, N., Curto, V.F., Erenas, M.M., Benito-Lopez, F., Diamond, D., Palma, A.J., Capitan-Vallvey, L.F., 2014. Anal. Chem. 86: 9554-9562.

Lopreside, A., Calabretta, M. M., Montali, L., Roda, A., & Michelini, E. 2022. Live Cell Immobilization. Handbook of Cell Biosensors, 479-496.

Lopreside, A., Calabretta, M.M., Montali, L., Ferri, M., Tassoni, A., Branchini, B.R., Southworth, T., D'Elia, M., Roda, A., Michelini, E., 2019. Anal. Bioanal. Chem. 411: 4937-4949.

Lu, Y., Shi, W., Jiang, L., Qin, J., Lin, B., 2009. Electrophoresis. 30: 1497–1500.

Luzi, E., Minunni, M., Tombelli, S., Mascini, M., 2003. Trend Anal. Chem. 22: 810–8.

Marks, P., Campbell, M., Aron, J., Lipson, H., 2011 New Sci. 2823: 17–20.

Martín-Betancor, K., Rodea-Palomares, I., Muñoz-Martín, M.A., Leganés, F., Fernández-Piñas, F., 2015. Front. Microbiol. 6: 186.

Martinez, A.W., Phillips, S.T., Butte, M.J., Whitesides, G.M., 2007. Angew. Chem. Int. Ed., 46: 1318-1320.

Martinez, A.W., Phillips, S.T., Carrilho, E., Thomas, S.W., Sindi, H., Whitesides, G.M., 2008. Anal. Chem. 80: 3699-3707.

Martinez, A.W., Phillips, S.T., Whitesides, G.M., 2010. Anal. Chem., 82: 3–10.

Mathew, F.P., Alocilja, E.C., 2005. Biosens. Bioelectron. 20 (205): 1656-1661.

Mbeunkui, F., Richaud, C., Etienne, A.L., Schmid, R.D., Bachmann, T.T., 2002. Appl. Microbiol. Biotechnol. 60:306-12.

McNaught, A.D., Wilkinson, A., 1997 IUPAC Compendium of Chemical Terminology, 2nd ed. (the "Gold Book"), Blackwell Scientific Publications, Oxford.

Mentele, M.M., Cunningham, J., Koehler, K., Volckens, J., Henry, C.S., 2012. Anal. Chem. 84: 4474-4480.

Michelini, E., Calabretta, M.M., Cevenini, L., Lopreside, A., Southworth, T., Fontaine, D.M., Simoni, P., Branchini, B.R., Roda, A., 2019. Biosens. Bioelectron. 123:269-77.

Michelini, E., Roda, A., 2012. Anal. Bioanal. Chem. 402(5): 1785-97.

Minunni, M., Tombelli, S., Gullotto, A., Luzi, E., Mascini, M., 2004. Biosens. Bioelectron. 20: 1149–56.

Mirasoli, M., Bonvicini, F., Dolci, L.S., Zangheri, M., Gallinella, G., Roda, A., 2013. Anal. Bioanal. Chem. 398: 227-238.

Mirasoli, M., Guardigli, M., Michelini, E., Roda, A., 2014. J. Pharmaceut. Biomed. 87: 36-52.

Morales, M.A., Halpern, J.M., 2018. Bioconjug. Chem. 29(10): 3231-3239.

Morbioli, G.G., Mazzu-Nascimento, T., Stockton, A.M., Carrilho, E., 2017. Anal. Chim. Acta. 970: 1-22.

Mudanyali, O., Dimitrov, S., Sikora, U., Padmanabhan, S., Navruz, I., Ozcan, A., 2012. Lab. Chip. 12: 2678-2686.

Mulvaney P., 1996. Langmuir. 12: 788-800.

Nakatsu, T., 2006. Nature. 372-6.

Nath, P., Arun, R.K., Chanda, N., 2015. RSC Adv. 5: 69024–69031.

Nelson, C.M., Bissell, M.J., 2005. Semin. Cancer. Bio 15: 342-352.

Ngoepe, M., Choonara, Y., Tyagi, C., Tomar, L.K., Du Toit, L.C., Kumar, P., Ndesendo, V.M.K., Pillay, V., 2013. Sensors 13: 7680-7713.

Nomura, Y., Ikebukuro, K., Yokoyama, K., Takeuchi, T., Arikawa, Y., Ohno, S., Karube, I., 1998. Bios. Bioel. 13(9): 1047-53.

Oncescu, V., O'Dell, D., Erickson, D., 2013. Lab. Chip. 13(16): 3232-3238.

Palenzuela, C.L.M., Pumera, M., 2018. TrAC Trends Anal. Chem. 103:110-8.

Pasini, P., Musiani, M., Russo, C., Valenti, P., Aicardi, G., Crabtree, J.E., Baraldini, M., Roda, A., 1998. J. Pharmaceut. Biomed. Anal. 18: 555-564.

Pessela, B.C., Mateo, C., Carrascosa, A.V., Vian, A., García, J.L., Rivas, G., et al. 2003. Biomacromol. 4: 107-113.

Petänen, T., Romantschuk, M., 2002. Anal. Chim. Act. 456(1): 55-61.

Pfeiffer, F., Mayer, G., 2016. Front. Chem. 4: 25.

Pham, D., Gault, R., 1998. Int. J. Mach. Tools. Manuf. 38: 1257-87.

Philippu, A., In Vivo Neuropharmacology and Neurophysiology. Springer New York, ed. 2017

Poce-Fatou, J.A., Bethencourt, M., Moreno-Dorado, F.J., Palacios-Santander J.M., 2011. J. Chem. Educ., 88: 1314-1317.

Polizzi, K. M., Bommarius, A. S., Broering, J. M., Chaparro-Riggers, J. F., 2007. Curr. Op. Chem. Biol., 11: 220-225.

Pundir, C.S., Chauhan, N., 2012. Anal. Biochem. 429: 19-31.

Quesada-González, D., Merkoçi, A., 2016. Biosens. Bioelectron. pp. 0-1

Ranmadugala, D., Ebrahiminezhad, A., Manley-Harris, M., Ghasemi, Y., Berenjian, A., 2018. Biotec. 40: 237-48.

Rantala, A., Utriainen, M., Kaushik, N., Virta, M., Välimaa, A.L., Karp, M., 2011. Anal. Bioanal. Chem. 400: 1041-1049.

Reshetilov, A.N., Semenchuk, I.N., Iliasov, P.V., Taranova, L.A., 1997. Anal. Chim. Acta

Riglar, D.T., Giessen, T.W., Baym, M., Kerns, S.J., Niederhuber, M.J., Bronson, R.T., Kotula, J.W., Gerber, G.K., Way, J.C., Silver, P.A., 2017. Nat. Biotechnol. 35(7): 653-8.

Roda, A., Calabretta, M.M., Calabria, D., Caliceti, C., Cevenini, L., Lopreside, A., Zangheri, M., Smartphone-Based Biosensors, In Past, Present and Future Challenges of Biosensors and Bioanalytical Tools in Analytical Chemistry: A Tribute to Professor Marco Mascini, Elsevier, Amsterdam, The Netherlands, 2017; Volume 77, p. 237

Roda, A., Cevenini, L., Borg, S., Michelini, E., Calabretta, M.M., Schüler, D., 2013. Lab. Chip. 13: 4881-4889.

Roda, A., Cevenini, L., Michelini, E., Branchini, B.R., 2011a. Biosens. Bioelectron. 26: 3647-3653.

Roda, A., Guardigli, M., 2012. Anal. Bioanal. Chem. 402: 69–76.

Roda, A., Mirasoli, M., Dolci, L.S., Buragina, A., Bonvicini, F., Simoni, P., Guardigli, M., 2011b. Anal. Chem. 83: 3178-3185.

Roda, A., Mirasoli, M., Michelini, E., Di Fusco, M., Zangheri, M., Cevenini, L., Roda, B., Simoni, P., 2016. Biosens. Bioelectron. 76: 164-179.

Roda, A., Pasini, P., Guardigli, M., Baraldini, M., Musiani, M., Mirasoli, M., 2000. Fresenius J. Anal. Chem. 366: 752-759.

Rodrigues, ERGO, LAPA, R.A.S., 2010. Anal. Bioanal. Chem. 397: 381-388.

Rowe, L., Dikici, E., Daunert, S., 2009. Anal. Chem. 8662-8.

Ruan, B., Wu, P., Chen, M., Lai, X., Chen, L., Yu, L., Gong, B., Kang, C., Dang, Z., Shi, Z., Liu, Z., 2018. Ecotox. Environ. Saf. 162:103-111.

Ruffinatti, F.A., Lomazzi, S., Nardo, L., Santoro, R., Martemiyanov, A., Dionisi, M., Tapella, L., Genazzani, A.A., Lim, D., Distasi, C., Caccia, M., 2020. ACS Sens. 5: 2388– 2397.

Sadik, O.A., Wanekaya, A.K., Andreescu, S., 2004. J. Environ. Monit. 6: 513-522.

Saini, R., Hegde, K., Brar, S.K., Verma, M., 2019. Tool Tec. Prot. Mon. Env. Cont. 263-84.

Santangelo, M.F., Libertino, S., Turner, A.P.F., Filippini, D., Mak, W.C., 2018. Biosens. Bioelectron. 99: 464-470.

Sciuto, E.L., Corso, D., Libertino, S., van der Meer, J.R., Faro, G., Coniglio, M.A., 2021. Int. J. Environ. Res. Public Health. 18: 7580.

Scordo, G., Moscone, D., Palleschi, G., Arduini, F., 2018. Sens. Actuat. B. Chem. 258: 1015-1021.

Shallan, A.I., Smejkal, P., Corban, M., Guijt, R.M., Creadmore, M.C., 2014. Anal. Chem. 86: 3124–30.

Sharafeldin, M., Jones, A., Rusling, J.F., 2018. Micromac. 9(8): e394.

Sharma, S.K., Leblanc, R.M., 2017. Anal. Biochem. 2017. 535: 1-11.

Sharma, S.K., Li, S., Micic, M., Orbulescu, J., Weissbart, D., Nakahara, H., Shibata, O., Leblanc, R.M., 2016. J. Phys. Chem. B. 120: 12279-12286.

Shin, H.J., 2011. Appl. Microbiol. Biotechnol. 89: 867-877.

Silva, N., Gil, D., Karmali, A., Matos, M., 2009. Biocat. Biotrans. 27(2): 143-51.

Singh, R.R., Lengh, L., Guenther, A., Genov, R., 2011. IEEE J. Solid-state circuits. 47: 282-2833.

Songa, E.A., Okonkwo, J.O., 2016. Talanta. 155: 289-304.

Sood, A.K., Ohdar, R., Mahapatra, S., 2009. Mater. Des. 30: 4243-5.

Souiri, M., Gammoudi, I., Mora, L., 2012. J. Environ. Sci. Eng. 1: 924-935.

Statistics, Int. Telecommun. Union (2019) http://www.itu.int/en/ITU-D/Statistics/Pages/stat/default.aspx

Stolper, P., Fabel, S., Weller, M.G., Knopp, D., Niessner, R., 2008. Anal. Bioanal. Chem. 390(4): 1181–7.

Sun, G., Liu, H., Zhang, Y., Yu, J., Yan, M., Songand, X., He, W., 2015. New J. Chem., 39: 6062–6067.

Tag, K., Riedel, K., Bauer, H., Hanke, G., Baronian, K.H.R., Kunze, G., 2007. Sens. Act. B: Chem. 2007; 122(2): 403-9.

Tang, D., Sauceda, J.C., Lin, Z., Basova, S., Goryacheva, I., Biselli, S., Lin, J., Niessner, R., Knopp, D., 2009. Biosens. Bioelectron. 25: 514–518.

Tavernier, F., Steyaert, M., From light to electric current—The photodiode, in: High-Speed Optical Receivers with Integrated Photodiode in Nanoscale CMOS, Springer, New York, NY, 2011, pp. 41-76.

Therriault, D., White, S.R., Lewis, J.A., 2003. Nat. Mater. 2: 265–271.

Valdman, E., Gutz, I.G.R., 2008. Sens. Actuat. B. 133(2): 656-663.

Velu et al., 2015

Vincent, G., Chantre, A., Bois, D., 1979. Int. J. Appl. Phys. 50: 5484-5487.

Waldbaur, A., Rapp, H., Lange, K., Rapp, B.E., 2011. Anal. Methods 3: 2681-716.

Wanekaya, A.K., Chen, W., Mulchandani, A., 2008. J. Environ. Monit. 10: 703-712.

Wang, J., 2008. 108(2): 814-825.

Wang, J., Monton, M.R.N., Zhang, X., Filipe, C.D.M., Pelton, R., Brennan, J.D., 2014. Lab. Chip. 14: 691–695.

Wang, J., Wu, C., Hu, N., Zhou, J., Du, L., Wang, P., 2012a. Biosensors. 2: 127-170.

Wang, S., Ge, L., Song, X., Yu, J., Ge, S., Huang, J., Zeng, F., 2012b. Biosens. Bioelectron. 31: 212–218.

Wang, W., Zhao, Q., Luo, M., Li, M., Wang, D., Wang, Y., Liu, Q., 2015. ACS Appl. Mater. Interfaces, 7: 20046-20052.

Weaver, V.M., Petersen, O.W., Wang, F., Larabell, C.A., Briand, P., Damsky, C., Bissel, M.J., 1997. J. Cell. Boil. 37: 231-245.

Wei, Q., Nagi, R., Sadeghi, K., Feng, S., Yan, E., Ki, S.J., Caire, R., Tseng, D., Ozcan, A., 2014. ACS Nano. 8:1121-9.

Whitesides, G.M., Grzybowski, B., 2002. Science 295: 2418-2421.

Wilson R., 2008. Chem. Soc. Rev. 37: 2028-2045.

Wolter, A., Niessner, R., Seidel, M., 2007. Anal. Chem. 79: 4529–4537.

Wüst, S., Müller, R., Hofmann, S., 2011. J. Funct. Biomat. 2:119–54.

Xia, Y., Si, J., Li, Z., 2016. Biosens. Bioelectron. 77: 774–789.

Xu, T., Jin, J., Gregory, C., Hickman, J.J., Boland, T., 2005. Biomat. 26:93–9.

Xu, Y., Mawatari, K., Konno, T., Kitamori, T., Ishihara, K., 2015. ACS Appl. Mater. (7): 23089–97.

Yagur-Kroll, S., Lalush, C., Rosen, R., Bachar, N., Moskovitz, Y., Belkin, S., 2014. App. Microbiol. Biotechnol. 98(2): 885-895.

Yagur-Kroll, S., Schreuder, E., Ingham, C.J., Heideman, R., Rosen, R., Belkin, S., 2015. Biosens. Bioelectron. 64: 625-632.

Yang, K., Peretz-Soroka, H., Liu, Y., Lin, F., 2016. Lab. Chip. 16: 943-958.

Yang, W., Pang, P., Gao, X., Cai, Q., Zeng, K., Grimes, C.A., 2007. Sens. Lett. 5: 405-410.

Yotter, R.A., Wilson, D.M., 2003. IEEE Sens. J. 3: 288-303.

Yousefi-Nejad, M., Hosseinkhani, S., Khajeh, K., Ranjbar, B., 2007. Enzym. Microb. Technol., 40: 740-746.

Zangheri, M., Di Nardo, F., Anfossi, L., Giovannoli, C., Baggiani, C., Roda, A., Mirasoli, M., 2015. Analyst. 140: 358-365.

Zhou, Z., Xu, L.R., Wu, S.Z., Su, B., 2014. Analyst. 139: 4934-4939.

2

Aim of the thesis

The activity carried out during PhD was mainly focused on the development of different types of portable paper-based biosensors for multianalyte detection and their implementation into portable analytical devices for point-of-care and point-of-need applications. In particular, enzymes and cells (bacteria and mammalian cell lines) have been exploited as biorecognition elements, in some cases even by coupling different elements in the same biosensor to increase its robustness. The final goal of biosensors developed during these years was the application in the environmental and forensic field, since the target analytes are organophosphorus pesticides (OPs), heavy metals, such as mercury (Hg^{2+}), present in liquid samples and molecules with androgenic activity, including new drugs or endocrine disrupting chemicals. Moreover, different optical detection principles (chemiluminescence, bioluminescence, colorimetry) have been exploited and integrated in the same device for achieving orthogonal detection, which allows to obtain more accurate and robust results. The assays were validated and characterized in terms of analytical performance and applied to different fields, from environmental monitoring to clinical diagnostics. Different portable detectors, such as coupled-charged device, smartphone cameras and silicon photomultiplier, and also benchtop laboratory instruments have been used to validate and support the developed biosensors. Several paper-based platforms have been designed and printed to better adapt to the type of assay, reagents, samples and detection method. Paper-based platforms and assays were implemented with adaptors and devices fabricated using a dual-extrusion 3D printer, using thermoplastic material (ABS). OPs detection has been obtained coupling three different enzymatic reaction while bioluminescent whole-cell biosensors have been obtained by genetically engineered cells that respond to different analytes. At the end, a new intracellular nanosensor that exploits intermolecular NanoLuc complementation for the fast and sensitive detection of androgenic-like compounds has been developed exploiting 3D cells models.

In Chapter 3, a foldable paper-based biosensor with chemiluminescent (CL) detection based on the origami technique is proposed. This biosensor is based on the inhibition process of acetylcholinesterase by molecules such as organophosphorus pesticides (OPs), nerve gases and some drugs. As regards the CL reaction, AChE activity is measured through a series of coupled enzymatic reactions exploiting AChE, choline oxidase (ChOx) and horseradish peroxidase (HRP) leading to light emission. When AChE is inhibited, there is a decreased production of hydrogen peroxide, and consequently a reduction in light emission. An improved luminol substrate is also reported that provides improved sensitivity, possibly having broad applicability in CL-based biosensing.

In Chapter 4, the implementation of BL- CL reactions in a SiPM device is evaluated and a side-by-side comparison of its performance with other portable light detectors, that showed very good performance in previous works, is performed. As model analytes, a green emitting *P. pyralis* firefly luciferase mutant Ppy-GR-TS (λ_{max} 550 nm) and the blue-emitting NanoLuc luciferase (λ_{max} 460 nm) are exploited. The SiPM device outperforms other portable detectors, providing adequate sensitivity for detecting low light intensities and making it suitable for on-site and forensic applications. As a proof-of-concept application, a CL origami sensing paper for the rapid detection of organophosphorus pesticides (OPs) is implemented in the device to assess its analytical performance.

Chapter 5 reports the development of an orthogonal biosensor providing the detection of mercury (II) via two different biorecognition elements, a bioluminescent mercury sensitive *Escherichia coli* bioreporter and an immobilized enzyme, β-gal, with bioluminescent and colorimetric detection, respectively. In addition, the inclusion of another bioluminescent strain, *Aliivibrio fischeri*, provides an internal toxicity control to correct the analytical signal, thus enabling the analysis of complex matrices. Both sensory elements and substrates necessary for the BL and colorimetric detection are integrated into a paper sensor to provide an all-in-one disposable cartridge and a reusable 3D-printed case for smartphone signal acquisition. Thanks to the correction of BL signal obtained from the *E. coli* mercury-sensitive paper with the *A. fischeri* toxicity paper signal, a LOD of 0.58 ± 0.07 ppb for Hg2+ was obtained, thus allowing the measurements of the maximum allowed concentration of mercury(II) in drinking water of 2 ppb (10 nM) and 6 ppb fixed by U.S. Environmental Protection Agency (EPA) and the World Health Organization (WHO), respectively (U.S. EPA, 2009; WHO, 2011).

Chapter 6 reports an intracellular nanosensor for androgenic activity detection relying on the human androgen receptor (hAR) fused to NanoBiT that can be employed in 2D and 3D cell models. Human Embryonic Kidney (HEK-293) cells are transiently transfected with vectors expressing the two chimeric proteins LgBiT-hAR and hAR-SmBiT under the control of a constitutive promoter. This genetically encoded sensor also represents a new tool for real time imaging of the activation state of the androgen receptor, thus being suitable for analysing molecules with androgenic activity, including new drugs or endocrine disrupting chemicals.

3

Multienzyme chemiluminescent foldable biosensor for on-site detection of acetylcholinesterase inhibitors

3.1 Introduction

Acetylcholine (ACh) is one of the key neurotransmitters in the human body, acting as a chemical messenger for conveying signals through the nerve synapse. The impairment of central cholinergic transmission has been related to a plethora of diseases, including Alzheimer's disease, Parkinson's disease, schizophrenia, and epilepsy (Ahmed et al., 2019). In both the central and peripheral nervous systems, the termination of impulse transmission occurs via rapid ACh hydrolysis by the enzyme acetylcholinesterase (AChE). AChE converts ACh into choline and acetic acid, thus causing the return of a cholinergic neuron to its resting state. The enzyme can be inactivated by several inhibitors, leading to acetylcholine accumulation and disrupted neurotransmission caused by hyperstimulation of nicotinic and muscarinic receptors (Andreani et al., 2005; Colovic et al., 2013). Reversible AChE inhibitors are widely used for treating neurodegenerative diseases, while irreversible inhibitors are associated with toxic effects (Andreani et al., 2008). Irreversible AChE inhibitors include chemical warfare agents and many organophosphorus (OP) compounds used as pesticides and insecticides. These inhibitors deactivate AChE by a nucleophilic attack to the serine residue (Ser200) located in the active site, thus generating a phosphorylated enzyme. This inhibition causes accumulation of ACh with severe respiratory impairment, paralysis, and death (Patel and Sangeeta, 2019). The rapid detection of these chemicals in water, soil, and food rep- resents a major challenge to current analytical technologies. Apart from warfare agents, OP pesticides are among the most important environmental pollutants because of their increasing use in agriculture as insecticides, fungicides, herbicides, contributing for about 38% of the total employed pesticides (Pundir and Malik, 2019). Most countries, including Europe, have fixed maximum residue levels (MRL) for food and animal feed. European legislation (Regulation EC 396/2005 and amendments) covers around 1100 pesticides currently or formerly used in agriculture in or outside the EU, with a general default MRL of 0.01 mg/kg. Recently, on 10 January 2020, the European Commission formally adopted two regulations to not renew the approvals of chlorpyrifos and chlorpyrifos-methyl. As a consequence, all Member States should, within one month, withdraw all authorizations for plant protection products containing these active substances (https://ec.europa.eu/food/plant/pesticides/approval_active_substances/ chlorpyrifos_chlorpyrifos-methyl_en).

Since chlorpyrifos-methyl shows significant hepatotoxicity and nephrotoxicity (Deng et al., 2016), its detection is of primary concern for agriculture workers and for the general

population. Thanks to their excellent sensitivity, High Performance Liquid Chromatography (HPLC) and Gas Chromatography (GC) coupled to mass spectrometry (MS) are widely used for OP compounds detection (Samsidar et al., 2018; Garlito et al., 2019). However, these techniques require specialized laboratory and skilled personnel, thus are not suitable for on-site detection. After the pioneering work by G. Guilbault (Guilbault et al., 1962), several successful examples of the use of AChE inhibition were reported to detect OP pesticides (Del Carlo et al., 2002; Roda et al., 1994; Guardigli et al., 2005). Biosensors targeting AChE inhibition are being considered suitable approaches for real-time, cost-effective and on-field OP compounds monitoring (Pundir and Malik, 2019). Most biosensors for OP pesticide detection rely on fluorescence, electrochemiluminescence and electrochemical detection (Chang et al., 2016; Liang and Han, 2020; Yao et al., 2019; Arduini et al., 2010, 2019; Capoferri et al., 2018; Uniyal and Sharma, 2018; Cui et al., 2019; Huang et al., 2019), generally being amperometric biosensors those showing the lowest detection limits. The possibility of implementing enzymatic assays with smartphone-based bio-chemiluminescence (BL-CL) detection has been explored by us and others (Roda et al., 2016, 2017; Huang et al., 2018; Calabretta et al., 2020). In recent years, smartphone-based biosensors have had an exponential growth as the integrated smartphone detector provides sufficient sensitivity to replace portable light detectors such as Charge-Coupled Devices (CCDs) and Complementary Metal Oxide Semiconductor (CMOS) sensors (Roda et al., 2014a; Cevenini et al., 2016b). Paper-based sensors were proposed for fabricating simple, low-cost, portable and disposable analytical devices suitable for clinical diagnosis, food and environmental monitoring (Liana et al., 2012; Meredith et al., 2016; Cinti, 2019; Martinez et al., 2010; Zangheri et al., 2015; Devi, 2012; Liu et al., 2019). Thanks to its hydrophilic cellulose fiber composition, paper is porous, enables passive liquid transport without the need of pumps and it is highly compatible with several types of reactions (Hu et al., 2014; Clegg, 1950; Lopez-Marzo and Merkoçi, 2016). Moreover, paper based analytical devices mimicking the origami art of paper folding are suitable alternatives for triggering the reactions catalyzed by specific enzymes during the folding (Liu et al., 2013). In 2012, Ge et al. developed a sandwich-type chemiluminescence immunoassay based on 3D origami device for the detection of tumor markers. This 3D origami-based immunodevice has the capability to separate the operational procedures into several steps including (i) folding pads above/below and (ii) addition of reagent/buffer under a specific sequence, showing excellent analytical performance for the simultaneous detection of four tumor markers (Ge et al., 2012). Very recently an origami-like paper-based electrochemical biosensor was developed

to detect mustard agent simulants, achieving limits of detection of 1 mM and 0.019 g min/m^3 for the targets in liquid and aerosol phase, respectively (Colozza et al., 2019).

Till now, the implementation of CL as detection technique in origami-paper based biosensors has been seldomly explored, with only few examples mostly relying on immunoassays (Ge et al., 2012; Liu et al., 2013). While several CL biosensors based on enzymatic reactions have been developed (Li et al., 2019; Chen et al., 2016; Jin et al., 2020; Yeh and Ai, 2019), till now there are no examples of implementation of coupled enzyme reactions with CL detection into foldable paper-based smartphone biosensors. This approach benefits from the high detectability of CL signals and simplicity of use deriving from easy folding of the paper, providing an instrument-free biosensor that only requires a smartphone for detection.

In this work we propose a foldable paper-based biosensor with CL detection based on the origami technique. This biosensor is based on the inhibition process of AChE by molecules such as OP pesticides, nerve gases and some drugs. As regards the CL reaction, AChE activity is measured through a series of coupled enzymatic reactions exploiting AChE, choline oxidase (ChOx) and horseradish peroxidase (HRP) leading to light emission. When AChE is inhibited, there is a decreased production of hydrogen peroxide, and consequently a reduction in light emission. An improved luminol substrate is also reported that provides improved sensitivity, possibly having broad applicability in CL-based biosensing.

3.2 Experimental section

3.2.1 Materials and chemicals

Acetylcholinesterase (AChE) from *Electrophorus electricus* (EC 3.1.1.7), choline oxidase (ChOx) from *Alcaligenes sp.* (EC 1.1.3.17), peroxidase (HRP) Type VI-A from horseradish (EC 1.11.1.7), acetylcholine (ACh) chloride and luminol sodium salt were provided by Sigma Aldrich, St. Louis, MO, USA. Stock solutions of the enzymes (AChE: 100 U/mL in 20 mM Tris-HCl buffer pH 7.5; ChOx: 20 U/mL in 10 mM Tris- HCl buffer pH 8.0 containing 2.0 mM EDTA and 134 mM KCl; HRP: 108 U/mL in 20 mM Tris-HCl buffer pH 7.5) were prepared and stored at - 20°C. Whatman 1 CHR cellulose chromatography paper from GE Healthcare (Chicago, IL, USA) was used for the origami paper-based analytical device. Commercial Reldan®22 insecticide containing 225 g/L of chlorpyrifos methyl was purchased from

Corteva Agriscience (Wilmington, DE, USA). SuperSignal ELISA Femto Maximum Sensitivity was provided by Thermo Scientific (Waltham, Massachusetts, USA).

3.2.2 Design and fabrication of the foldable paper biosensor

The foldable biosensor pattern (Fig. 3.1a) was designed using PowerPoint (Microsoft, Redmond, WA, USA) and printed onto the Whatman 1 CHR chromatography paper using a ColorQube 8570 office wax printer (Xerox, Norwalk, CT, USA). The biosensor consisted of four circular hydrophilic "wells" (diameter 5 mm), numbered from 1 to 4 according to the folding sequence, surrounded by hydrophobic areas. After printing, the waxed pattern was cured for 1 min at 100°C to allow wax to diffuse in the paper thickness to create the hydrophobic areas. Enzymes were then loaded in the biosensor by dispensing appropriate volumes of enzyme solutions in the wells (5 µL of a 100 U/mL AChE solution in well No.1, 15 µL of a 20 U/mL ChOx solution in well No. 2, and 15 µL of a 108 U/mL HRP solution in well No. 3). Finally, the biosensor was let drying for 30 min at 37°C.
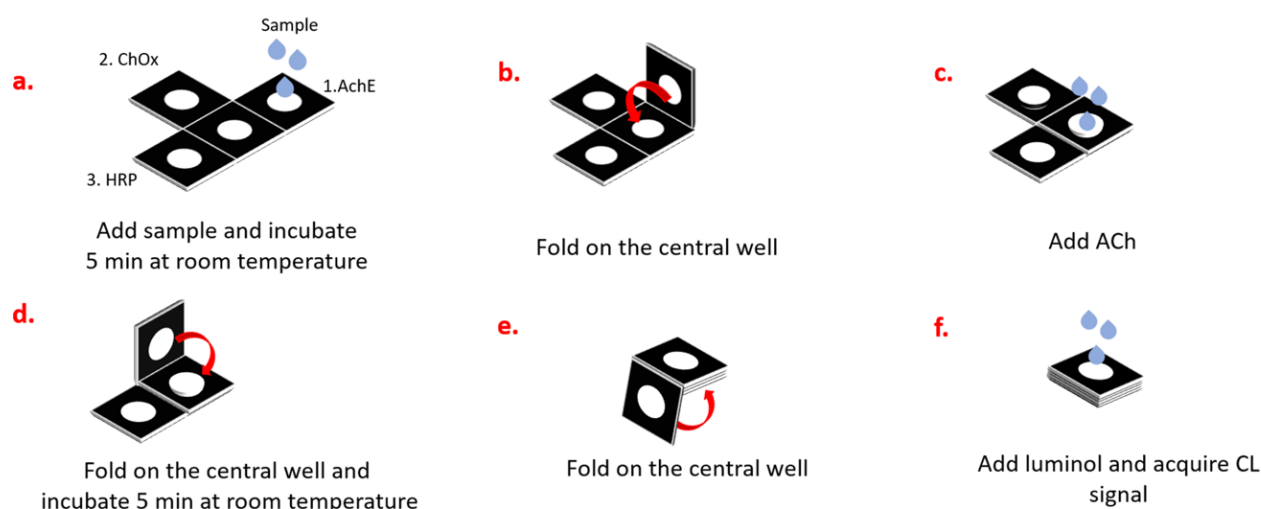

Fig. 3.1: *Schematic representation of the foldable paper-based biosensor and assay procedure.*

3.2.3 3D-printed analytical device

Accessories for performing the assay (i.e., a holder for the foldable paper biosensor and a mini dark box for CL imaging of the biosensor with a smartphone) were fabricated using a Replicator 2X 3D printer (Makerbot, Boston, MA, USA), which allows rapid prototyping of the device components by exploiting the Fused Deposition Modeling (FDM) technology.

Three-dimensional models of device components were created using the SketchUp Free browser-based 3D design platform (Trimble, Sunnyvale, CA, USA) and saved in the stereolithography file format (STL). Then the proprietary software MakerWare v.2.4 (Makerbot) was used for slicing the 3D models (i.e., converting the 3D models into a series of thin layers for printing) and producing a file (X3G) with the appropriate printing instructions for the 3D printer. All components were printed in black acrylonitrile-butadiene-styrene copolymer ("True Black" ABS, Makerbot) at 250-μm layer thickness, 10% infill.

The holder for the paper biosensor (Fig. 3.2c) consisted of two parts (Fig. 3.2d), which are held together by four N52 grade neodymium magnets (diameter 6 mm, thickness 2 mm), and was designed to keep the paper biosensor folded during the steps of the analytical procedure (Fig. 3.2e–f). Holes in the two parts of the holder allowed addition of luminol solution and imaging of the CL signal from the folded biosensor. The mini dark box comprised a slot for inserting the holder and an adapter for connecting a smartphone used as a portable light detector (Fig. 3.2a–b), thus allowing to perform measurements out-of-lab without any interference from ambient light. The distance between the holder and the smartphone (about 5 cm) was long enough to permit correct focusing of the biosensor by the smartphone camera. In our experiments, we used a OnePlus 6 smartphone (OnePlus, Shenzen, China), equipped with a dual integrated camera (primary sensor: 16 MP Sony Exmor RS IMX 519, BSI CMOS 1/2.600 color sensor with 1.22-μm pixels, f/1.7 aperture; secondary sensor: 20 MP Sony Exmor RS IMX 376K, BSI CMOS 1/2.800 color sensor with 1.0-μm pixels, f/1.7 aperture). Images were acquired using the secondary 20 MP camera. Experiments were also performed using as light detector an ATIK 383L camera (ATIK Cameras, Norwich, England) equipped with a thermoelectrically cooled CCD sensor (8.3 MP On Semiconductor (former Kodak) KAF-8300 Full Frame CCD 4/300 monochrome sensor, with 5.4-μm pixels) coupled with a Xenon 25 mm objective, f/0.95 aperture (Schneider-Kreuznach, Bad Kreuznach, Germany). In comparison with the smartphone, the higher sensitivity of the CCD camera allowed use of shorter exposure times, thus permitting a more precise characterization of the CL emission kinetics and/or detection of weak signals.
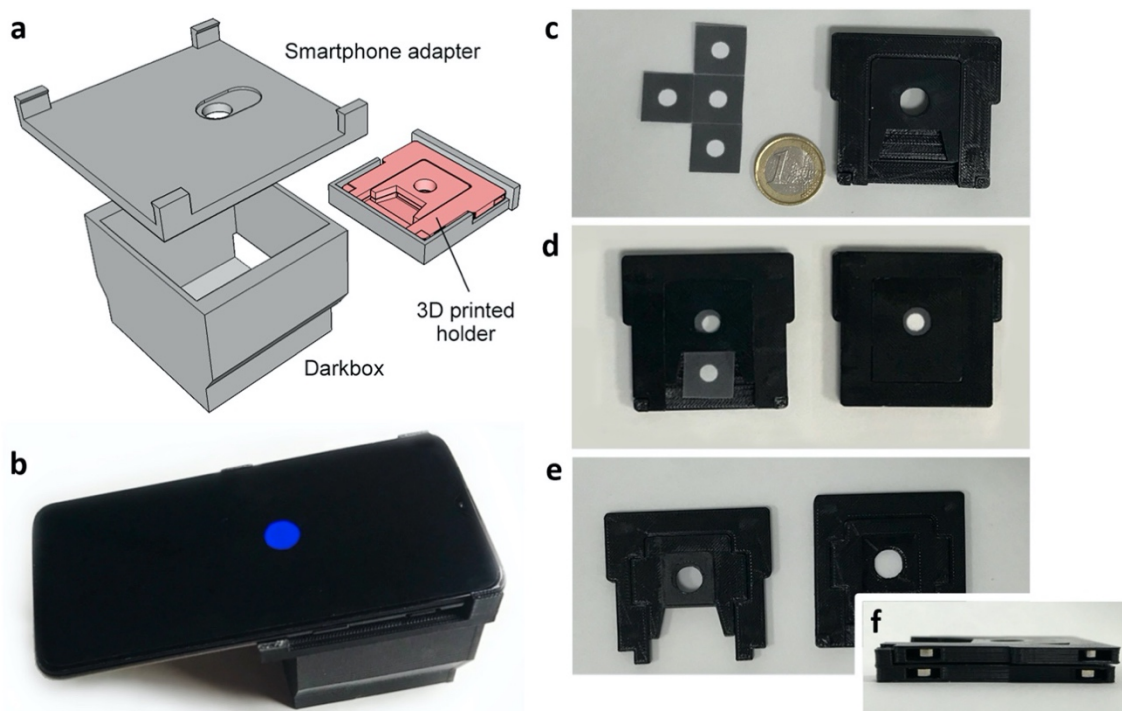
Fig. 3.2: *a) Schematic drawing of the device. b) Device connected to the One Plus 6 smartphone. c) Unfolded paper-based biosensor and 3D printed holder. d) The two parts composing the 3D printed holder; each part contains a 5-mm hole to enable addition of luminol solution and acquisition of the CL signal with the smartphone. e) 3D printed holder (top and bottom view) housing the paper-based biosensor. f) Detail of the assembled holder showing the N52 grade neodymium magnets designed to keep the paper biosensor folded.*

3.2.4 Assay procedure

The optimized analytical procedure for the evaluation of the activity of AChE inhibitors in a liquid sample is schematized in Fig. 3.1. First, a 10 µL-volume of sample is added to the well No. 1 of the biosensor (which contains the AChE enzyme) and pre-incubated for 5 min at room temperature so that inhibition of AChE takes place (Fig. 3.1a). After folding of well No. 1 on the central well (Fig. 3.1b) and addition of 10 µL of ACh solution (10 mM in deionized water) the AChE-catalyzed hydrolysis of ACh takes place (Fig. 3.1c). Then, the well No. 2 (which contains ChOx) is folded on the central well to activate the enzyme reactions leading to choline and then to hydrogen peroxide, and the partially folded biosensor is clamped by the 3D-printed biosensor holder (Fig. 3.1d). After a second 5-min incubation, the well No. 3 containing HRP is folded on under the already stacked wells to obtain the completely folded biosensor (Fig. 3.1e). After clamping the biosensor in the holder again, 20 µL of a 0.025 M luminol solution in NaOH (pH 12.0) are added to trigger the final HRP-catalyzed CL reaction

leading the production of the CL signal (Fig. 3.1f). The holder is then inserted in the mini dark box and after 10 min of incubation an image of the CL emission (30-sec exposure time, ISO 800 sensitivity) is acquired using the OnePlus 6 smartphone and saved as an RGB file. Quantitative analysis of the CL images was performed with the open source Image J software (v. 1.52s, National Institutes of Health, Bethesda, MD, USA). A circular region of interest (ROI) was defined in the correspondence of the biosensor well and the CL signal was evaluated by integrating the CL image intensity over the ROI area (since the maximum of the CL emission is at about 460 nm, integration was performed by considering only the blue channel of the RGB image). For all experiments, evaluation of AChE inhibition required two separate measurements, carried out either in the presence or in the absence of the inhibitor (in such case 10 μL of deionized water were used in the pre-incubation step). A blank experiment was also performed to measure the background CL signal by replacing the ACh solution with deionized water. All measurements were performed in triplicate and repeated at least three times. The AChE inhibition was then calculated from the CL signals as follows, where $CL_{inhibitor}$, $CL_{no\ inhibitor}$ and CL_{blank} represent the CL signals recorded in the presence and in the absence of the inhibitor and the CL background signal, respectively.

$$AChE\ inhibition\ (\%) = \frac{(CL_{no\ inhibitor} - CL_{blank}) - (CL_{inhibitor} - CL_{blank})}{(CL_{no\ inhibitor} - CL_{blank})} \times 100$$

For quantitative analysis, chlorpyrifos methyl concentrations were obtained by interpolating the AChE inhibition measured for the sample on a calibration curve generated by analyzing chlorpyrifos methyl solutions in the concentration range 0.01–10.0 mM and fitting the dose/inhibition graph with a four-parameter logistic equation.

3.2.5 Detection of AChE in spiked food matrices and recovery study

The applicability of the foldable biosensor to the analysis of complex samples was also evaluated by detecting chlorpyrifos methyl in spiked white cabbage juice. White cabbage was chopped with a mixer and 30 g were mixed with 50 mL of deionized water and under magnetic stirring for 1 h at room temperature (22°C). The cabbage mush was then centrifugated at 1000xg for 10 min and the supernatant was spiked with Reldan®22 to obtain white cabbage juice samples containing low (0.6 mM), medium (3.0 mM) and high (10.0 mM) concentrations of chlorpyrifos methyl. Spiked samples (10 μL) were then assayed with the foldable biosensor following the procedure previously described and the recovery of the

assay was evaluated by comparison between the measured and spiked chlorpyrifos methyl concentrations.
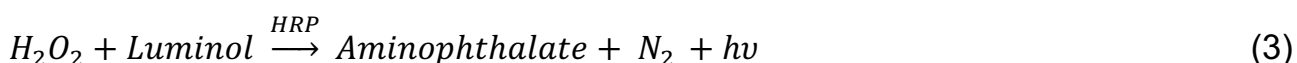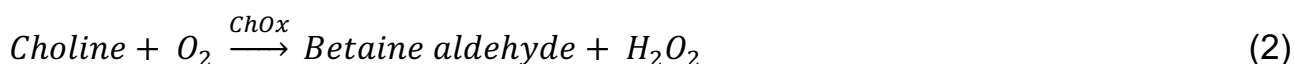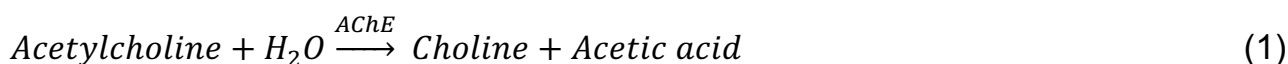
3.2.6 Biosensor stability evaluation

Stability of the paper-based biosensor was investigated by simulating different storage and shipment conditions. A series of biosensors were produced and vacuum-packed in plastic bags by employing a simple commercial vacuum machine used to preserve food. The biosensors were stored at different temperatures, i.e., room temperature (25°C), 4°C and –20°C. At different time points (up to 30 days) sets of three biosensors stored in different conditions were tested following the procedure reported in the section "Assay procedure". To assess biosensor stability, both the CL intensity in the absence of inhibitors and the AChE inhibition obtained in the presence of 3.0 mM chlorpyrifos methyl. The CL signals in the absence of the inhibitor and the AChE inhibitions measured in the presence of chlorpyrifos methyl were compared to those obtained at day 0, i.e., with newly produced biosensors.

3.3 Results and discussion

3.3.1 Design, fabrication and characterization of the foldable paper-based biosensor

The foldable paper-based CL biosensor allows detection of OP compounds by exploiting their capability to inhibit AChE, thus affecting the chain of coupled enzymatic reactions by decreasing the intensity of light emission:

$$Acetylcholine + H_2O \xrightarrow{AChE} Choline + Acetic\ acid \qquad (1)$$

$$Choline + O_2 \xrightarrow{ChOx} Betaine\ aldehyde + H_2O_2 \qquad (2)$$

$$H_2O_2 + Luminol \xrightarrow{HRP} Aminophthalate + N_2 + h\upsilon \qquad (3)$$

The use of cellulose chromatography paper (Whatman 1 CHR, having a pore size of 11 μm), on which wells were delimited by hydrophobic walls obtained by wax printing technique, permitted to obtain a ready-to-use biosensor containing the enzymes (AChE, ChOx, and HRP) required for the assay. Enzymes were loaded in the wells of the biosensor via adsorption by physical interactions with cellulose matrix, thus avoiding loss of catalytic activity (Hernandez and Fernandez-Lafuente, 2011; Hwang and Gu, 2013; Huang and Cheng, 2008). The values of pH of the enzyme solutions loaded in the biosensor were

selected to maintain the optimal activity for the enzymes (AChE and ChOx have an optimum activity at pH 7.0 and 8.0, respectively (Kano et al., 1994). Addition of sample and reagent solutions (ACh and luminol) and sequential folding of the biosensor allowed solubilization of the enzymes loaded in the biosensor and occurrence of the enzymatic reactions (Fig. 3.1), from preincubation of the sample with AChE to production of H_2O_2 by exploiting the reactions catalyzed by AChE and ChOx (reactions (1) and (2)). At the end, the biosensor was completely folded to obtain a single well in which the produced H_2O_2 was detected thanks to the HRP-catalyzed CL oxidation of luminol (reaction (3)).

3.3.2 Assay optimization

Several working conditions were optimized to improve the effectiveness of the foldable biosensor for measuring the AChE activity, including the diameter of the wells, the enzyme concentrations and the timing for the sequential folding to enable sequential reactions. Moreover, a luminol solution was optimized to improve CL signal detectability with the OnePlus 6 smartphone. As concerns the biosensor design, to ensure adequate enzyme loadings two different well sizes were tested (diameter of 5 and 8 mm). A 5-mm diameter was selected for the wells since it provided a uniform CL signal. Conversely, the use of 8-mm diameter wells did not allow a uniform reaction distribution, as confirmed by the detection of CL signal only in the peripheral region of the well (Fig. 3.3).
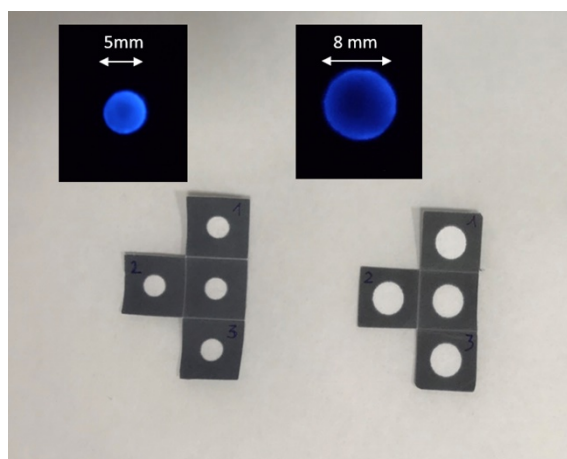

Fig. 3.3: *Paper-based biosensors designed with 5-mm (left) and 8-mm (right) diameter wells and CL signals obtained with paper-based biosensors with adequate enzymes loading (AChE, ChOx and HRP) in 5-mm and 8-mm diameter wells. In optimized experimental conditions CL signals were obtained with OnePlus6 smartphone (30 s, ISO 800) after 10 minutes of substrate reaction.*

Different concentrations of enzymes loaded in the biosensor (AChE from 0.5 to 1 U/well, ChOx from 0.3 to 0.6 U/well, HRP from 0.16 to 1.62 U/well) as well as of ACh (from 0.01 to 10.0 mM) were tested keeping all other factors constant (Fig. 3.4). This enabled to identify the conditions providing the best compromise between low reagent loading and high CL signal, thus providing a cost-effective yet sensitive tool for detection of AChE inhibitors. Higher AChE, ChOx and HRP enzyme concentrations led to a small increase in the CL emission intensity but also to higher limit of detection (LOD) of AChE inhibitors, thus the lowest enzyme concentrations were used in the assay.
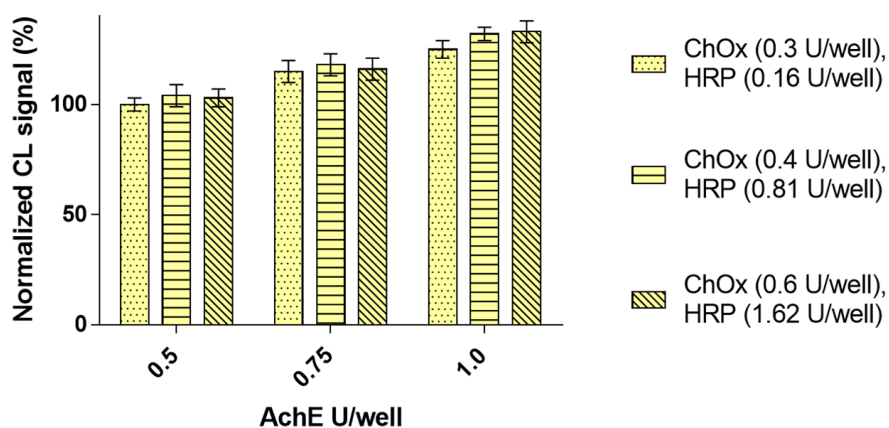

Fig. 3.4: *Optimization of the paper-based biosensors with different enzyme loadings: AChE (0.5, 0.75 and 1.0 U/well) with different concentrations of ChOx and HRP (0.3 and 0.16 U/well, 0.4 and 0.81 U/well and 0.6 and 1.62 U/well, respectively). CL signals were measured with the OnePlus6 smartphone (30 s, ISO 800) 10 minutes after the complete folding of the biosensor. Results are normalized to the signal obtained in the optimal experimental conditions (AChE 0.5 U/well, ChOx 0.3 U/well, HRP 0.16 U/well)*

To obtain a CL signal easily detectable with the smartphone-integrated CMOS camera, the effect of luminol substrate formulation on the CL emission was also studied. The commercial SuperSignal ELISA Femto Maximum Sensitivity luminol-based HRP CL substrate, which contains proprietary enhancers that improve CL emission intensity, was tested as well as home-made luminol solutions at different pH (i.e., 0.025 M luminol solutions in deionized water and NaOH solutions at pH 10.0 and pH 12.0). Indeed, the pH of the luminol solution should be a compromise between the optimal pH for HRP activity (the highest peroxidase activity is in the pH interval 6.0–7.0) and that for the luminol CL reaction (which is stronger at alkaline pH). To select the optimal substrate formulation and the most suitable time window for CL measurement, the CL emission in the absence of AChE inhibitors was

monitored for 30 min after the addition of luminol substrates. As shown in Fig. 3.5a, thanks to the presence of the enhancers the commercial luminol substrate provided the highest CL signal. However, despite the high signal, the fast emission kinetics drastically reduced the time window for CL signal acquisition. The strict time control required for CL measurement made such substrate not suitable for reproducible smartphone-based detection (indeed, the peak of the CL emission was not actually recorded with the OnePlus 6 smartphone). Conversely, 0.025 M luminol both in deionized water and in NaOH solution pH 10.0 showed weak CL signals, which were hardly detectable with the OnePlus 6 CMOS camera. The luminol solution in NaOH at pH 12.0 proved the most suitable for smartphone-based measurement: even though the CL signal intensity was lower than obtained with the SuperSignal ELISA Femto substrate, the CL emission was still easily detectable by the smartphone and it showed a glow-type kinetics. Indeed, the CL signal remained almost constant between 10 and 20 min after the addition of the substrate, thus facilitating the measurement. In accordance to the CL signal kinetics, all CL measurements were performed 10 min after the addition of the luminol substrate.
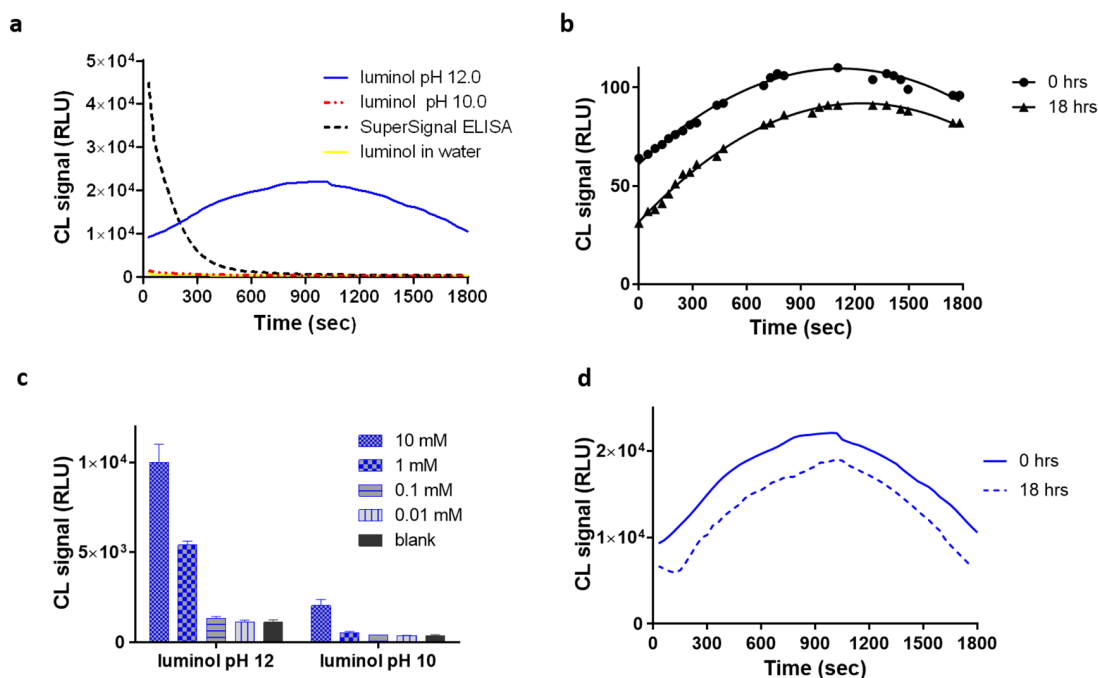

Fig. 3.5: *a) CL emission kinetics of the paper-based biosensor obtained with four different substrates (the commercial SuperSignal ELISA Femto substrate and 0.025 M luminol in water and in NaOH solutions at pH 10.0 and pH 12.0). CL measurements were performed with CCD ATIK 383L-camera*

integrating CL signals for 30 s at room temperature. b) Optimization of the incubation time (from 0 to 15 min) of ACh (10 mM) with the AChE and ChOx previously adsorbed on the paper biosensor. CL emission kinetics were obtained with CCD ATIK 383L-camera integrating CL signals (30 s at room temperature) after the addition of luminol solution at pH 12.0; c) Dose-response curves for ACh obtained with the paper-based biosensor (concentration range 0.01–10.0 mM). CL measurements were performed with ATIK 383L CCD (integration time of 30-sec at room temperature) after 10 min of the addition of home-made luminol pH 12.0 and normal luminol pH 10.0; d) Comparison of CL emission kinetics obtained with the paper-based biosensor without storage (0 h) and after 18 h storage at room temperature using a CCD ATIK 383L-camera (CL signal integration of 30 s at room temperature).

It should be noted that the selected pH value is higher than the optimal pH value reported in the literature for the luminol/H_2O_2/HRP system (between pH 9.5 and pH 10.0 according to Khan et al., 2014), but the discrepancy could be due to the partial neutralization of NaOH by the buffers loaded into the biosensor with the AChE and ChOx enzyme solutions. Once selected the optimal experimental conditions for performing H_2O_2 detection with the smartphone camera, we optimized the incubation time of ACh with AChE and ChOx. As shown in Fig. 3.5b, CL signals were proportional to the reaction time up to 15 min, but their intensities remained in the same order of magnitude. As the best compromise in terms of detectability of the CL signal with the smartphone and time-saving analysis, a reaction time of 5 min was selected.

As a performance test of the foldable paper biosensor, we obtained a dose-response curve for ACh. To this end, 10 µL-volumes of ACh solutions (concentration range 0.01–10.0 mM) were analyzed in triplicate with the foldable biosensor and the CL measurements were performed with the ATIK 383L CCD camera, using both luminol solutions at pH 10.0 and pH 12.0. Fig. 3.5c illustrates CL signals obtained with different ACh dilutions, showing as expected stronger CL signals with the luminol solution in NaOH pH 12.0, thus confirming the suitability of this luminol solution for smartphone-based detection. By using the latter luminol solution, a LOD for ACh, calculated as 3 times the standard deviation of the blank (deionized H_2O), of 160 µM was obtained.

3.3.3 Evaluation of AChE inhibition

To prove the suitability of the biosensor to evaluate AChE inhibition, a simulated inhibition experiment was performed by measuring the CL signal obtained from biosensors in which decreasing amounts of AChE (starting from 0.5 U/well, i.e., the concentration used in the biosensor) were loaded in the biosensor. The experiments were performed in the optimized

experimental conditions without AChE inhibitor (replaced by deionized H_2O) and the CL signal was correlated to the amount of AChE in the biosensor. As shown in Fig. 3.6a, the intensity of the CL signal showed a linear correlation with the amount of AChE, thus suggesting that comparison of the CL signals obtained in the presence and in the absence of an inhibitor allowed to estimate the AChE inhibition (indeed, the relative decrease of the CL signal represented the actual inhibition of AChE). Considering the reproducibility of the CL measurements, it can be assumed that AChE inhibitions as low as 15% could be reliably detected with the developed foldable biosensor.
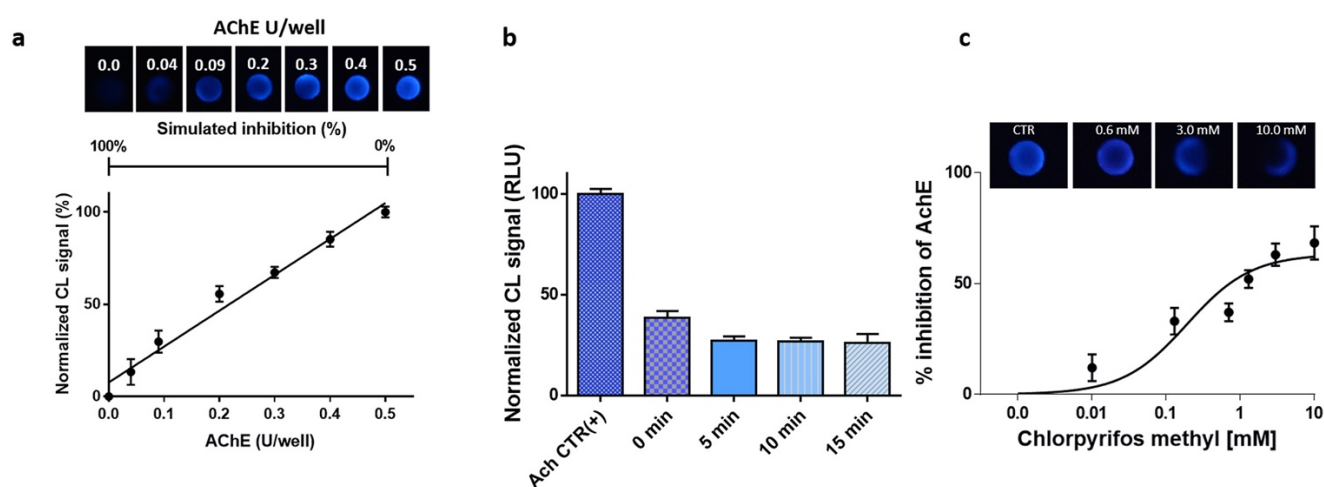

Fig. 3.6: *a) Simulated inhibition curve performed by measuring the CL signal obtained with paper-based biosensors in which decreasing amounts of AChE (from 0.5 U to 0.04 U) were previously adsorbed in well No. 1. In optimized experimental conditions CL signals were obtained with OnePlus6 smartphone (ISO 800, 30 s) after 10 min of substrate reaction and analyzed with ImageJ Software; b) Optimization of the pre-incubation time with the OP with the paper-based biosensor. Several incubation times (0, 5, 10, and 15 min) of chlorpyrifos-methyl (3.0 mM) were evaluated with the origamiPAD biosensor and CL measurement were performed with CCD ATIK 383L-camera integrating CL signals for 30 s at room temperature after 10 min of luminol solution at pH 12.0. The obtained CL signals were compared with the control, without pesticide (10 µL of water solution); c) Chlorpyrifos-methyl inhibition curve obtained with the foldable biosensor testing a concentration range of Reldan® 22 suggested by the manufacturer (concentration range of chlorpyrifos-methyl from 0.01 to 10 mM in deionized water). CL images corresponding to the Chlorpyrifos-methyl inhibition curve were obtained acquiring CL signals with Oneplus 6 camera after 10 min of substrate reaction (ISO 800, 30 s) and analyzed with ImageJ Software.*

3.3.4 Detection of AChE inhibitors

The suitability of the smartphone-based foldable biosensor to detect AChE irreversible inhibitors was investigated using chlorpyrifos methyl as a model OP pesticide able to irreversibly inhibit AChE. Chlorpyrifos methyl is an OP pesticide commonly used in

agriculture, for which exposure may occur either directly or via the food chain. Several commercial pesticides contain chlorpyrifos methyl, including Reldan®22, a broad-spectrum insecticide for control of insects and mites containing 225 g/L of chlorpyrifos methyl.

To obtain a calibration curve suitable for quantitative analysis of chlorpyrifos methyl, spiked Reldan®22 solutions in water corresponding to chlorpyrifos methyl concentrations, in the range 0.01–10.0 mM, were analyzed using the procedure described in section "Analytical procedure". As stated before, because we correlated the concentration of OP compounds with the decrease of the biosensor response upon enzyme inhibition, each experiment was conducted by comparing the CL signals obtained in the presence and in the absence of the inhibitor.

Before generating the dose-response curve, the incubation time of the biosensor with the sample was optimized by analyzing an intermediate concentration sample (3.0 mM chlorpyrifos methyl) after different incubation times with AChE and comparing the CL signals with that obtained from the control without pesticide (10 µL of deionized water). As shown in Fig. 3.6b, the irreversible inhibition by the pesticide is almost immediate and the decrease in the CL signal reached a constant value upon only 5 min of incubation. This incubation time was thus used in the subsequent experiments.

Fig. 3.6c showed representative CL images obtained for the various chlorpyrifos methyl concentrations and the corresponding dose-response curve generated as reported in Section 2.4. According to the dose-response curve, the LOD for chlorpyrifos methyl was 45.0 µM. When compared to other biosensors for OP detection relying on amperometric and potentiometric detection (Pundir and Malik, 2019), our CL paper-based biosensor provided a higher LOD. In fact, reported limits of detection ranged from µM to sub-nM for different OPs; however, it must be pointed out that the smartphone-based biosensor is intended to be a low-cost device to be used without any specialized laboratory instrumentation. In the last five years CL has been used as detection technique for a limited number of smartphone-based biosensors, mainly for nucleic acid and immunosensors (Ghosh et al., 2020; Kalligosfyri et al., 2019). To the best of our knowledge this is the first CL enzyme paper-based smartphone-integrated biosensor. In comparison with a previously reported CL enzyme smartphone biosensor for lactate that provided LOD at the mM level (Roda et al., 2014b), we were able to significantly improve detectability, thus confirming that this

approach is suitable for smartphone-based sensing, although its full potential has yet to be reached.

As additional feature, this paper-based "green biosensor" can be easily produced in any laboratory (only an office wax printer is required) in a sustainable way and disposed after use without safety concerns. Most importantly, the foldable paper biosensor is highly versatile, and, by proper selection of the loaded enzymes, it could be easily repurposed to obtain low-cost disposable cartridges for detecting analytes in a rapid and simple way.

3.3.5 Recovery in spiked samples

To investigate potential matrix effects and evaluate the performance of the developed foldable biosensor for detection of pesticides in real samples, a recovery study was carried out on a vegetable sample (i.e., white cabbage juice). White cabbage juice samples were spiked with Reldan® 22 at three different chlorpyrifos-methyl concentrations (0.6, 3.0 and 10.0 mM) and analyzed with the foldable biosensor. The recovery values for chlorpyrifos methyl (Table 3.1) were in the range 92%– 99%, thus suggesting a low matrix effect and further confirming the suitability of the proposed biosensor for real sample analysis. Conversely, no OPs were detected in blank white cabbage juice.

Added (mM)	Found (mM)	Recovery (%)	RDS (%)
0.00	*n.d.*	*n.d.*	*n.d.*
0.60	0.59±0.04	95	1
3.00	2.72±0.03	99	3
10.00	9.73±0.05	92	6

Table 3.1: *Recovery of chlorpyrifos methyl in white cabbage juice (n = 3). n.d.: not detectable*

3.3.6 Biosensor precision and stability

Different figures of merit of the biosensor including repeatability, reproducibility and stability and were studied. As concerns the repeatability, a relative standard deviation (RSD, n 1⁄4 5) of 9.8% was obtained for biosensors produced in the same day and used for detecting an intermediate concentration (3.0 mM) of chlorpyrifos-methyl. Conversely, a reproducibility (RSD, n = 5) of 13.2% was obtained by analyzing the same sample in consecutive days

using biosensors produced in the same day and maintained until use in the optimal storage conditions (see below).

As concerns biosensor stability, Fig. 3.7b shows the CL signals measured for biosensors vacuum-packed in plastic bags and stored at different temperatures (22 °C, 4 °C and - 20 °C) and for different periods of time (up to 30 days). The measurements were performed in the optimized experimental conditions without any AChE inhibitor and, for reference, the CL signals have been normalized to the value obtained immediately after the production of the biosensors. Storage of the bio- sensors at room temperature (22 °C) or at 4 °C resulted in a decrease of the CL signal, which is reasonably due to a loss of enzyme activity. After 48 h at room temperature the loss of the CL signal was 35 ± 5%, while a smaller, but still significant, reduction (20 ± 6%) was observed during storage at + 4 °C. After one week the decreases of the CL signals were 61 ± 3% and 19 ± 4% at room temperature and 4 °C, respectively. Conversely, storage at -20 °C proved suitable for long-term storage of the biosensors since after 30 days we observed a decrease of the CL signal of only 2-3%. Additionally, the overall kinetics of the CL emission remained unchanged upon storage at - 20 °C for up to 30 days.
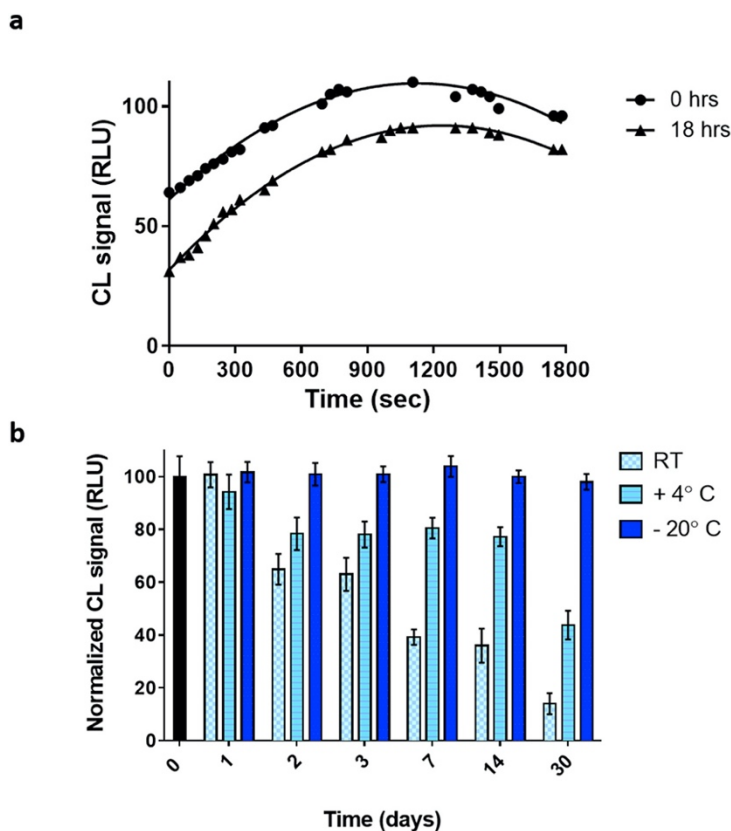
Fig. 3.7: *a) Comparison of CL emission kinetics of the paper-based biosensor obtained with the biosensor without storage (0 h) and after 18 h storage at room temperature. CL measurements were performed using the maximum performance settings of OnePlus6 smartphone (30 s, ISO 800) and CL images were elaborated by ImageJ Software; b) Stability of the paper-based biosensor stored at room temperature (23 °C), +4 °C and −20 °C. Each indicated day (from 0 to 30 days), triplicate paper-based biosensors were tested following the procedure reported in the section "Assay procedure". CL measurements were obtained with OnePlus 6 (30 s at ISO 800) and analyzed with ImageJ software. CL signals are normalized with respect to day 0.*

Short-term stability at room temperature was also investigated to confirm that the biosensor remained useable for a reasonable time after unpacking. As shown in Fig. 3.7a the catalytic activity of the enzymes, as well as the overall kinetics of the CL emission, were maintained stable after up to 18 h of storage of the unpacked biosensor at 22°C, with a decrease of the CL signal of 20 ± 3%. These results support the fact, if adequately refrigerate, that the biosensor has an adequate shelf-life to allow storage and shipping.

3.4 Conclusions

We presented a foldable CL paper biosensor that capitalizes on well-established assays based on enzyme inhibition, sensitive CL detection relying on luminol/ H_2O_2/HRP system, foldable paper biosensors and the possibility to use the smartphone integrated CMOS as light detector. We integrated for the first time these concepts to provide a CL biosensor that enables a very rapid and straightforward analysis of compounds inhibiting AChE, by exploiting coupled enzymatic reactions involving AChE, ChOx and HRP and an improved luminol solution as the CL substrate. The biosensor here described allows the measurement of the AChE inhibitory activity in very short times (less than 30 min) using small volumes of samples and, thanks to high intensity of the CL signal, enables smartphone-based detection. Thanks to the 3D printing technology, biosensor's housing interfacing with smartphone is straightforward and different smartphone adaptors can be easily designed and produced according to various smartphone models. Biosensor validation was performed using chlorpyrifos methyl and spiked cabbage juice samples, showing its potential applicability to rapidly detect the presence of OP pesticides along the food chain. Moreover, the developed biosensor could be applied to replace currently employed colorimetric papers used to rapidly detect nerve agents and OP insecticides.

3.5 Acknowledgements

3.6 References

Ahmed, N.Y., Knowles, R., Dehorter, N., 2019. Front. Mol. Neurosci. 12, 204. Andreani, A., Burnelli, S., Granaiola, M., Guardigli, M., Leoni, A., Locatelli, A., Morigi, R., Rambaldi, M., Rizzoli, M., Varoli, L., Roda, A., 2008. Eur. J. Med. Chem. 43, 657–661.

Andreani, A., Granaiola, M., Guardigli, M., Leoni, A., Locatelli, A., Morigi, R., Rambaldi, M., Roda, A., 2005. Eur. J. Med. Chem. 40, 1331–1334.

Arduini, F., Amine, A., Moscone, D., Palleschi, G., 2010. Microsc. Acta 170, 193–214. Arduini, F., Cinti, S., Caratelli, V., Amendola, L., Palleschi, G., Moscone, D., 2019. Biosens. Bioelectron. 126, 346–354.

Calabretta, M.M., Álvarez-Diduk, R., Michelini, E., Roda, A., Merkoçi, A., 2020. Biosens. Bioelectron. 150, 111902.

Capoferri, D., Della Pelle, F., Del Carlo, M., Compagnone, D., 2018. Foods 7, 148. Cevenini, L., Calabretta, M.M., Lopreside, A., Tarantino, G., Tassoni, A., Ferri, M., Roda, A., Michelini, E., 2016. Anal. Bioanal. Chem. 408, 8859–8868.

Chang, J., Li, H., Hou, T., Li, F., 2016. Biosens. Bioelectron. 86, 971–977.

Chen, Z., Tan, Y., Xu, K., Zhang, L., Qiu, B., Guo, L., Lin, Z., Chen, G., 2016. Biosens. Bioelectron. 75, 8–14.

Cinti, S., 2019. Anal. Bioanal. Chem. 411, 4303–4311.

Clegg, D.L., 1950. Anal. Chem. 22, 48–59.

Colovic, M.B., Krstic, D.Z., Lazarevic-Pasti, T.D., Bondzic, A.M., Vasic, V.M., 2013. Curr. Neuropharmacol. 11, 315–335.

Colozza, N., Kehe, K., Dionisi, G., Popp, T., Tsoutsoulopoulos, A., Steinritz, D., Moscone, D., Arduini, F., 2019. Biosens. Bioelectron. 129, 15–23.

Cui, H.F., Zhang, T.T., Lv, Q.Y., Song, X., Zhai, X.J., Wang, G.G., 2019. Biosens. Bioelectron. 141, 111452.

Del Carlo, M., Mascini, M., Pepe, A., Compagnone, D., Mascini, M., 2002. J. Agric. Food Chem. 50, 7206–7210.

Deng, Y., Zhang, Y., Lu, Y., Zhao, Y., Ren, H., 2016. Sci. Total Environ. 544, 507–514. Devi, D.L., 2012. Burkhard. R., J. Justin gooding 2 and edith chow 1. Sensors 12 (9), 11505–11526.

Garlito, B., Ibáñez, M., Portolés, T., Serrano, R., Amlund, H., Lundebye, A.K., Sanden, M., Berntssen, M.H.G., Hernández, F., 2019. Anal. Bioanal. Chem. 411, 7281–7291.

Ge, L., Wang, S., Song, X., Ge, S., Yu, J., 2012. Lab Chip 12, 3150–3158.

Ghosh, S., Aggarwal, K., Vinitha, T.U., Nguyen, T., Han, J., Ahn, C.H., 2020. Microsyst & Nanoeng, 6-5.

Guardigli, M., Pasini, P., Mirasoli, M., Leoni, A., Andreani, A., Roda, A., 2005. Anal. Chim. Acta 535, 139–144.

Guilbault, G.G., Kramer, D.N., Cannon Jr., P.L., 1962. Anal. Chem. 34, 1437–1439. Hernandez, K., Fernandez-Lafuente, R., 2011. Enzym. Microb. Technol. 48, 107–122.

https://ec.europa.eu/food/plant/pesticides/approval_active_substances/chlorpyrifos_chlorpyrifos-methyl_en.

Hu, J., Wang, S., Wang, L., Li, F., Pingguan-Murphy, B., Lu, T.J., Xu, F., 2014. Biosens. Bioelectron. 54, 585–597.

Huang, L., Cheng, Z.M., 2008. Chem. Eng. J. 144, 103–109.

Huang, S., Yao, J., Chu, X., Liu, Y., Xiao, Q., Zhang, Y., 2019. J. Agric. Food Chem. 67, 11244–11255.

Huang, X., Xu, D., Chen, J., Liu, J., Li, Y., Song, J., Ma, X., Guo, J., 2018. Analyst 143, 5339–5351.

Hwang, E.T., Gu, M.B., 2013. Eng. Life Sci. 13, 49–61.

Jin, L., Hao, Z., Zheng, Q., Chen, H., Zhu, L., Wang, C., Liu, X., Lu, C., 2020. Anal. Chim. Acta 1100, 215–224.

Kalligosfyri, P.M., Sevastou, A., Kyriakou, I.K., Tragoulias, S.S., Kalogianni, D.P., Christopoulos, T.K., 2019. Anal. Chim. Acta 1088, 123–130.

Kano, K., Morikage, K., Uno, B., Esaka, Y., Goto, M., 1994. Anal. Chim. Acta 299, 69–74. Khan, P., Idrees, D., Moxley, M.A., Corbett, J.A., Ahmad, F., von Figura, G., Sly, W.S.,

Waheed, A., Hassan, M.I., 2014. Appl. Biochem. Biotechnol. 173, 333–355.

Li, F., Liu, J., Guo, L., Wang, J., Zhang, K., He, J., Cui, H., 2019. Biosens. Bioelectron. 141, 111472.

Liana, D.D., Raguse, B., Gooding, J.J., Chow, E., 2012. Sensors 12, 11505–11526. Liang, B., Han, L., 2020. Biosens. Bioelectron. 148, 111825.

Liu, W., Cassano, C.L., Xu, X., Fan, Z.H., 2013. Anal. Chem. 85, 10270–10276.

Liu, X., Li, X., Gao, X., Ge, L., Sun, X., Li, F., 2019. ACS Appl. Mater. Interfaces 11, 15381–15388.

López-Marzo, A.M., Merkoçi, A., 2016. Lab Chip 16, 3150–3176.

Martinez, A.W., Phillips, S.T., Whitesides, G.M., Carrilho, E., 2010. Anal. Chem. 82 (1), 3–10.

Meredith, N.A., Quinn, C., Cate, D.M., Reilly, T.H., Volckens, J., Henry, C.S., 2016. Analyst 141, 1874–1887.

Patel, S., Sangeeta, S., 2019. ESPR 26, 91–100.

Pundir, C.S., Malik, A., 2019. Biosens. Bioelectron. 111348.

Roda, A., Calabretta, M.M., Calabria, D., Caliceti, C., Cevenini, L., Lopreside, A., Zangheri, M., 2017. Smartphone-based biosensors. In: Comprehensive Analytical Chemistry, Past, Present and Future Challenges of Biosensors and Bioanalytical Tools in Analytical Chemistry: A Tribute to Professor Marco Mascini, pp. 237–286.

Roda, A., Guardigli, M., Calabria, D., Calabretta, M.M., Cevenini, L., Michelini, E., 2014b. Analyst 139, 6494–6501.

Roda, A., Michelini, E., Cevenini, L., Calabria, D., Calabretta, M.M., Simoni, P., 2014a. Anal. Chem. 86, 7299–7304.

Roda, A., Michelini, E., Zangheri, M., Di Fusco, M., Calabria, D., Simoni, P., 2016. TrAC Trends Anal. Chem. (Reference Ed.) 79, 317–325.

Roda, A., Rauch, P., Ferri, E., Girotti, S., Ghini, S., Carrea, G., Bovara, R., 1994. Anal. Chim. Acta 294, 35–42.

Samsidar, A., Siddiquee, S., Shaarani, S.M., 2018. Trends Food Sci. Technol. 71, 188–201.

Uniyal, S., Sharma, R.K., 2018. Biosens. Bioelectron. 116, 37–50.

Yao, T., Liu, A., Liu, Y., Wei, M., Wei, W., Liu, S., 2019. Biosens. Bioelectron. 145, 111705.

Yeh, H.W., Ai, H.W., 2019. Annu. Rev. Anal. Chem. 12, 129–150.

Zangheri, M., Cevenini, L., Anfossi, L., Baggiani, C., Simoni, P., Di Nardo, F., Roda, A., 2015. Biosens. Bioelectron. 64, 63–68.

4

Ultrasensitive On-Field Luminescence Detection Using a Low-Cost Silicon Photomultiplier Device

4.1 Introduction

In recent years, with the increasing necessity to perform rapid, cheap, and sensitive on-site detection of different analytes such as environmental pollutants, pathogens, and food contaminants, researchers have sought to develop new bioanalytical tools and new portable detectors. This urgency stems from different areas spanning diagnostics to food safety and quality control, environmental monitoring, and forensic fields (Ouyang et al., 2021; Ligler and Gooding, 2019; de Araujo et al., 2018). A number of portable devices and biosensors have been reported; however, most of them are currently at the prototype stage, and very few reached the market, with glucose sensors and adenosine triphosphate (ATP) detection devices dominating the landscape (Turasan and Kokini, 2021; Hernández-Neuta et al., 2019; Cesewski and Johnson, 2020; Viator et al., 2017). Among main bottlenecks that hamper commercialization and use of these devices for real life applications, the relatively high cost, inadequate sensitivity when applied to real samples, and difficulty of interfacing with electronics are surely some of the main factors (Turner, 2013). Different optical detection techniques have been implemented in portable analytical devices, including fluorescence, bio-chemiluminescence (BL-CL), and colorimetric detection (Tsai et al., 2015; Zhou et al., 2021; Wang et al., 2021; Lopreside et al., 2019).

BL-CL presents significant advantages especially in terms of sensitivity, low cost, and ease of integration with miniaturized systems (Love and Prescher, 2020; Wang et al., 2020). Different portable light detectors have been exploited to detect BL-CL signals, including photomultipliers (PMT), charge-coupled devices (CCDs), complementary metal oxide semiconductor (CMOS) sensors, and smartphone-integrated CMOS (Rodrigues and Lapa, 2010; Chen et al., 2021; Cevenini et al., 2016b; Lopreside et al., 2019; Cevenini et al., 2018). Due to their high efficiency, PMTs are the most used detectors. However, the PMT technology has relevant drawbacks, such as intrinsic complexity and fragility, high energy consumption and requirement of high voltages (Li et al., 2020). Portable CCD and CMOS showed feasible alternatives for both bioluminescence (BL) and chemiluminescence (CL). In the last years smartphone-integrated sensors (CMOS) showed suitable to replace other portable detectors, including CCDs and CMOS (Sevastou et al., 2020; Montali et al., 2020; Calabretta et al., 2020). Silicon photomultipliers (SiPMs) have also been proposed as sensitive light detectors for BL (Li et al., 2012; Jung et al., 2020). SiPMs are arrays of avalanche photodetectors working in Geiger mode (GM-APDs), each one having integrated passive-quenching resistor and connected in parallel (Gola et al. 2019). Due to their high

quantum efficiency, low energy and bias voltage requirements, and rapid fast response time (in nanosecond time scale), SiPMs have attracted significant interest for various applications, providing in some cases better performance than smartphones (Li et al., 2012; Jung et al., 2020; Gola et al. 2019; Ruffinatti et al., 2020).

Despite jeopardized efforts, there is no clear evidence about the selection of the most suitable light detector for implementation into portable devices and scaled-up deployments. This choice in fact should consider not only the sensitivity but also the cost, ruggedness, and ease of integration. In the present study we evaluated the implementation of BL- CL reactions in a SiPM device and performed a side-by-side comparison of its performance with other portable light detectors that showed very good performance in previous works. We selected as model analytes a green emitting *P. pyralis* firefly luciferase mutant Ppy-GR-TS (λ_{max} 550 nm) (Branchini et al., 2007) and the blue-emitting NanoLuc luciferase (λ_{max} 460 nm) (Biewenga et al., 2020). The SiPM device outperformed other portable detectors, providing adequate sensitivity for detecting low light intensities and making it suitable for on-site and forensic applications. As a proof-of-concept application, a CL origami sensing paper for the rapid detection of organophosphorus (OP) pesticides was implemented in the device to assess its analytical performance.
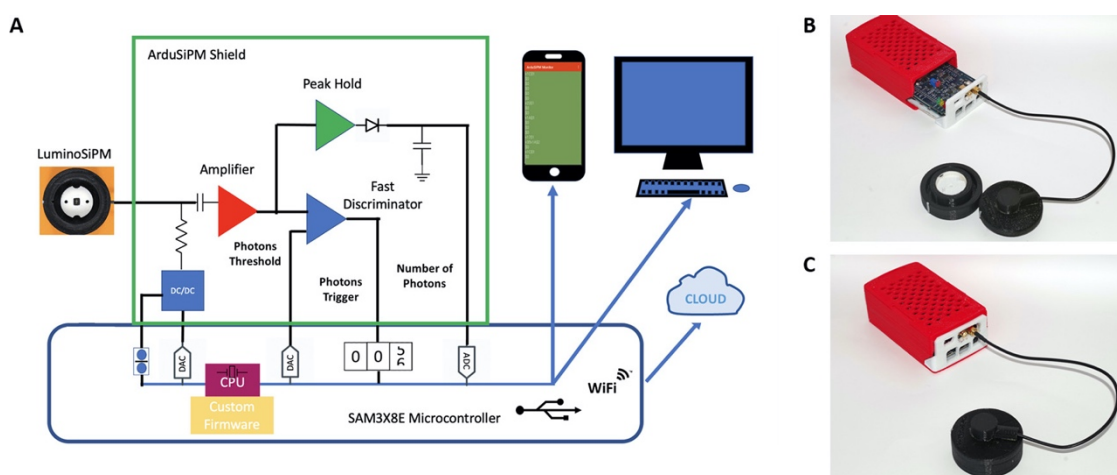

Fig. 4.1: *(A) ArduSiPM block diagram composed by the dark box with SiPM and temperature sensors, an internal digital controlled DC-DC converter as voltage supply, a voltage amplifier, a fast discriminator with programmable threshold, a peak hold circuit for pulse amplitude, LEDs for monitoring; all outputs from analog circuit and digital controls are connected to the Arduino DUE board. (B) ArduSiPM (red-white box) connected to LuminoSiPM dark box (black cell) ready for sample addition and (C) closed for acquisition.*

4.2 Experimental section

4.2.1 Reagents

E. coli competent cells (JM109) for plasmid propagation and SOC medium (tryptone 20g/L, yeast extract 5 g/L, NaCl 5M 2 mL/L, KCl 1.0 M 2,5 mL/L, MgCl$_2$ 1.0 M 10mL/L, MgSO$_4$ 1.0 M 1 0 mL/L, D-Glucose 1.0 M 20 mL/L) were from Sigma (St. Louis, MO, USA), *E. coli* competent cells (BL21) for protein expression were from Agilent Technologies (Santa Clara, USA). Luria-Bertani (LB) medium and LB-Agar plates used for cell cultures were prepared with Select Agar and LB (Lennox L Broth) from Sigma (St. Louis, MO, USA) added with ampicillin (1 µg/mL). All media and materials were autoclaved for 20 minutes at 121°C. Expression plasmids, kits for plasmid extraction and purification, BrightGlo and NanoGlo substrates were from Promega (Madison, WI, USA). Enzymes required for cloning were from Fermentas (Vilnius, Lithuania). B-PER^{TM} Bacterial Protein Extraction Reagent was from Thermo Scientific (Rockford, USA). Protino Ni-IDA Resin and 14 mL Protino Columns required for protein extraction were purchased from MACHEREY-NAGEL GmbH & Co. (Düren, Germany). Microcon 30K device used for protein concentration and buffer exchange was purchased from Merck Millipore Ltd. (Tullagreen, Carrigtwohill, Co. Cork, IRL). Acetylcholinesterase (AChE) from *Electrophorus electricus* (EC 3.1.1.7), choline oxidase (ChOx) from *Alcaligenes sp.* (EC 1.1.3.17), peroxidase (HRP) Type VI-A from horseradish (EC 1.11.1.7), acetylcholine (ACh) chloride, luminol sodium salt and all other chemicals were purchased from Sigma (St. Louis, MO, USA).

4.2.2 LuminoSiPM Fabrication and 3D printed dark box

The LuminoSiPM device is composed of a SiPM sensor (Hamamatsu MPPC 13360-1325CS) read by means of the ArduSiPM system (Bocci et al., 2014; Kim and Paulmurugan, 2020) integrated in a portable case and designed with FreeCAD software. It is able to accommodate in its inner cavity different types of disposable sample holders for hosting biospecific reactions (Fig. 4.1 and Fig. 4.2). In particular, a previously developed ArduSiPM board, the first all-in-one system for SiPM in literature, was selected as a compact data acquisition system for SiPM sensor with low-power consumption. ArduSiPM uses SAM3X8E 32-bit ARM® Cortex-M3 CPU as processor unit, an open hardware/software development board, that contains all circuits to acquire analog and digital signals and, if programmed with suitable firmware, can output processed data (Ligler and Gooding, 2019; de Araujo et al., 2018, Turasan and Kokini, 2021). The detector can measure the relative time of occurrence

of each photon burst, the number of occurrences within a specified acquisition window (one second as default), and the intensity of each blinking with single photon precision. The Hamamatsu MPPC 13360-1325CS SiPM sensor was used. This sensor contains a sensitive matrix of 2668 GM-APD cells with a pixel pitch of 25 μm, an active photosensitive area of 1.3 x 1.3 mm and a fill factor of 47%. The sensor is protected by a silicon resin window and has a spectral response in the visible region, with a declared maximum photon detection efficiency (PDE) at 450 nm of 25%. The typical driving voltage is around of 50-60 V. The operative voltage (Vop), defined as Vbreak down + 5V, is 56.45 V, with a leakage current "Id" (the intrinsic current which flows when the sensor is in the dark) of 0.013 μA at 25 °C.
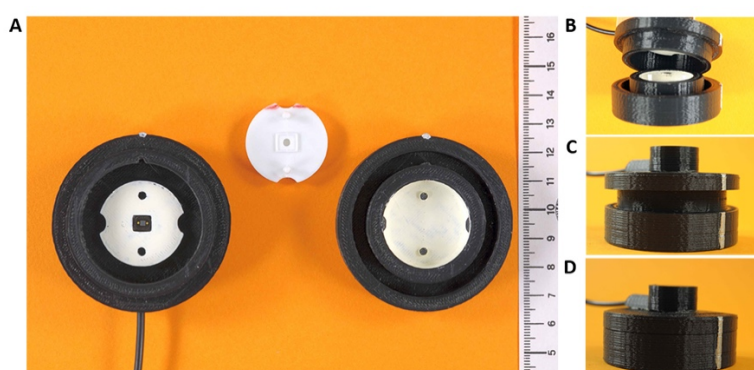

Fig. 4.2: *(A) The three components of LuminoSiPM dark box. (B) The assembly of sample holder in the dark box. (C) Mechanical protrusions and complementary alignment holes guarantee light tightness. (D) The box closed and ready for measurement.*

The two parts of LuminoSiPM dark box were fabricated with a 3D printer (3DiELLE - ver. L) using thermoplastic black polylactic acid (PLA) polymer to shield from environmental light both sensor and sample holder. Sample-holder cartridges, designed in different versions according to the analysis format, were printed in PLA and in UV 405 nm sensitive resin, using an Anycubic Photon 3D printer (Anycubic Shenzhen, China). For measurements with liquid samples, a central cylindrical well was designed (radius 1.75 mm, height 3.0 mm, inner volume about 30 μL) (Fig. 4.2). A sample-holder with an inner, square cavity (19 x 19 mm) was 3D printed in UV sensitive resin, to accommodate the foldable paper disposable device.

The sample holder was fabricated with stereolithography 3D printing, providing, when compared to components printed with PLA, better resolution and reduced surface porosity, thus preventing liquid leakage. The complete polymeric composition insulated the sensor contacts operating at a static voltage of around 56 V. To simplify the use of the device and reduce issues related to incorrect positioning of removable sample holders in the box, specific reference points were included with custom mechanical protrusions (pins height 5.5

mm, diameter 1.15 mm) and complementary alignment holes in the box parts and in sample holders (Fig. 4.2). This ensured that, when the LuminoSiPM dark box was operative, samples were always placed in the same position, in front of the detector, at about 1.5 mm from the sensitive surface.

4.2.3 Preliminary dark count rate evaluation

To select the most suitable instrumental condition, especially regarding the dark (thermal) noise, two series of 5 min signals acquisitions were performed, with the sensor shielded from light and varying gradually the discriminator threshold admittance in the range 3.39 - 4.57 mV. Measures were repeated at two different temperature conditions: series "A" between 24 - 26 °C, Series "B" between 26 - 28 °C (Fig. 4.3).
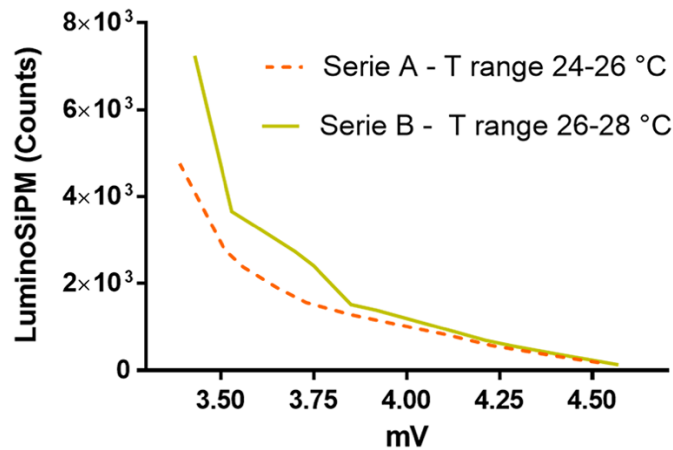

Fig. 4.3: *Series of SiPM Dark Noise acquisitions: Series A measurements acquired at room temperature range 24-26 °C (dotted line); Series B measurements acquired at room temperature range 26-28 °C (solid line).*

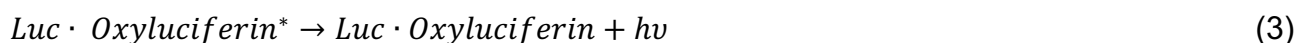### 4.2.4 LuminoSiPM signal acquisition and data treatment

The ArduSiPM is an all-in-one detector that processes the SiPM signal independently using customized firmware and shows all measurements about the events directly throughout a serial interface. For an improved treatment of BL-CL signal acquisition, a specific Microsoft Windows software was used (https://ardusipm.filippocurti.it/download). In all measurements, the sensor's signal was acquired for 5 min with data sampling cycles of 1 s. A total of 300 numerical acquisitions were recorded in the form of counts per second (cps) for any single experiment and stored in CSV format.

4.2.5 Evaluation of LuminoSipM analytical performance in detecting bioluminescence and comparison with other portable light detectors and benchtop instrumentation

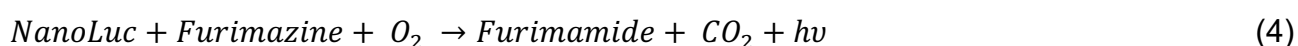To investigate the suitability of LuminoSipM to detect low light intensities of BL reactions, two luciferases PpyGR-TS and NanoLuc (Branchini et al., 2007; Biewenga et al., 2020) were purified as previously described by Cesewski and Johnson. (Cesewski and Johnson, 2020). Briefly, a 6-histidine sequence and a spacer (GCGHHHHHH) were fused with the C-terminal of NanoLuc and PpyGR-TS luciferases via standard Polymerase Chain Reaction (PCR) technique. PCR products were subsequently inserted into pGex-6P-2 plasmid using BamHI and NotI for high protein expression in *E. coli* strain BL21. Protein purification was performed using whole cell extracts after 4 h incubation with isopropyl β-D-1-thiogalactopyranoside (IPTG) 0.1 mM at 25°C, with Protino Ni-IDA Resin according to the manufacturer's instructions. Cell extract was obtained using a cell-lysis-extraction buffer consisted of B-PER^{TM} Reagent (from Thermo Scientific, Rockford, USA), Lysozyme (0.1 mg/mL) and phenylmethylsulfonyl fluoride (10 µM), incubated for 20 min, on ice. Proteins were purified using Protino Ni-IDA Resin and LEW Buffer as solution. LEW Buffer pH 8.0 was prepared using NaCl 300 mM and NaH$_2$PO$_4$ 50 mM. LEW Buffer plus Imidazole 250 mM and glycerol 2% was used for protein elution and storages (at 4 °C). Protein concentrations were determined with the Bradford Reagent from Sigma (St. Louis, MO, USA) using bovine serum albumin (BSA) as standard. Protein purification yields were ~5 mg/0.25 L culture for both the luciferases.

A 5 µL volume of purified protein solution (concentration range from 1.0 to $1.0×10^{-6}$ mg/mL) was dispensed in the sample holder cartridge shown in Fig. 4.2, and BL acquisition was performed after addition of 10 µL of BL substrate, i.e., BrightGlo and NanoGlo substrates (Promega) for PpyGR-TS and NanoLuc, respectively. Acquisitions with LuminoSipM were performed for 5 min with data sampling cycles of 1 s. Comparative studies were performed with different portable light detectors, including a Oneplus 6 smartphone (Oneplus, Shenzhen, China) equipped with an integrated dual camera (16 MP Sony Exmor IMX 519 sensor and F1.7 aperture +20 MP Sony Exmor IMX 376 K sensor and F1.7 aperture) and a portable CCD camera (ATIK 383L+ mono cromo CCD) equipped with a high-resolution monochrome CCD sensor (Kodak KAF 8300, sensor size 17.96 × 13.52 mm). The limit of detection (LOD) was calculated as the blank plus three times the standard deviation.

The sensitivity, dynamic range, and linearity of the system response were assessed using luciferin-luciferase solutions containing all substrates and cofactors required for the firefly luciferase BL reaction:

$$Luc + LH_2 + ATP \overset{Mg^{2+}}{\longleftrightarrow} Luc \cdot LH_2 - AMP + Ppi \tag{1}$$

$$Luc \cdot LH_2 - AMP + O_2 \rightarrow Luc \cdot Oxyluciferin^* + AMP + CO_2 \tag{2}$$

$$Luc \cdot Oxyluciferin^* \rightarrow Luc \cdot Oxyluciferin + hv \tag{3}$$

and for the NanoLuc-catalyzed BL reaction:

$$NanoLuc + Furimazine + O_2 \rightarrow Furimamide + CO_2 + hv \tag{4}$$
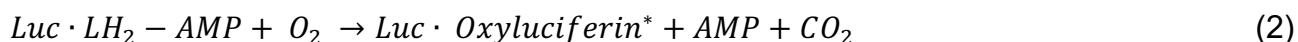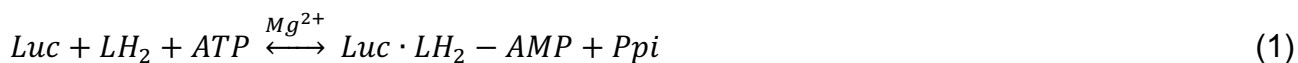
BL measurements obtained with ATIK 383L+ monochrome CCD were performed integrating BL signals for 5 min at +25°C (room temperature). For BL measurements performed with Oneplus 6 smartphone, images were taken for 30 sec with different sensitivity settings, from ISO 100 to ISO 3200. Images were elaborated with ImageJ software (National Institutes of Health, Bethesda, MD) to quantify the signal over the sample spot area and expressed as relative light units (RLUs). GraphPad Prism v.5 software (GraphPad Software, La Jolla, USA) was used to analyze data.

Limit of Detection (LOD) was calculated as the blank signal plus three times the standard deviation. All measurements were performed in triplicate for each concentration tested and repeated at least three times with the same disposable sample-holder cartridge used for LuminoSiPM. A standard benchtop luminometer Varioskan Flash multimode reader (ThermoFisher Scientific) was used for characterization of the purified PpyGR-TS and Nanoluc luciferases. BL emission spectra (350–700 nm) and kinetics (30 min, 300 ms integration time) were obtained with a black 384-well microtiter plate after the addition of a 5 μL-volume of 0.1 mg/mL purified protein solution and 10 μL of BL substrate (BrightGlo substrate for PpyGR-TS and NanoGLo for NanoLuc) (Fig. 4.4). Calibration curves of PpyGR-TS and NanoLuc luciferases were also obtained with the Varioskan Flash multimode reader (Fig. 4.5).

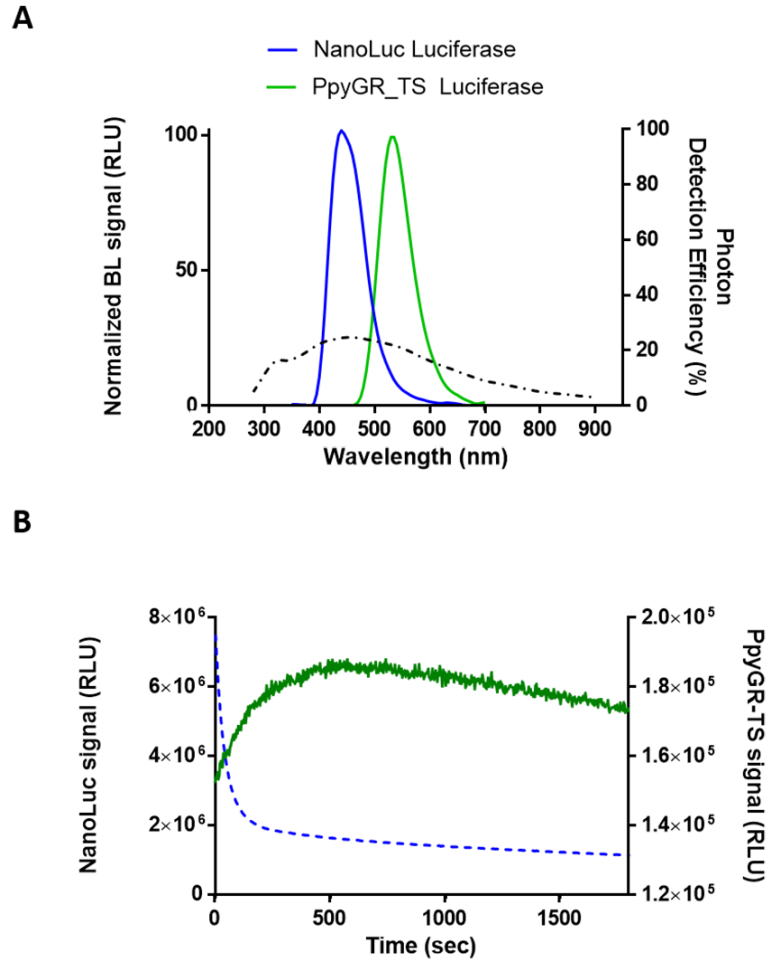**Fig. 4.4:** *(A) Normalized emission spectra of NanoLuc and PpyGR-TS luciferases with the photon detection efficiency of the Hamamatsu MPPC 13360-1325CS SiPM Sensor (dash dotted line); (B) Emission kinetics of NanoLuc (dashed blue line) and PpyGR-TS (solid green line).*
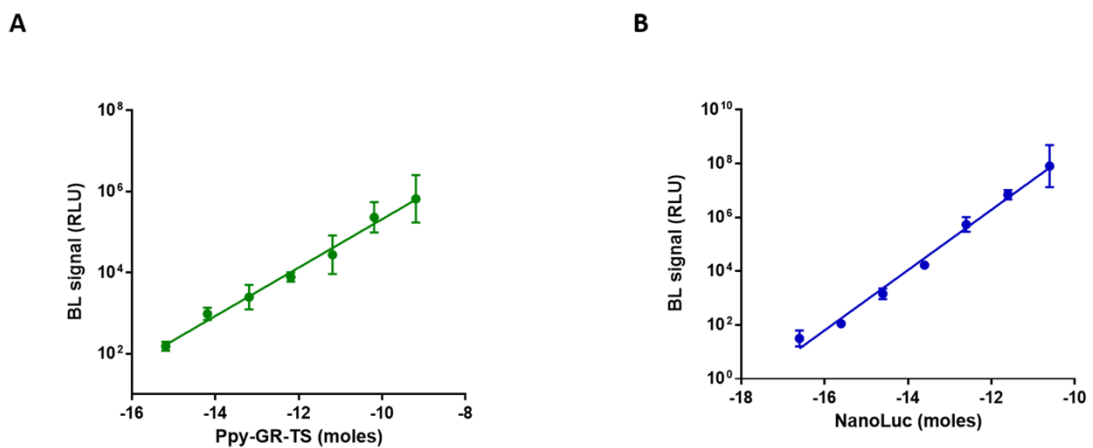

Fig. 4.5: *Calibration curves of PpyGR-TS (A) and Nanoluc (B) luciferases obtained with the Varioskan Flash multimode reader.*

4.2.6 LuminoSiPM-Based Detection of Acetylcholinesterase (AChE) Inhibitors with a Chemiluminescent Origami Sensing Paper: Analytical Procedure

An origami sensing paper previously described (Montali et al., 2020) was modified to fit the LuminoSiPM and the analytical procedure adapted. The sensing paper consisted of four circular hydrophilic "wells" with a diameter of 5 mm, surrounded by hydrophobic areas obtained by wax printing. The enzymes, i.e, AChE, choline oxidase (ChOx), and horseradish peroxidase (HRP), were loaded in the wells of the sensing paper via physical adsorption with cellulose matrix.

The origami sensing paper, composed by Whatman 1 CHR cellulose chromatography paper from GE Healthcare (Chicago, IL, USA) was designed using PowerPoint (Microsoft, Redmond, WA, USA) and printed using a ColorQube 8570 office wax printer (Xerox, Norwalk, CT, USA). The origami sensing paper consisted of four circular hydrophilic "wells" (diameter 5 mm), numbered from 1 to 4 according to the folding sequence, surrounded by hydrophobic areas. The internal 3D-wax structure confining wells was obtained through a heating process for 2 min at 84°C. Acetylcholinesterase (AChE) from *Electrophorus electricus*, choline oxidase (ChOx) from *Alcaligenes sp.*, peroxidase (HRP) Type VI-A from horseradish were then loaded in the origami sensing paper by dispensing appropriate volumes of enzyme solutions in the wells (5 µL of a 100 U/mL AChE solution in well No.1, 15µL of a 20U/mL ChOx solution in well No.2, and 15 µL of a 108 U/mL HRP solution in well No. 3). Finally, the origami sensing paper was let drying for 30 min at 37°C. A 0.025 M luminol solution in NaOH at pH 12.0 was used as substrate for the chemiluminescent reaction.

The analytical procedure consists in addition of a 10 µL-volume of sample to well No. 1 (which contains AChE) and pre-incubation at room temperature for 5 minutes. After folding of well No. 1 on the central well, a 10 µL-volume of ACh solution (10 mM) is added and ACh hydrolysis occurs. Then, well No. 2 (which contains ChOx) is folded on the central well leading to production of choline and then to hydrogen peroxide. After 5-min incubation, well No. 3, containing HRP, is folded on the central well to obtain the completely folded paper. The biosensor is clamped into the sample holder (Fig. 4.6) and a 20 µL-volume of 0.025 M luminol in NaOH (pH 12.0) is added to trigger HRP-catalyzed CL reaction leading to the production of CL signal. The sample holder is then inserted in the LuminoSiPM dark box

and then, after 10 min of incubation, closed with the other section of the dark box (which supports the sensor) to acquire the CL signal.
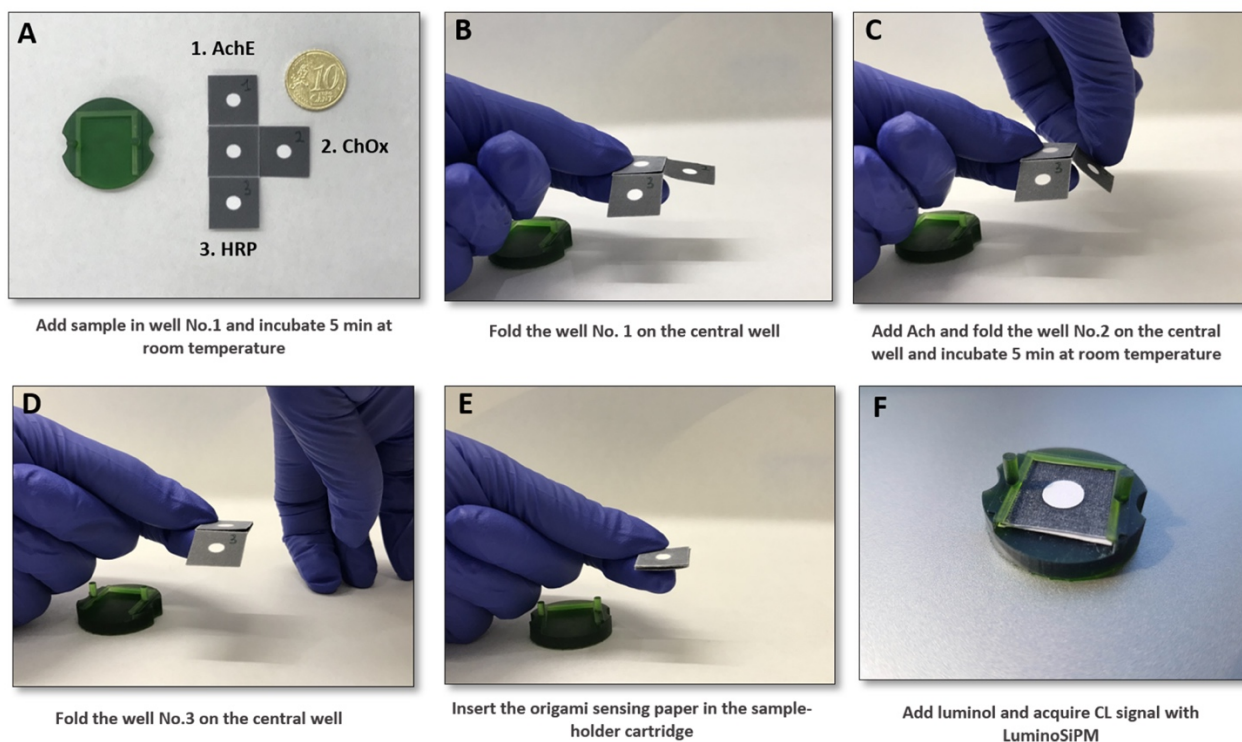

Fig. 4.6: *Schematic representation of the foldable origami sensing paper biosensor and assay procedure.*

For all experiments, two separate measurements were performed with the same LuminoSiPM settings described in previous section to assess AChE inhibition either in the presence or in the absence of the inhibitor (in this case 10 μL of deionized water were used in the pre-incubation step). All measurements were performed in triplicate and repeated at least three times. Calibration curves for chlorpyrifos-methyl were obtained by analyzing with the origami sensor and LuminoSiPM device chlorpyrifos methyl solutions in the concentration range 1.0×10^{-4} – 10.0 mM and fitting the dose/inhibition graph with a four-parameter logistic equation.

The optimized analytical procedure to evaluate the activity of AChE inhibitors in a liquid sample is shown in Figure 4.6. A 10 μL-volume spiked Reldan®22 solution in water corresponding to chlorpyrifos methyl (concentrations range 0.0001 – 10.0 mM) was added to the well No. 1 of the origami sensing paper (which contains the AChE enzyme) and let to incubated for 5 minutes at room temperature so that inhibition of AChE takes place (Fig.

4.6A). After folding of well No. 1 on the central well (Fig. 4.6B) and addition of 10 µL of ACh solution (10 mM in deionized water) the AChE-catalyzed hydrolysis of ACh takes place. Then, the well No. 2 (which contains ChOx) is folded on the central well to activate the enzyme reactions leading to choline and then to hydrogen peroxide, and the partially folded origami sensing paper is clamped by the 3D-printed sample-holder cartridge (Fig. 4.63C). After a second 5-min incubation, the well No. 3 containing HRP is folded on under the already stacked wells to obtain the completely folded origami sensing paper (Fig. 4.6D-E). After clamping the biosensor in the holder again, 20 µL of a 0.025 M luminol solution in NaOH (pH 12.0) are added to trigger the final HRP-catalyzed CL reaction leading the production of the CL signal (Fig. 4.6F). The sample-holder cartridge is then inserted in the LuminoSiPM dark box and after 10 min of incubation, closed with the other section of the dark box (which supports the sensor) to acquire the CL signal for 5 min.

4.3 Results and discussion

4.3.1 LuminoSiPM Device Fabrication

A compact and portable device, called LuminoSiPM, was developed with the aim of exploiting SiPM technology to measure the photons produced by BL-CL systems as an alternative to more explored portable light detectors. To provide an all-in-one device, a removable plastic box was 3D printed to encase the ArduSiPM and enable easy inspections on functionality and operative conditions (Fig. 4.1B, C). The LuminoSiPM cell was connected to the signal inlet of ArduSiPM (SMA connector); data acquired were transferred in real-time to a PC via the ArduSiPM USB port for data storing and software treatment. Electric power was supplied by the PC USB port (5 V, current max 0.5 A) (Fig. 4.1A).

In SiPM sensors, increasing the operating voltage improves photon detection but produces a significant increase in noise components in terms of dark count and crosstalk. Nevertheless, the Hamamatsu SiPMs S13360 series, as declared by the company, has a reduced noise increase when operating voltage is increased. This is highly advantageous for detecting low-light signals similar to those generated by BL-CL reactions because the signal gain can reach the 1×10^6 limit in terms of photoelectrons' amplification, a value comparable with PMT's response. Improvement in material and design technology permitted reduction of dark counts down the Mcps threshold (range from 70 to 210 Kcps at 25 °C). As

concerns the LuminoSiPM data output, they are available as ASCII format through an RS232 serial interface with maximum speed of 115 200 Baud. Therefore, data can be easily acquired using high integrated computer platforms such as smartphone, Raspberry Pi, or simple microcontroller devices like M5Stack. These properties support the suitability of LuminoSiPM as a portable photometric instrument for operation in the field, even in uncontrolled settings.

4.3.2 Optimization of SiPM Sensor Driving Parameters

The original use of ArduSiPM was coupled with a scintillator in a radiation detector. In this application, the threshold usually adopted is in the range of five photoelectrons. This value provides a dark count near to zero cps suitable for rare, yet intense signals produced when an ionizing particle hits the scintillator and yields a few-nanosecond burst of photons. Conversely, for BL detection, reactions lead to a continuous emission of photons. With a threshold of five photons, the detector does not count events when there is an emission of one, two, three, or four photons in a microsecond-scale window. Therefore, considering the typical photon generation of BL reactions, a threshold of about 2−3 photoelectrons was selected. With a two-photoelectron threshold, a composed dark count of a few hundreds of cps was obtained. Although this threshold did not allow the detector to reach the physical limit of one photoelectron, it was still suitable to measure very low light intensities as BL-CL signals with a good signal-to-noise ratio (SNR) even at room temperature. A series of measurements was performed to identify the optimal conditions to achieve the highest SNR. After the preamplification stage of the SiPM signal, a photoelectron corresponded to a voltage of about 2.0 mV. Dark noise optimization was achieved by varying the threshold with 0.1 mV increments in the range of 3.39 − 4.57 mV. Measurement sessions were performed at 25 ± 1°C (A series) and 27 ± 1°C (B series) with the sensor blinded in a time window of 5 min to avoid the contribution of temperature drift. Besides an expected temperature dependence, a significant noise increase was observed with variation of a few millivolts, highlighting the threshold mechanism of the process (Fig. 4.3). The optimal threshold was in the range of 3.55−3.60 mV, corresponding to two photons hitting the sensor with an integrated noise between 2300 and 1900 Hz (cps). Below the 3.0 mV threshold (1.5 photoelectron equivalent), the dark count increased rapidly up to tens of thousands of cps. A lower threshold value produced an abrupt increase both in the absolute number of counts and in the occurrence of multiple pulses of noise. The bias voltage was set at 3.60 mV to

maximize sensor sensitivity while keeping acceptable dark noise figures (approximately 2000 spurious counts in 5 min acquisition at 25 °C).

4.3.3 Evaluation of LuminoSiPM Performance and Comparison with Other Light Detectors

To assess the feasibility of employing LuminoSiPM as a light detector for low light intensities, we first compared the sensitivity of the system in detecting BL emitted by purified luciferase solutions. A blue emitting luciferase (NanoLuc) and a green emitting luciferase variant of the *P. pyralis* luciferase (Ppy-GR-TS) having λ max at 460 (half bandwidth 70 nm) and 548 nm (half bandwidth 66 nm), respectively, were selected as models of BL emission (Fig. 4.4). We obtained calibration curves for the two luciferases (in the range 1 pg μL^{-1} to 1 μg μL^{-1}) employing either D-luciferin/ATP/Mg$_2^+$ or furimazine substrates, respectively. A LOD of 4.2×10^{-8} M, corresponding to 2.1×10^{-13} moles, and a LOD of 1.7×10^{-10} M, corresponding to 8.7×10^{-16} moles, were obtained for Ppy-GR-TS luciferase and NanoLuc luciferase, respectively. We compared the LODs and linear range with those obtained with a benchtop luminometer, a portable CCD camera (ATIK 383L+), and CMOS-smartphone integrated sensors (OnePlus6). Both the selected CCD camera and the CMOS-smartphone sensors previously demonstrated their suitability as portable light sensors for BL and CL assays (Montali et al., 2020; Calabretta et al., 2020). The OnePlus smartphone-integrated CMOS was reported to be the best performing smartphone-integrated sensor by Kim et al., who performed a comparison with five different types of smartphones and reported that best results were achieved by OnePlus One (Kim et al., 2017). Figure 4.7 shows concentration−response curves obtained with the three portable light detectors (ATIK 383L+, OnePlus 6 smartphone, and SiPM sensor).
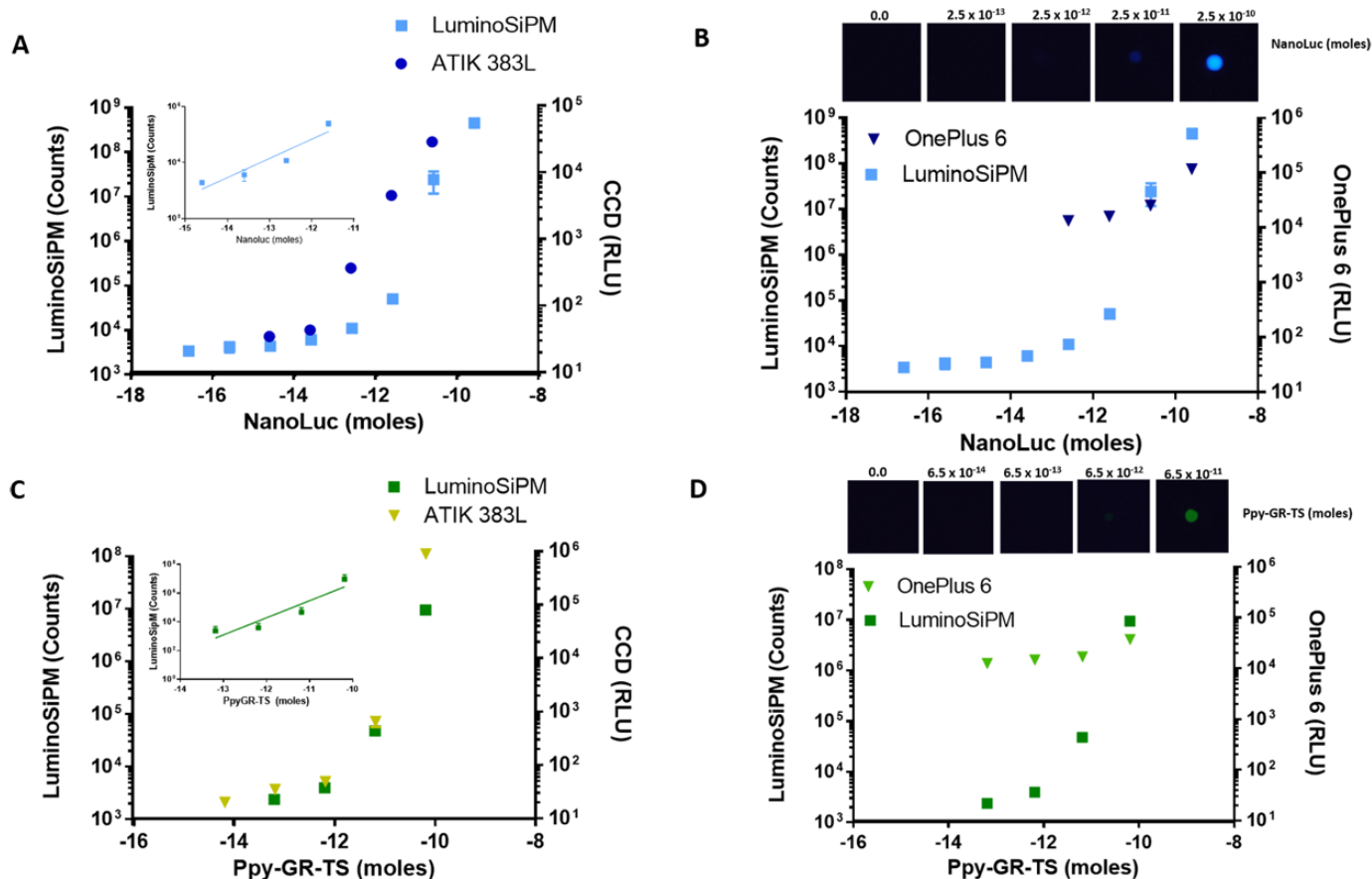
Fig. 4.7: *Calibration curves for Nanoluc and PpyGR-TS obtained with the LuminoSiPM, Oneplus 6, and CCD camera. (A) Calibration curve for NanoLuc and (C) PpyGR-TS obtained with the LuminoSipM and CCD camera. (B) Calibration curve for NanoLuc and (D) PpyGR-TS obtained with the LuminoSipM and OnePlus 6 smartphone. Representative images obtained with the Oneplus6 are also shown.*

Calibration curves obtained with a benchtop luminometer, used as reference instrumentation, provided an LOD of 4.3×10^{-10} M (2.1×10^{-15} moles) and an LOD of 6.4×10^{-11} M (3.2×10^{-16} moles) for PpyGR-TS and NanoLuc luciferases, respectively (Fig. 4.5). The calculated LODs for Ppy-GR-TS and NanoLuc were one and two orders of magnitude lower, respectively, than those obtained with the CCD ATIK 383L. This unexpected result was only partially explained by the high sensitivity of the SiPM sensor at the wavelengths of the NanoLuc emission spectrum (quantum efficiency of 25% at 450 nm) (https://www.hamamatsu.com/resources/pdf/ssd/s13360_ series_kapd1052e.pdf) because reported quantum efficiency of the KAF-8300 sensor of the ATIK 383L+ camera shows a similar behavior, reaching about 45% efficiency at 450 nm according to data sheet values (Hampf et al., 2020). In addition, the sensing area of the KAF-8300 sensor is 243 mm^2, while the sensing area of LuminoSiPM is only 1.69 mm^2.

As concerns results obtained with the OnePlus6 CMOS-integrated sensors, LODs of 1.3×10^{-6} M (6.5×10^{-12} moles) and of 2.5×10^{-8} M (corresponding to 1.3×10^{-13} moles) were obtained for PpyGR-TS and NanoLuc, respectively (Fig. 4.7B, D). These values were one and three orders of magnitude higher, respectively, than the LODs obtained with the LuminoSiPM. As concerns the linear range, LuminoSiPM was able to maintain a linear correlation between concentration and photon counts in the concentration range of 4.2×10^{-7} to 1.3×10^{-5} M for PpyGR-TS ($R^2 = 0.8666$) and for NanoLuc of 3.6×10^{-9} to 5.0×10^{-7} M ($R^2 = 0.8887$) (Fig. 4.7A, C). More details are shown in Table 4.1.

	PpyGR-TS LOD	NanoLuc LOD	PpyGR-TS LINEAR RANGE	NanoLuc LINEAR RANGE
LuminoSiPM	2.1×10^{-13} moles (4.2×10^{-8} M)	8.7×10^{-16} moles (1.7×10^{-10} M)	$2.1 \times 10^{-12} - 6.5 \times 10^{-11}$ moles ($4.2 \times 10^{-7} - 1.3 \times 10^{-5}$ M)	$1.8 \times 10^{-14} - 2.5 \times 10^{-12}$ moles ($3.6 \times 10^{-9} - 5.0 \times 10^{-7}$ M)
ATIK 383L+	7.0×10^{-13} moles (1.4×10^{-7} M)	2.2×10^{-14} moles (4.3×10^{-9} M)	$3.0 \times 10^{-12} - 6.5 \times 10^{-11}$ moles ($6.0 \times 10^{-7} - 1.3 \times 10^{-5}$ M)	$3.8 \times 10^{-14} - 2.5 \times 10^{-11}$ moles ($5.0 \times 10^{-6} - 7.6 \times 10^{-9}$ M)
OnePlus6 Smartphone	6.5×10^{-12} moles (1.3×10^{-6} M)	1.3×10^{-13} moles (2.5×10^{-8} M)	n.d.	$6.5 \times 10^{-12} - 2.5 \times 10^{-10}$ moles ($1.3 \times 10^{-6} - 5.0 \times 10^{-5}$ M)

Table 4.1: *Limit of detection (LODs) and linear range obtained for PpyGR-TS and NanoLuc luciferase with LuminoSiPM, ATIK 383L and OnePlus6 smartphone.*

According to a recent work, most smartphone-based sensing platforms reported in the literature are not optimized due to suboptimal design and intrinsic limitations of smartphones with very small lens apertures (Li et al., 2020). Because smartphone-integrated lenses remain the factor that plays a major role in determining the final sensitivity of the sensing platform, alternative systems such as SiPM could represent a more suitable alternative to improve the assay sensitivity while keeping cost contained. Another consideration is related to the fact that most 3D-printed prototypes that have been reported by us and others fit only one model of smartphone. This reduces the general applicability of the sensors and surely hampers their market entrance. Instead, more sensitive yet cheap platforms that could be easily connected to a smartphone used only for data handling could be more advantageous. In the current configuration, the electric power was supplied by the PC USB port, but a smartphone or a cheap microcontroller display unit could be deployed for data storage and/or elaboration in perspective of having a standalone portable battery powered device

with direct cloud connection. The use of the smartphone/tablet option is under development using USB CDC instead of the RS232 interface. The USB OTG port of the LuminoSiPM micro can theoretically reach 480 Mbit/s data output, thus allowing management of a higher data rate.

4.3.4 LuminoSiPM Detection of Acetylcholinesterase Inhibitors with a Chemiluminescent Origami Sensing Paper

The suitability of LuminoSiPM for the detection of CL signals was also evaluated. An origami sensing paper based on the inhibition of AChE activity by molecules such as OP pesticides and nerve agents (Montali et al., 2020) was optimized and adapted to fit the LuminoSiPM device (Fig. 4.8).
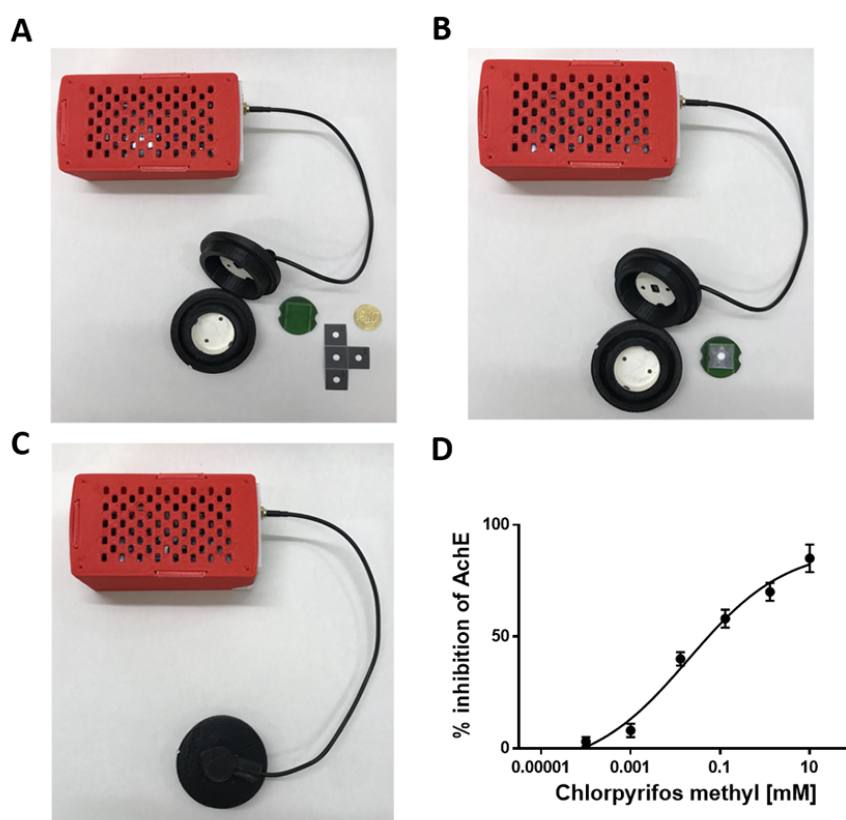

Fig. 4.8: *(A) Picture of the LuminoSiPM with the unfolded paper sensor, (B) the folded sensor, and (C) the assembled device. (D) Chlorpyrifos-methyl inhibition curve.*

The origami sensing paper is based on enzyme inhibition with three enzymatic reactions relying on the luminol/H_2O_2/ HRP system. This sensing paper allows the measurement of AChE inhibitory activity via coupled enzymatic reactions in very short times (less than 30 min) using small volumes of samples (10 µL) and a very straightforward procedure (Fig. 4.6). We used chlorpyrifos-methyl as the model analyte, commercially sold as insecticide

Reldan 22. The calculated LOD for chlorpyrifos methyl was 0.4 µM. The use of LuminoSiPM enabled significant improvement of the LOD, corresponding to 45 µM, previously obtained exploiting CMOS-smartphone integrated detector (Montali et al., 2020). This proof-of-principle assay demonstrated that LuminoSiPM can be used for quantitative and rapid detection of pesticides acting on ACh and can be easily adapted to different analytical formats.

4.4 Conclusion

In this work, we exploited SiPM technology to develop a low-cost device suitable for measuring enzyme-catalyzed bio-chemiluminescent reactions. In view of its application for detecting low light intensities in critical fields such as environmental and forensic analysis, the performance of the device was evaluated and compared to more explored portable light detectors such as smartphone-integrated CMOS and a portable CCD camera. A remarkable improvement of the LOD was obtained for both luciferin-luciferase reactions and in a proof-of-principle application based on a paper sensor for detecting ACh inhibitors. An impressive LOD in the femtomolar range was reported for NanoLuc with a linearity of response extending up to three orders of magnitude, thus confirming the suitability of LuminoSiPM for on-site applications. In addition, due to the temperature dependence of detector noise figures, we envisage that the implementation of temperature stabilization systems based on Peltier elements might further improve the sensitivity. Our results support the use of the LuminoSiPM for on-site analysis, which also benefits from a relatively small footprint and low power demand.

4.5 Acknowledgements

4.6 References

Biewenga, L.; Rosier, B. J. H. M.; Merkx, M. Biochem. Soc. Trans. 2020, 48, 2643−2655.
Bocci, V.; Chiodi, G.; Iacoangeli, F.; Nuccetelli, M.; Recchia, L. 2014 IEEE Nuclear Science Symposium and Medical Imaging Conference (NSS/MIC); Seattle, WA, United States, 2014; pp 1−5.

Branchini, B. R.; Ablamsky, D. M.; Murtiashaw, M. H.; Uzasci, L.; Fraga, H.; Southworth, T. L. Anal. Biochem. 2007, 361, 253−262.

Calabretta, M. M.; Álvarez-Diduk, R.; Michelini, E.; Roda, A.; Merkoçi, A. Biosens. Bioelectron. 2020, 150, 111902,

Cesewski, E.; Johnson, B. N. Biosens. Bioelectron. 2020, 159, 112214.

Cevenini, L.; Calabretta, M. M.; Tarantino, G.; Michelini, E.; Roda, A. Sens. Actuators, B 2016, 225, 249−257.

Cevenini, L.; Lopreside, A.; Calabretta, M. M.; D'Elia, M.; Simoni, P.; Michelini, E.; Roda, A. Anal. Bioanal. Chem. 2018, 410, 1237−1246.

Chen, W.; Yao, Y.; Chen, T.; Shen, W.; Tang, S.; Lee, H. K. Biosens. Bioelectron. 2021, 172, 112788.

de Araujo, W. R.; Cardoso, T. M. G.; da Rocha, R. G.; Santana, M.H.P.; Muñoz, R.A.A.; Richter, E.M.; Paixaõ, T.R.L.C.; Coltro, W. K. T. Anal. Chim. Acta 2018, 1034, 1−21.

Gola, A.; Acerbi, F.; Capasso, M.; Marcante, M.; Mazzi, A.; Paternoster, G.; Piemonte, C.; Regazzoni, V.; Zorzi, N. Sensors 2019, 19, 308.

Hampf, R.; Ulrich, A.; Wieser, J. EPJ. Techn Instrum 2020, 7, 5.

Hernández-Neuta, I.; Neumann, F.; Brightmeyer, J.; Ba Tis, T.; Madaboosi, N.; Wei, Q.; Ozcan, A.; Nilsson, M. J. Intern. Med. 2019, 285, 19−39.

https://ardusipm.filippocurti.it/download (accessed 22 April 2021).

https://www.hamamatsu.com/resources/pdf/ssd/s13360_ series_kapd1052e.pdf (accessed 22 April 2021).

Jung, Y.; Coronel-Aguilera, C.; Doh, I. J.; Min, H. J.; Lim, T.; Applegate, B. M.; Bae, E. Appl. Opt. 2020, 59, 801−810.

Kim, H.; Jung, Y.; Doh, I. J.; Lozano-Mahecha, R. A.; Applegate, B.; Bae, E. Sci. Rep. 2017, 7, 40203.

Kim, S. B.; Paulmurugan, R. Anal. Sci. 2020, 20R003.

Li, H.; Lopes, N.; Moser, S.; Sayler, G.; Ripp, S. Biosens. Bioelectron. 2012, 33, 299−303.

Li, Y.; Ma, X.; Wang, W.; Yan, S.; Liu, F.; Chu, K.; Xu, G.; Smith, Z. J. J. Biophotonics 2020, 13, No. e201900241.

Ligler, F. S.; Gooding, J. J. Anal. Chem. 2019, 91, 8732−8738.

Lisi, F.; Peterson, J. R.; Gooding, J. J. Biosens. Bioelectron. 2020, 148, 111835.

Lopreside, A.; Calabretta, M. M.; Montali, L.; Ferri, M.; Tassoni, A.; Branchini, B. R.; Southworth, T.; D'Elia, M.; Roda, A.; Michelini, E. Anal. Bioanal. Chem. 2019, 411, 4937−4949.

Lopreside, A.; Wan, X.; Michelini, E.; Roda, A.; Wang, B. Anal. Chem. 2019, 91, 15284−15292.

Love, A. C.; Prescher, J. A. Cell Chem. Biol. 2020, 27, 904−920.

Montali, L.; Calabretta, M. M.; Lopreside, A.; D'Elia, M.; Guardigli, M.; Michelini, E. Biosens. Bioelectron. 2020, 162, 112232.

Ouyang, M.; Tu, D.; Tong, L.; Sarwar, M.; Bhimaraj, A.; Li, C.; Coté, G. L.; Di Carlo, D. Biosens. Bioelectron. 2021, 171, 112621.

Rodrigues, E. R. G. O.; Lapa, R. A. S. Anal. Bioanal. Chem. 2010, 397, 381−388.

Ruffinatti, F. A.; Lomazzi, S.; Nardo, L.; Santoro, R.; Martemiyanov, A.; Dionisi, M.; Tapella, L.; Genazzani, A. A.; Lim, D.; Distasi, C.; Caccia, M. ACS Sens. 2020, 5, 2388−2397.

Sevastou, A.; Tragoulias, S. S.; Kalogianni, D. P.; Christopoulos, T. K. Anal. Bioanal. Chem. 2020, 412, 5663−5669.

Tsai, H. F.; Tsai, Y. C.; Yagur-Kroll, S.; Palevsky, N.; Belkin, S.; Cheng, J. Y. Lab Chip 2015, 15, 1472−1480.

Turasan, H.; Kokini, J. Annu. Rev. Food Sci. Technol. 2021, 12, 539−566.

Turner, A. P. Chem. Soc. Rev. 2013, 42, 3184−3196.

Viator, R.; Gray, R L.; Sarver, R.; Steiner, B.; Mozola, M.; Rice, J. J. AOAC Int. 2017, 100, 537−547.

Wang, C.; Liu, M.; Wang, Z.; Li, S.; Deng, Y.; He, N. Nano Today 2021, 37, 101092.

Wang, R.; Yue, N.; Fan, A. Analyst 2020, 145, 7488−7510.

Zhou, M.; Li, T.; Xing, C.; Liu, Y.; Zhao, H. Anal. Chem. 2021, 93, 769−776.

<div style="text-align: right; font-size: 4em; color: #1F3864;">**5**</div>

Orthogonal paper biosensor for mercury(II) combining bioluminescence and colorimetric smartphone detection

5.1 Introduction

Mercury is a global contaminant that causes severe health effects including neurological and gastrointestinal disorders in humans and wildlife. Contamination of water with mercury and its inorganic and organic compounds is still very frequent in several areas worldwide, deriving from both natural and anthropogenic sources. According to the European Environment Agency, about 41% of EU surface water bodies have a mercury concentration exceeding the safety limits, with alarming cases, such as Sweden, with all surface bodies not meeting the environmental quality standard for mercury in biota (European Commission, 2012; Lemm et al., 2021). Notably, mercury speciation and transport between aqueous and solid phases are responsible for different levels of toxicity. In aquatic environments, such as water bodies, sediments, aquatic flora and fauna, mercury occurs mostly as divalent cation in organic and inorganic complexes and as Hg(0) dissolved in the aqueous phase (Leopold et al., 2010). Due to bioaccumulation phenomenon mercury is also present in food, in particular seafood and dairy products, as reported by EFSA (EFSA, 2015). The Minamata Convention on mercury, supported by the World Health Organization (WHO), entered into force in 2017 providing binding measures, such as the banning of mercury in batteries, thermometers, and light bulbs with the goal of protecting the environment and human health from adverse effects of mercury. Accordingly, it is mandatory to monitor mercury and its compounds in aquatic environments, drinking water and food (European Environment Agency, 2018; Minamata Convention, Progress Report, 2020).

Accurate analysis of mercury can be achieved with standard analytical techniques and physico-chemical methods that are generally expensive, not suitable for on-site analysis and require non-green procedures. Cost-effective and eco-friendly methods that enable a rapid and on-site analysis are highly valuable to prioritize samples that need to undergo a more accurate analysis (Calabretta et al., 2021). This would enable a more capillary and widespread screening of water samples and reduce the number of samples to be sent to specialized laboratories for confirmatory analysis. Different biosensors were developed targeting mercury ions, and whole-cell biosensors are among the most sensitive ones (Wang et al., 2013). Microbial biosensors can be easily embedded within portable devices, enabling rapid, on-site and low-cost monitoring (Gu et al., 2004; Lee et al., 2005; Stocker et al., 2003). Highly sensitive whole-cell biosensors were developed based on genetically reprogrammed cells for detecting several heavy metals, including arsenic, zinc, copper, cadmium and mercury (Selifonova et al., 1993; Van der Meer and Belkin, 2010; Wan et al., 2019). Cell

engineering with fluorescent (FL) and bioluminescent (BL) reporter proteins, such as the green fluorescent protein and its variants and luciferases, under the regulation of specific regulatory pathways, such as mercury sensitive proteins (i.e. MerR) and their cognate regulated promoter (i.e. PmerT) provided new tools enabling the detection of mercury down to the femtomolar levels after 30 min of incubation with $HgCl_2$ using benchtop instrumentation (Lopreside et al., 2019b). However, the implementation of such powerful tools in portable analytical devices is not trivial and several attempts showed the difficulty of keeping cells viable and responsive not only during the analysis but also during storage and shipping. Different matrices and polymeric materials were explored to entrap microbial cells. The ideal material should have defined properties in terms of biocompatibility, absence of toxicity, ability to enable diffusion of sample and substrates, biodegradability, mechanical stability, and transparency for optical detection (Bae et al., 2020; Lobsiger et al., 2019; Lopreside et al., 2019b; Shemer et al., 2020; Jung et al., 2014). The well-established lyophilization method provided unbeatable results in terms of long-term stability. However lyophilized cells are not ready-to-use reagents, they must be "awakened" before use with incubation in liquid medium at a defined temperature for a given period of time (Bergua et al., 2021). Instead, the ideal biosensor should be a stable all-in-one device embedding cells that are viable and responsive at use without prior treatments.

Other (bio)sensors were developed for the detection of Hg^{2+} exploiting, among others, aptamer and oligonucleotide-based strategies and different detection techniques such as electrochemical, FL and colorimetric ones (Sahin et al., 2020; Zhong et al., 2021). Besides aptamers, enzymes, such as β-galactosidase (β-gal), were also successfully integrated into paper sensors to detect irreversible inhibitors such as mercury and other heavy metals (Hossain and Brennan, 2011). Despite diverse prototypes for on-site analysis have been proposed, low-cost devices having the required sensitivity and robustness and able to analyze complex environmental matrices have not yet reached the market.

We aim to address the main issues that impede a true market penetration of current biosensors, such as lack of robustness and insufficient sensitivity, by developing an orthogonal biosensor providing the detection of mercury (II) via two different biorecognition elements, a BL mercury sensitive *Escherichia coli* bioreporter and an immobilized enzyme, β-gal, with BL and colorimetric detection, respectively. In addition, the inclusion of a BL strain, *Aliivibrio fischeri*, provides an internal toxicity control to correct the analytical signal, thus enabling the analysis of complex matrices. Both sensory elements and substrates

necessary for the BL and colorimetric detection have been integrated into a paper sensor to provide an all-in-one disposable cartridge and a reusable 3D-printed case for smartphone signal acquisition (Fig. 5.1).

5.2 Experimental section

5.2.1 Strains, chemicals and reagents

β-gal from *E. coli* (G6008-1KU), chlorophenol red-β-D-galactopyranoside (CPRG) substrate and all reagents required for colorimetric reaction were from Sigma-Aldrich (St. Louis, MO). *E. coli* TOP10 J23109-merR-PmerT-NanoLuc bacterial strain for mercury detection via NanoLuc luciferase expression has been obtained by PCR and Gibson Assembly (Lopreside et al., 2019b). Naturally BL bacteria *A. fischeri* were kindly gifted from Prof. Stefano Girotti (Camanzi et al., 2011). Lysogeny broth (LB) medium and all reagents required for bacterial cell cultures were from Sigma-Aldrich (St. Louis, MO). Cryoprotectant R18 medium was prepared with 7.5 g/L tryptone, 100 g/L sucrose, 50 g/ L bovine serum albumin (BSA) in ddH$_2$O.). B-PER^{TM} lysing buffer for bacterial cell lysing was from Thermo Fisher Scientific (Waltham, MA, USA). Furimazine from NanoGlo Luciferase Assay System was from Promega (Madison, WI, USA).
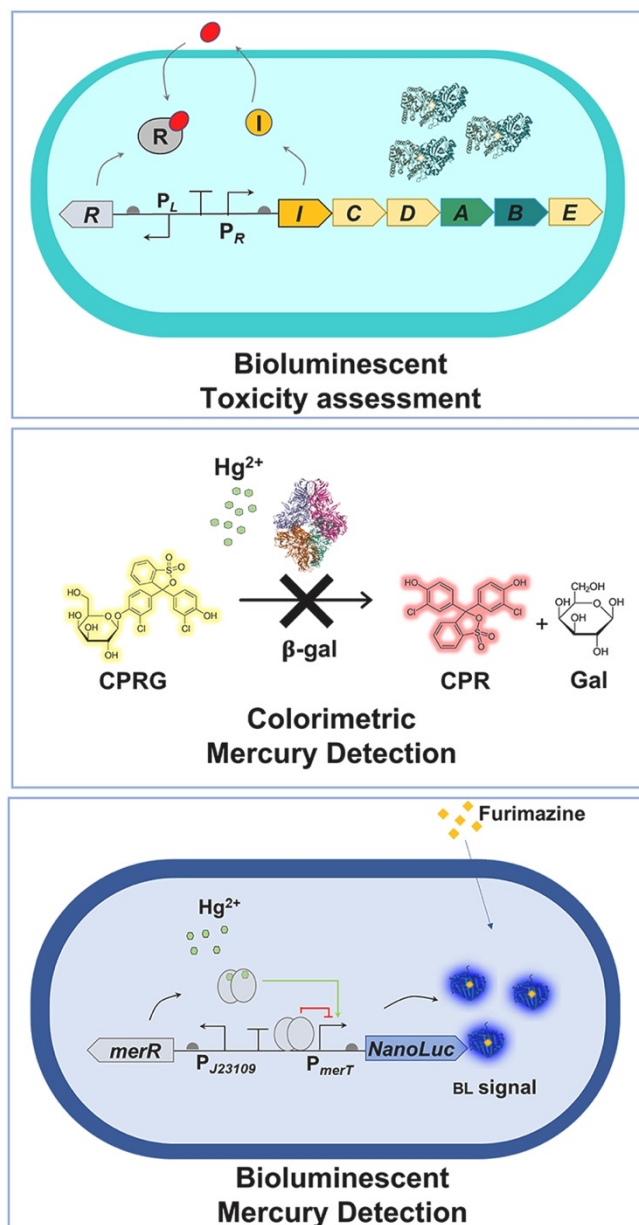
Fig. 5.1: *Schematic showing the design of the three-leaf biosensor. The paper sensor integrates two mercury-specific biorecognition elements, BL bacteria carrying NanoLuc luciferase induced by Hg^{2+} and β-gal enzyme irreversibly inhibited by Hg^{2+}, with a BL A. fischeri strain, used to correct the analytical signals according to sample toxicity. BL and colorimetric signals are measured with the smartphone camera. A 3D printed dark box protects the sensing papers from ambient light for BL detection and enables the use of smartphone-integrated flash for β-gal colorimetric detection.*

5.2.2 Design of disposable sensing paper and 3D-printing of smartphone-based device

Whatman 1 CHR cellulose chromatography paper from GE Healthcare (Chicago, IL, USA) was used as support for the paper-based analytical device. A modular biosensor pattern was designed using PowerPoint (Microsoft, Redmond, WA, USA) and printed onto the Whatman 1 CHR chromatography paper using a Phaser 8400 office wax printer (Xerox,

Norwalk, CT, USA). After printing, the waxed pattern was cured for 1 min at 100°C to allow wax to diffuse in the paper thickness to create the hydrophobic areas (Montali et al., 2020). The paper-based disposable cartridge consisted of 12 circular hydrophilic "wells" (diameter 5 mm), named "CTR" (control well) and "T" (sample well), surrounded by hydrophobic areas (Fig. 5.2A). A central bigger well (8 mm diameter) connected with each sample well (5 mm diameter) by tree channels (15 mm of length) was designed for single step sample addition. Two separate modules containing chromogenic and BL substrates, defined substrate-papers, were also designed overlapping the three-leaf sensing paper for independent substrate addition (Fig. 5.2B). Adaptor and dark box for signal acquisition via smartphone were designed with the online 3D modeling program Tinkercad and printed with a desktop 3D printer Makerbot Replicator 2X. Black thermoplastic polymer acrylonitrile butadiene styrene (ABS) (FormFutura, Nijmegen, NL) at 300 µm layer resolution was used with 30% infill. A dark box (65 × 65 mm, 60 mm high) with smartphone adaptor (80 × 85 mm, 20 mm high) was designed with a front-side port (40 × 40 mm, 8 mm high) for cartridge integration. A reusable holder for the sensing paper was also designed (composed of 3 squares joined together, each one 40 × 40 mm and 8 mm high) with two subunits that can be held together by six N52 grade neodymium magnets (diameter 6 mm, thickness 2 mm) to assemble sample-paper and substrate-paper for signal acquisition (Fig. 5.2A).

5.2.3 Colorimetric β-galactosidase paper (β-gal paper)

β-gal (500 U/mL) stock solution was prepared in 2 mL of PBS 0.1 M pH 7.4, sealed under nitrogen flow and stored at +4 °C. 400 mg of CPRG were solubilized in 10 mL of ddH$_2$O to obtain a 68.4 mM (10x) stock solution. CPRG stock solution was stored protected from light at −20°C. Different concentrations, from 0.12 to 4 U/mL of β-gal were tested for immobilization on paper. β-gal concentration was optimized on paper with the preliminary absorption of 2 µL of 6.84 mM CPRG, subsequent addition of 10 µL of ddH$_2$O or sample and the addition of 5 µL of β-gal. Two alternative methods were evaluated, i.e., adsorption and lyophilization, to integrate β-gal on paper. For lyophilization, a 5 µl-volume of β-gal (1 U/mL) was deposited on a 5 mm-diameter paper well with R18 medium (from 0 to 50 %v/v). Due to the low sample volume, lyophilization was performed without sample freezing step using a Christ Alpha 1-2LD Plus Lyophilizer (Martin Christ Gefriertrocknungsanlagen GmbH, Germany), for 3 h, 0.029 mbar, −60°C (Calabretta et al., 2020). The optimized protocol involves the addition of a 5 µl-volume of β-gal (1 U/mL) with 20%$_{v/v}$ of R18 medium for each

well of the sensing paper and a lyophilization step at – 60°C for 3 h at 0.029 mbar. The β-gal paper was then sealed into plastic bag and stored at + 4°C until use.
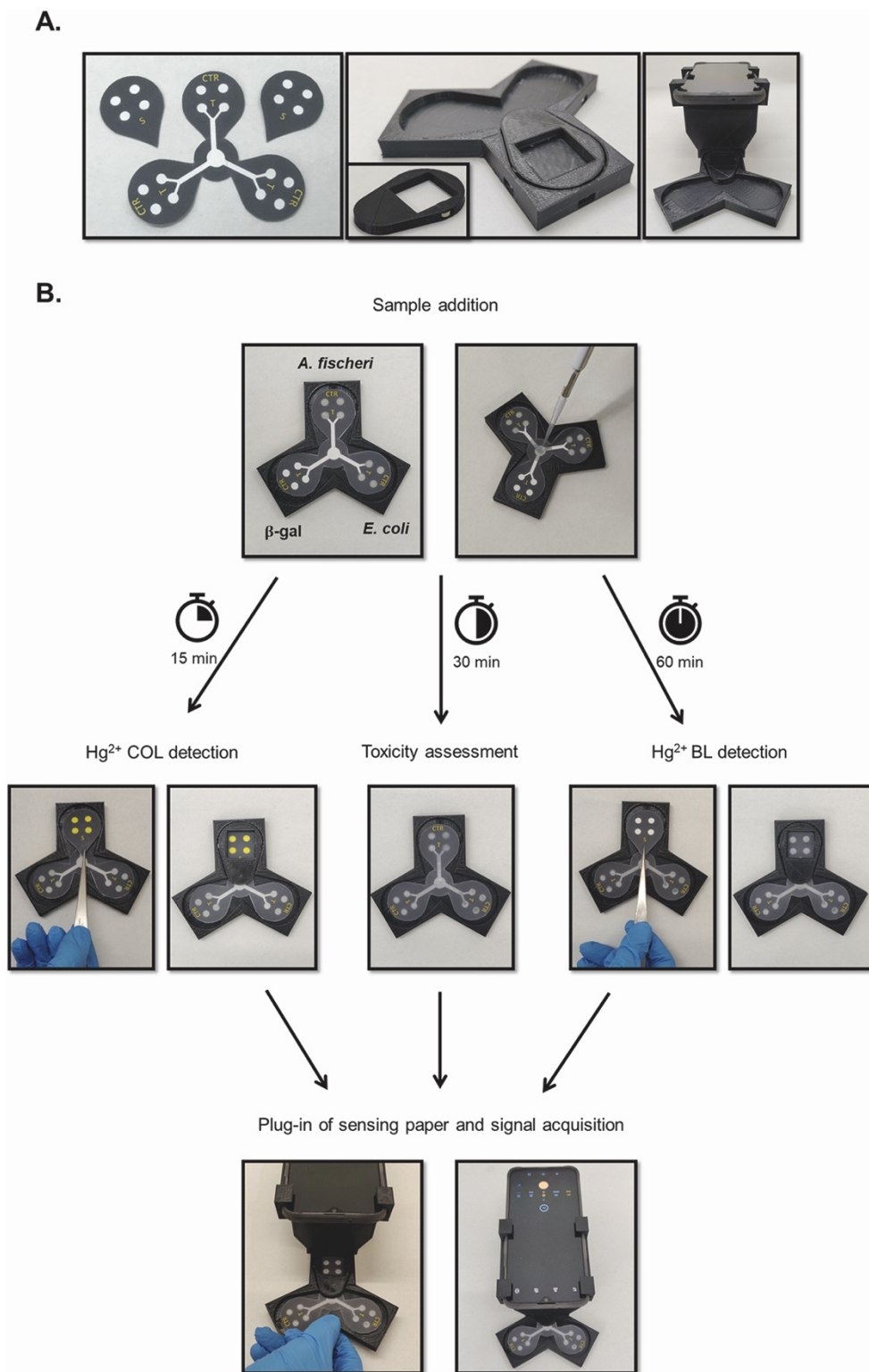

Fig. 5.2: *3D-printed device and user-friendly procedure for sample testing. A) Components of the orthogonal biosensor device. Disposable paper cartridge including a three-leaf sensing paper, enabling analysis of test sample (T) and control (CTR) in duplicate, two substrate papers (S), containing either CPRG or BL substrate for separate analysis, magnetic reusable 3D-printed holder and dark box with smartphone adaptor. B) Step-by-step procedure for sample analysis.*

5.2.4 Substrate-papers (CPRG-paper and Furimazine-paper)

The substrates for the colorimetric and BL reactions, CPRG and Furimazine, were lyophilized on paper for the development of a biosensor integrating all reagents required for the reactions. Different volumes from 2 μL to 4 μL of CPRG (6.84 mM) and from 10 μL to 20 μL of Furimazine (1:1000 and 1:500 dilutions in ddH$_2$O or B-PER lysing buffer) were tested. Cryoprotectant or cofactors such as R18 medium (from 0 to 50%$_{v/v}$) and B-PER lysing buffer (from 0 to 99%$_{v/v}$) were co-lyophilized to increase biosensors responsiveness and stability. Liquid-dry lyophilization was performed as described before. In optimized conditions, CPRG-paper and Furimazine-paper were obtained lyophilizing 2 μL of CPRG (6.84 mM) and 10 μL of BL substrate (Furimazine 1:500 from Promega stock solution and 98%$_{v/v}$ of B-PER lysing buffer).

5.2.5 Signal acquisition and data analysis

BL signal acquisitions were carried out with a OnePlus 6 T smartphone (OnePlus, Shenzhen, China), equipped with a dual integrated camera (primary sensor: 16 MP Sony Exmor RS IMX 519, BSI CMOS 1/ 2.600 color sensor with 1.22-μm pixels, f/1.7 aperture; secondary sensor: 20 MP Sony Exmor RS IMX 376 K, BSI CMOS 1/2.800 color sensor with 1.0-μm pixels, f/1.7 aperture). Images were acquired using the secondary 20 MP camera from a 55 mm distance (height of the designed dark-box). BL images were acquired with Pro mode, with a selected ISO of 1600 and an acquisition time of 30 s. Reflectance of colorimetric biosensor was acquired in standard mode using the integrated smartphone flash and the black box. Quantitative analysis of both colorimetric and BL signals was performed with the open-source Image J software (v. 1.52s, National Institutes of Health, Bethesda, MD, USA). A circular region of interest (ROI) was defined in correspondence of the biosensor well and the reflectance (colorimetric signal) was evaluated by the RGB analysis over the ROI area, while the BL signal was evaluated by integrating the BL image intensity over the ROI area (since maximum BL emission is at about 460 – 480 nm, integration was performed by considering only the blue channel of the RGB image). Regarding data obtained from images of the colorimetric biosensor, RGB system was considered as a three-dimensional space, whose 3 axes (x, y and z) correspond respectively to the 3 primary colors (red, green and blue). The x-axis (red) was considered constant since the CPRG colorimetric reaction varies from red-violet to yellow-orange, thus maintaining high and constant red color values. The two-dimensional Euclidean distance between the points on the y-axis and the points on the z-axis was then calculated to determine the curves,

i.e. the two-dimensional distance between the green color and the blue color (Li et al., 2018). The maximum two-dimensional Euclidean distance obtained between the green and the blue channels, corresponding to yellow color and complete enzyme inhibition by mercury(II), was set as 100%. GraphPad Prism v.5 (GraphPad Software, LaJolla, USA) was used to fit the data of samples with unknown concentration for the Hg(II) dose–response curves with a four parameter non-linear regression curve. As concerns the mercury-sensitive strain, the limit of detection (LOD) was calculated as mean value of control sample (ddH$_2$O) plus three times the standard deviation. For the β-gal, LOD was calculated as mean value of the control sample (red color) minus three times the standard deviation of the control sample.

5.2.6 Orthogonal biosensor assay procedure

After evaluating the optimal conditions in terms of analytical performances and incubation times of each sensing element of the biosensor, a straightforward procedure for simultaneous orthogonal detection of mercury(II) in liquid samples with the three different sensing papers in a single cartridge was developed and optimized. Briefly, the three-leaf sensing paper is placed in the 3D printed holder and a 150 µL-volume of sample is added to the central well. By capillarity the sample flows through the wax printed channels reaching sample wells. A 20 µL-volume of distilled water is added to control wells. Incubation times of 15, 30 and 60 min at room temperature are required for β-gal paper, *A. fischeri* toxicity paper, and *E. coli* mercury-sensitive paper, respectively. After 15-min of incubation, the CPRG-paper overlapped to the sensing paper and closed with a complementary 3D printed adaptor. After 10 min, the colorimetric image is acquired introducing the β-gal paper inside a dark-box to avoid external light noise and using a OnePlus 6 T smartphone camera with automatic mode and flashlight on. After 30-min incubation, *A. fischeri* toxicity paper is inserted into the dark box and BL signal acquired using a OnePlus 6 T smartphone camera in Pro mode, with 30 s of integration time and ISO 1600. After 60 min of incubation the Furimazine-paper is placed on the *E. coli* mercury-sensitive paper and is magnetically closed. The BL image is then acquired introducing the *E. coli* mercury-sensitive paper inside the dark-box using the OnePlus 6 T smartphone camera.

5.2.7 Real sample analysis, and characterization of sensor recovery and selectivity

As proof-of-concept of the applicability of the developed biosensor with real samples, water samples, including tap water and lake water were spiked with different concentrations of

mercury, interferents and toxic chemicals. Biosensor responsiveness to complex samples at different pH was assessed with tap water samples spiked with $HgCl_2$ (0.25 and 1.00 μM) with pH ranging from 2.5 to 7.5. Toxic samples were simulated with different concentrations of DMSO (from 0.50 to 50%$_{v/v}$) and fixed concentrations of mercury (0.50 μM and 0.25 μM). To evaluate the specificity of the biosensors, potential interferents like $CaCl_2$, $CdCl_2$, $NiCl_2$, $AgCl$ and $MgCl_2$ were evaluated using the optimized procedure. Recovery studies were performed using the optimized procedure and water samples spiked with mercury (from 5.00×10^{-3} to 1.00 μM) and DMSO (from 0.25 to 50%$_{v/v}$). Recoveries were calculated by applying a signal correction for *E. coli* mercury-sensitive paper. The corrected BL value was obtained by multiplying the raw value, obtained from the sensing paper, by a correction factor, calculated as the ratio, for each tested sample, between the BL signal of *A. fischeri*-toxicity paper incubated with ddH$_2$O (control) and the signal of *A. fischeri* toxicity-paper incubated with the sample. All experiments were performed in triplicate and repeated at least three times.

5.2.8 Biosensor stability evaluation

The stability for *E. coli* and *A. fischeri* immobilized in agarose (0.75%$_{w/v}$) with 10%$_{w/v}$ of trehalose and lyophilized β-gal (1 U/mL) with 20%$_{v/v}$ of R18 medium was assessed by keeping the sensing papers in sealed plastic bags for several weeks at + 4°C. After 24, 48, 72, 96 h, 1 week, 2 weeks and 1 month, the plastic bags were opened to perform the assay at room temperature (25°C), as described previously. To assess substrate stability, the substrate-papers containing the lyophilized substrate (CPRG and Furimazine) were stored in sealed plastic bags at + 4°C and tested after 24, 48, 72, 96 h, 1 week and 2 weeks as described before.

5.3 Results and discussion

5.3.1 Design of disposable paper-based cartridge and 3D-printing of the integrated smartphone-based device

We developed a low-cost biosensor for orthogonal detection of mercury(II) integrating three different biorecognition elements on a disposable three-leaf paper: i) a mercury-specific BL *E. coli* bioreporter strain expressing the mercury receptor MerR under the regulation of a constitutive promoter (J23109) and NanoLuc luciferase under the regulation of promoter PmerT, ii) a purified β-gal enzyme which is irreversibly inhibited by mercury and other metal ions reacting on the sulfhydryl group of cysteine, and iii) a *A. fischeri* BL strain for sample toxicity evaluation and analytical signal correction (Fig. 5.1). The mercury-specific BL *E. coli* bioreporter strain expresses the mercury receptor MerR under the regulation of a constitutive promoter (J23109), and mercury interacts with this receptor constitutively produced by the *E. coli* strain. In the presence of increasing concentrations of mercury(II), The mercury receptor MerR derepresses its cognate promoter PmerT leading to the expression of the BL NanoLuc protein.

The purified β-gal enzyme is irreversibly inhibited by mercury and other metal ions reacting on the sulfhydryl group of cysteine in the active site of the enzyme. In the presence of increasing concentrations of mercury(II) the enzymatic function is inhibited and the color changes from red-purple to yellow color. The BL control signal emitted by the *A. fischeri* strain decreases due to sample toxicity. Paper was chosen as support to integrate the three biosensing elements since it is sustainable, allows passive transport of liquid and shows high biocompatibility with several biomolecules and living cells as well. Few examples report the integration of whole-cell biosensors into paper (Guo et al., 2020; Liu et al., 2018; Ma et al., 2020) and, to the best of our knowledge, the present biosensor represents the first attempt to integrate living cells, enzymes and their corresponding substrates, in the same device to create a stable biosensor providing an easy and rapid assay procedure. The first challenge was to address both cell and enzyme immobilization in the same paper support to enable storage of the device without activity loss. We decided to lyophilize the enzyme and entrap the cells in a hydrogel to combine advantages of the two approaches and to obtain a ready-to-use sensing paper that does not require any additional step for "awakening" the cells and that can be stored and shipped without a strict cold chain. As concerns the detection, we combined BL detection required for the two whole-cell biosensors, the mercury specific strain and the viability control strain, with colorimetric detection of β-gal obtained with the chromogenic substrate CPRG. A low-cost 3D-printed

case was fabricated to enable standardized rapid and robust smartphone detection for all the three biosensing reactions.
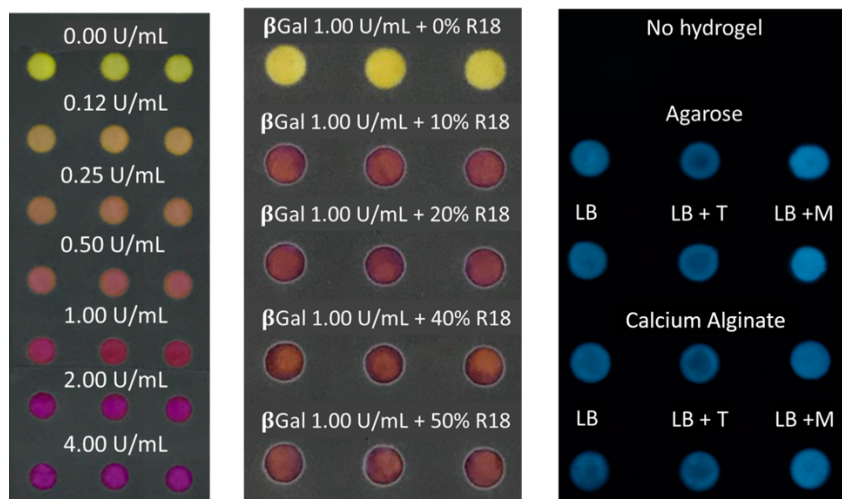

Fig. 5.3: *Optimization of ready-to-use paper-based biosensor with β-gal and BL bacterial sensors. Reflectance images of different β-galactosidase concentrations adsorbed on paper (from 0.0 to 4.00 U/mL) (left) and of the lyophilized β-galactosidase (1.00 U/mL) with different R18 medium percentages (concentration range from 0 to 50%$_{v/v}$) (center). BL images of A. fischeri immobilized on paper without hydrogel, with agarose (0.75%$_{w/v}$) and with calcium alginate (1.5%$_{w/v}$), supplemented with only LB (LB), LB plus trehalose (LB + T), and LB plus milk (10%$_{v/v}$) (LB + M).*

5.3.2 Colorimetric β-galactosidase paper

Preliminary experiments involving different concentrations and volumes of CPRG and β-gal were performed to identify the suitable combination providing the highest sensitivity of the paper sensor. A color change from yellowish-orange to red-purple was observed at increasing enzyme concentrations, leading to a decreased bidimensional distance between the green and blue channels of the RGB system (Fig. 5.3). The lowest concentration tested (0.12 U/mL) showed the maximum variation (48%) from the control. The highest concentration tested (4 U/mL) showed an opposite maximum variation from the control (155%) due to a negative Euclidean distance (purple color). No difference in reflectance was observed between the highest enzymatic concentrations (2 and 4 U/mL) in that the ratio of the Euclidean bi-dimensional distance between these two concentrations was 1.16.

Regarding response time, low enzyme concentrations required more time for color change (up to 10 min to obtain a red color, instead of 5 min for 1 U/mL β-gal) while higher enzyme concentrations (2 and 4 U/ mL) result in a rapid color change (from yellow to red color) and a saturated signal that leads to a negative distance between green and blue channel of RGB system. Accordingly, a β-gal concentration of 1 U/mL and a CPRG concentration of 6.84 mM, providing a positive Euclidean bi-dimensional distance close to zero and showing the maximum variation from the control of 95%, were selected.

Different lyophilization procedures and addition of cryoprotectants were evaluated. The addition of R18 at concentrations higher or equal than 10 %$_{v/v}$ caused the preservation of β-gal enzymatic function and a color change from yellow to red comparable to the one obtained before the freeze-drying process. Comparing the two-dimensional Euclidean distance between the green and blue channel obtained before and after freeze-drying, a 1.18 ratio was obtained with the lyophilization of a 5 µL volume of 1 U/mL β-gal with 20 %$_{v/v}$ of R18 medium. Higher concentrations of R18 medium resulted in a spurious color change (dark red), (Fig. 5.3). Therefore, the optimal lyophilization method was obtained with 5 µL of 1 U/mL β-gal with 20 %$_{v/v}$ of R18 medium for each well of the sensing paper.

5.3.3 Bioluminescent *E. coli* mercury-sensitive paper and *A. fischeri* toxicity paper

To develop a ready-to-use sensor integrating the two bacterial reporters with long stability we first tested lyophilization of bacterial cells with different cryoprotectants and conditions. The use of R18 medium and trehalose (10%$_{w/v}$) provided a significant improvement of cell viability after storage at + 4°C, up to 4 weeks, with an increased BL signal of 3.6 and 2.2 folds higher than that obtained with LB medium. Nevertheless, a minimum of 16 h of incubation at room temperature with liquid medium was required to reactivate cell metabolism and use the cells for biosensing. Accordingly, alternative approaches were investigated to develop a ready-to-use biosensor with active bacterial cells on paper. Agarose and calcium alginate were combined with different cell concentrations to improve cell viability and to obtain a BL signal detectable with smartphone-integrated CMOS. A 20 µL-volume of cell suspension with an OD600 of 0.1 for *E. coli* and OD600 5.0 for *A. fischeri* (corresponding to 1.6×10^6 and 8×10^7 cells, respectively) in LB medium with 10%$_{w/v}$ trehalose or 7.5%$_{w/v}$ of agarose were deposited on paper. A complete loss of BL signal was observed after bacterial dehydration on paper without hydrogel (Fig. 5.3); while a BL signal was produced by cells entrapped on hydrogel, corresponding to 123% of the BL signal obtained

with the liquid cell culture. The addition of milk (10%$_{v/v}$) in hydrogel caused a 1.4-fold signal increase when compared to the control (same cell concentration in LB medium). No change or signal increase was caused by trehalose addition (Fig. 5.3). No significant differences on cell viability were obtained with entrapment of cells into alginate, which provided a BL signal only 1.2 fold higher than obtained with agarose immobilization. Instead, cells entrapped in sodium alginate did not attach to the paper support and after drying almost complete detachment of cells was observed. Our results support those reported by Gu Z. et al., who demonstrated that agarose binds to filter paper fibers and that hydrogel coated region presents a relatively "slow" absorption of liquid, which may facilitate the interaction between the immobilized bacteria and the sample (Gu et al., 2011).

5.3.4 Chromogenic and bioluminescent substrate-papers

Two substrate papers have been designed complementary to the three-leaf sensing paper to obtain an all-in-one and liquid-free biosensor. A 2 µL-volume of CPRG (6.84 mM) and a 10 µL-volume of Furimazine were lyophilized on paper. CPRG was lyophilized without adding cryoprotectant because addition of 25%$_{v/v}$ and 50%$_{v/v}$ of R18 medium increased the Euclidean two-dimensional distance between the RGB signal in the green channel and the signal in the blue channel of 2.25 times and 6.64 times, respectively. The increase of the Euclidean distance corresponded to a lower reactivity of the substrate which did not allow the colorimetric reaction to proceed. Lyophilized CPRG, without cryoprotectant, is stable for a long time when stored at + 4°C sealed in plastic bags with a 100% stability up to 4 weeks post lyophilization. In addition, Furimazine substrate, required for the NanoLuc-catalyzed BL reaction, was lyophilized in the presence of a lysing buffer to obtain a stable reagent for the *E. coli* mercury-sensitive paper. Following 4 weeks storage at + 4°C sealed in plastic bags a BL signal corresponding to 98% of the signal obtained at day 0 was obtained. A high stability of Furimazine was also proven by Hall et al. who reported no loss in activity after 11 months at ambient temperature (Hall et al., 2021).

5.3.5 Three-leaf biosensor's characterization

A preliminary optimization of the three different sensing papers was performed using paper cartridges with 3x7 wells (5 mm diameter) in order to optimize LOD, analytical performances and incubation times of each component of the three-leaf biosensor separately.

Biosensor responsiveness and analytical performance were first evaluated with different concentrations of $HgCl_2$ as model analyte, from 1.00×10^{-4} to 1.00 μM. Limit of detection (LOD), fold response, incubation times and kinetic measurements from 0 to 120 min of incubation (at room temperature) for the three sensing papers were performed to identify the suitable temporal window for signal acquisition. For β-gal paper optimization, preliminary studies were performed using a 2 μL-volume of 6.84 mM CPRG solution absorbed on paper incubated with 5 μL of 1.00 U/mL β-galactosidase and 20 μL of 1.00 μM $HgCl_2$ solution. The β-gal paper was also tested with different $HgCl_2$ volumes from 5 to 25 μL to identify the optimal reaction conditions. The incubation time of $HgCl_2$ with β-gal paper was optimized by adding a 20 μL-volume of a 1.00 μM $HgCl_2$ solution on the well with β-galactosidase lyophilized and incubating up to 120 min. After incubation, a 2 μL-volume of 6.84 mM CPRG solution was added. As regards the final optimization of the β-gal paper, 20 μL of $HgCl_2$ (from 1.00×10^{-4} to 1.00 μM) were added on the well with the lyophilized β-galactosidase and left to incubate for 15 min at room temperature (25°C). After incubation, the substrate paper was positioned, and the colorimetric image acquired with the smartphone camera. To choose the optimal time window for the colorimetric image acquisition, kinetics of colorimetric signal obtained with CPRG substrate were evaluated, taking images every minute for 20 min. As concerns *E. coli* mercury-sensitive paper, different volumes (from 5 to 25 μL) of sample (1.00 μM $HgCl_2$) were tested to choose optimal condition for the BL reaction.

Different incubation times, from 0 up to 120 min, were tested, at room temperature, adding 20 μL of 1.00 μM $HgCl_2$ directly on wells with bacteria cells entrapped in agarose. Analytical performance of the *E. coli* mercury-sensitive paper was evaluated adding a 20 μL-volume of different concentrations of $HgCl_2$, from 1.00×10^{-4} to 1.00 μM. As for β-gal paper, after a 60 min-incubation of *E. coli* sensor cells with different concentrations of $HgCl_2$, the Furimazine-paper was positioned, and the bioluminescent image was taken. Also, for *A. fischeri* toxicity paper, volumes from 5 to 25 μL of sample (1.00 μM $HgCl_2$) were tested and incubation times from 0 to 120 min to choose the optimal condition for *A. fischeri* to respond. An inhibition curve with different concentrations of $HgCl_2$ (from 1.00×10^{-4} to 1.00 μM) was performed to evaluate the LOD for *A. fischeri* toxicity paper. Dimethyl sulfoxide (DMSO) was used as model toxic compound to investigate the biosensor response to toxic samples. Dose response curves were performed with DMSO dilutions ranging from 0.25 to 50%$_{v/v}$ prepared in ddH_2O. All experiments were performed at least three times in triplicate. The LOD was calculated as the BL signal of the control (ddH_2O) plus three times the standard deviation.

5.3.6 Analytical performance of the three-leaf bioluminescent colorimetric paper biosensor

The kinetics of the colorimetric and BL signals were obtained by incubating, up to 2 h, each well of three-leaf biosensor with 20 µL of 1 µM $HgCl_2$ as model analyte for induction and 25%$_{v/v}$ DMSO as model toxic compound. The β-gal paper produced a signal with a kinetic with a plateau reached after 15 min of incubation and a signal stable for at least 120 min, due to the irreversible inhibition of the enzyme. Accordingly, the incubation time for the colorimetric detection of mercury(II) was set at 15 min. Moreover, to standardize the measurement an optimal acquisition window from 10 to 13 min, after CPRG addition, was identified with stable reflectance signal (Figures 5.4; 5.5; 5.6). The *E. coli* mercury-sensitive paper produced an emission kinetic with a maximum BL signal over control after 60 min. This behavior is consistent with the time required to express the NanoLuc reporter protein (Lopreside et al., 2019b). Therefore, the incubation time for mercury(II) detection via BL *E. coli* sensor strain was set at 60 min.
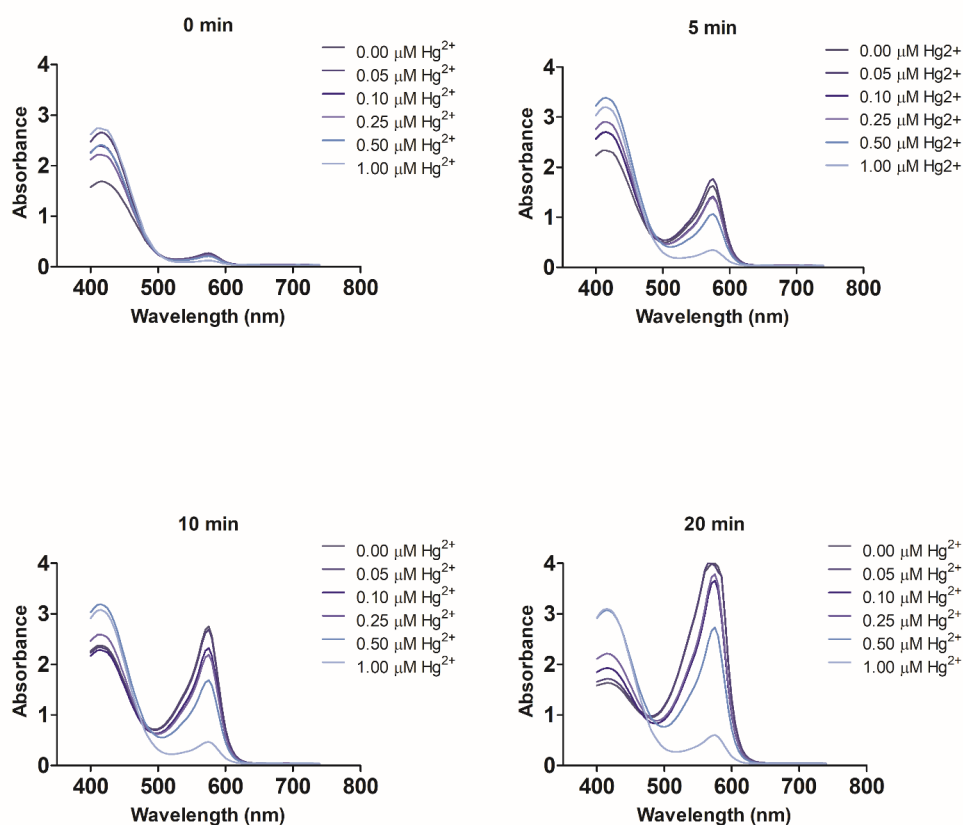

Fig. 5.4: *Optimization of β -gal/CPRG incubation time. UV-Visible absorption spectra of β -gal/CPRG in the presence of Hg2+ acquired with Thermo Scientific™ Varioskan™.*
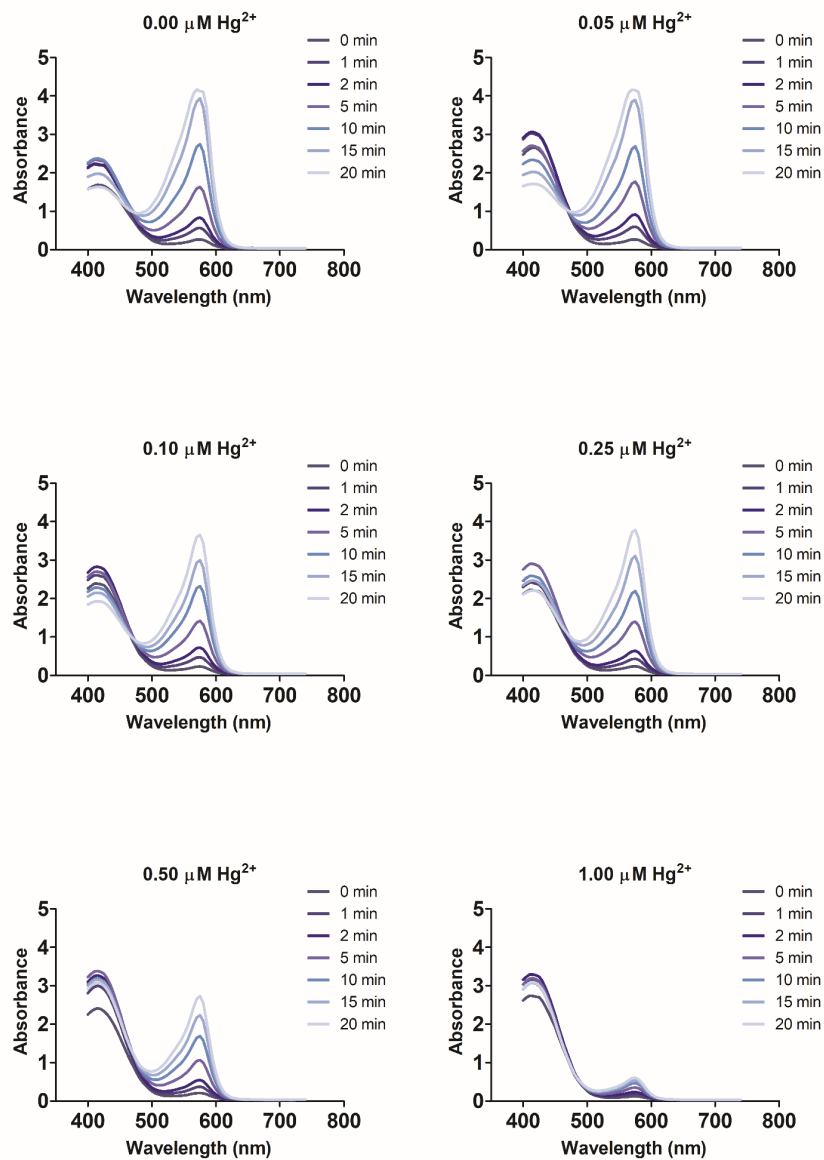
Fig. 5.5: *UV-Visible absorption spectra of β-gal paper with CPRG substrate. UV-Visible absorption spectra were obtained with Thermo Scientific™ Varioskan™ (from 0 to 20 min) with a fixed concentration of Hg²⁺.*

A decrease of the BL signal for *A. fischeri*-paper was observed over time due to DMSO toxicity. The 100% signal was set for *A. fischeri* incubated with ddH_2O (control) and a 43% of signal reduction was observed after 30 min of incubation. Since the curve reached a stable BL signal after 30 min, this incubation time was selected for *A. fischeri* paper.

Incubation times of 15, 30 and 60 min were selected for β-gal paper, *A. fischeri* toxicity paper and *E. coli* mercury-sensitive paper, respectively.
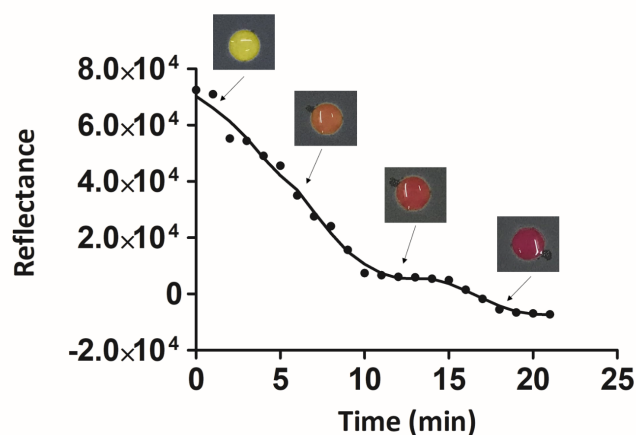

Fig. 5.6: *β-gal/CPRG reflectance kinetics on paper. Color development over time with on-paper immobilized β-gal/CPRG. Reflectance images were taken with Oneplus 6T smartphone camera.*

Fig. 5.7B shows the dose-response curves of *A. fischeri* toxicity paper and *E. coli* mercury-sensitive paper incubated with samples of varying $HgCl_2$ concentrations (from 5.00×10^{-4} to 1.00 µM). *A. fischeri* exhibited mercury toxicity at $HgCl_2$ concentrations higher than 0.25 µM. This toxicity assessment was necessary to correct the BL signal obtained with the *E. coli* mercury-sensitive paper and avoid underestimation due to sample toxicity or overestimations in the presence of matrix effects that improve cell metabolism. Signal correction according to cell viability and metabolism is required to obtain robust results from whole-cell biosensors (Mirasoli et al., 2002), especially for the analysis of complex matrices, however few examples of devices integrating analyte-specific bioreporters and general toxicity strains have been reported (Cevenini et al., 2018; Lopreside et al., 2019a; Roda et al., 2011a). By correcting the BL signal obtained from the *E. coli* mercury-sensitive paper with the *A. fischeri* toxicity paper signal, a dose-response curve was obtained showing a LOD of $2.87 \times 10^{-3} \pm 3.45 \times 10^{-4}$ µM for $HgCl_2$. This LOD corresponds to 0.58 ± 0.07 ppb for Hg^{2+}, thus allowing the measurements of the maximum allowed concentration of mercury(II) in drinking water of 2 ppb (10 nM) and 6 ppb fixed by U.S. Environmental Protection Agency (EPA) and the World Health Organization (WHO), respectively (U.S. EPA, 2009; WHO, 2011). The corrected dose-response curve obtained with *E. coli* mercury-sensitive paper was compared with the dose response curve obtained with the β-gal paper treated with samples of varying concentrations of $HgCl_2$ (Fig. 5.7). The LOD obtained with the β-gal

paper was $8.50 \times 10^{-2} \pm 0.01$ µM, corresponding to 17.0 ± 2.20 ppb for Hg^{2+}. Comparing the corrected signal of the *E. coli* mercury-sensitive paper with the β-gal paper, bacterial cells showed a lower LOD, albeit with a longer incubation time, 60 min vs 15 min. Both LODs are in the same order of magnitude obtained by others previously reported (Guo et al., 2020; Sajed et al., 2019) but faster response time (Fig. 5.8). For example, Guo et al. developed a whole-cell microbial biosensor based on FL reporter gene with a LOD of 1 mg/kg for total inorganic mercury pollutants in cosmetics with 6 h incubation time (Guo et al., 2020). In a pioneering work, three microbial bioreporters were developed to detect Hg(II) in waters in the 0.50 – 1000 nM range (0.10 – 200 ppb), thus similar to the analytical performance of the *E. coli* mercury-sensitive paper, albeit with benchtop instrumentation and necessity of growing bacterial cultures (Selifonova et al., 1993). Notably, Wan et al. combining different cascaded amplifying circuits in a FL whole-cell sensor array, were able to detect mercury down to 0.01 ppb, with 6 h incubation and benchtop laboratory instrumentation (Wan et al., 2019).
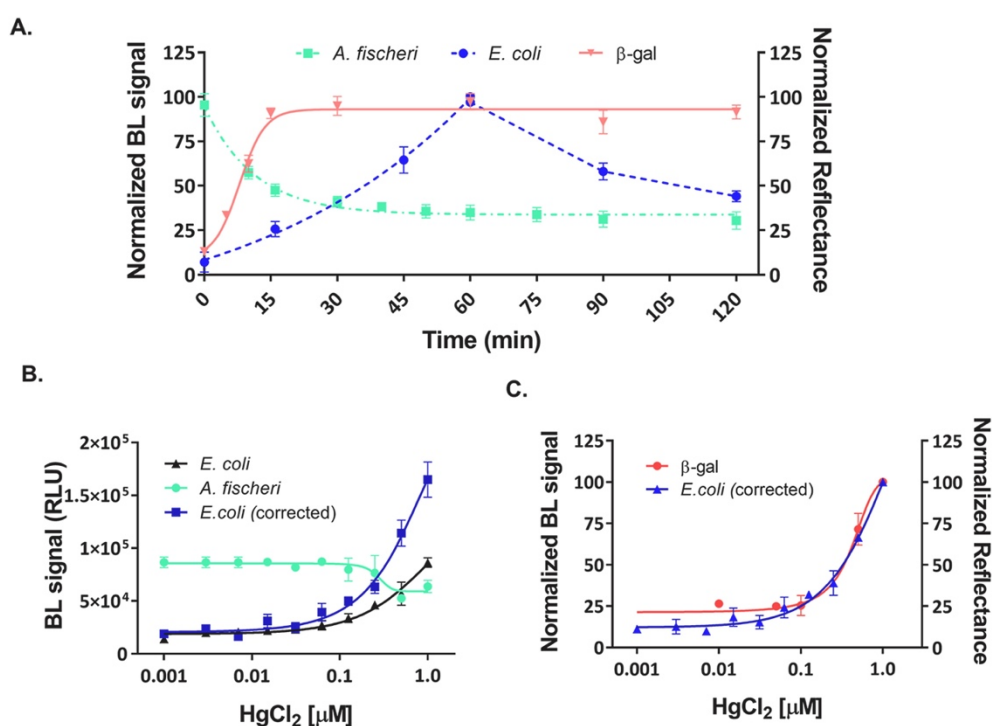

Fig. 5.7: *Analytical performance and characterization of the three-leaf bioluminescent-colorimetric paper biosensor. A) Biosensor's response over time with HgCl₂ (1 µM) for E. coli mercury-sensitive paper and β-gal paper, and DMSO-25%ᵥ/ᵥ for A. fischeri toxicity paper; B) Dose response curves of the E. coli mercury-sensitive paper (with/without signal correction) and A. fischeri toxicity paper with different concentrations of HgCl₂; C) Normalized dose response curves of E. coli mercury-sensitive paper (corrected curve) and β-gal paper with HgCl₂.*
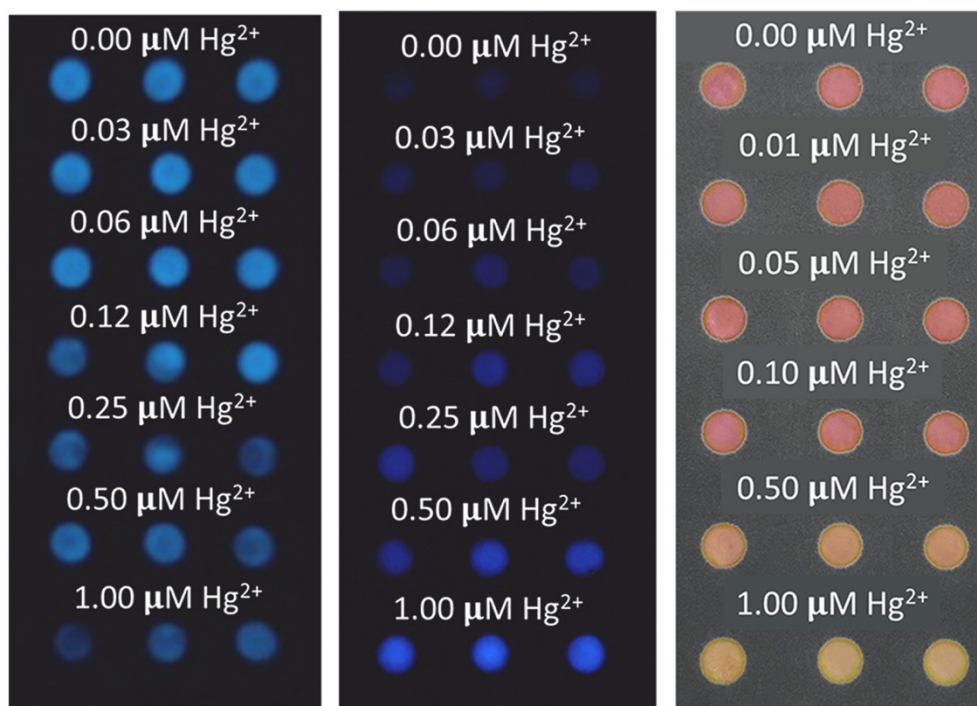
Fig. 5.8: *Pictures of the three-leaf bioluminescent-colorimetric paper biosensor. Pictures of sensing papers responding to samples with varying concentrations of Hg^{2+}: A. fischeri toxicity paper (left), E. coli mercury-sensitive paper (center) and β-gal paper (right).*

5.3.7 Biosensor analytical performance with simulated complex samples

Simulated complex samples with mixed toxic activity and mercury contamination were analyzed with the three-leaf biosensor (Fig. 5.9A, B). Both colorimetric and BL biosensors showed a signal decrease directly proportional to the increased toxicity. For example, in the presence of 0.50 µM Hg^{2+} at pH 4.6 and pH 7.0, a similar signal decrease of 16% and 17% were obtained, for the *E. coli*-mercury-sensitive paper and β-gal paper, respectively. For the same concentration, the signal decrease obtained with the *A. fischeri* toxicity paper was 11%, confirming its suitability for signal correction. We next analyzed solutions with more acidic pH (pH 3.0, Figs. 5.9A, 5.10) that caused an almost complete cell death of *A. fischeri* bacteria (BL signal corresponding to 4% of the control BL signal), supporting the necessity to perform a signal correction to avoid artefact results. In fact, in the presence of 0.50 µM of Hg^{2+} at pH 3.0, the *E. coli* mercury-sensitive paper showed a response decrease of 85%. On the other hand, the β-gal paper, on the basis of β-galactosidase inhibition in the presence of mercury, showed a false positive response. An enzyme inhibition of 90% was detected

for acidic water (pH 3.0) without mercury, compared to 88% of enzymatic inhibition in the presence of 1.00 mM of Hg^{2+} (Fig. 5.9A). *A. fischeri*-paper was able to respond to different pH changes from 2.5 to 5.5. BL signal decreases of 8% and 96% were observed at pH 5.3 and pH 2.7, respectively. Acute cytotoxicity was found starting at pH 4.0 with loss of 60% of cell viability. Therefore, to properly correct the analytical signal, we defined a viability threshold corresponding to 20% of cell toxicity, obtained at pH 4.5. DMSO was used as model toxic analyte to simulate general sample toxicity and to investigate the suitability of analytical signal correction according to the control signal obtained with the *A. fischeri* toxicity paper. A fixed concentration of Hg^{2+} (0.50 µM) was mixed with varying DMSO concentrations before biosensor response was evaluated. A signal decrease was observed with 0.50 µM Hg^{2+} and DMSO concentrations higher than 5%$_{v/v}$. A 5%$_{v/v}$ DMSO concentration caused *A. fischeri* cytotoxicity of 13% and a signal decrease of 41% and 15% for *E. coli* mercury-sensitive paper and β-gal paper, respectively (Fig. 5.9). With such high level of toxicity signal correction therefore could not be applied. A mercury(II) concentration of 0.49 ± 0.02 µM was calculated by applying the correction of analytical signal for a sample containing DMSO 0.5%$_{v/v}$ and 0.50 µM of Hg^{2+} while without the correction a concentration of mercury(II) of 0.45 ± 0.02 µM was obtained, demonstrating the usefulness of the signal correction for the analysis of toxic samples. The calculated recovery was 98%, while a 90% recovery was obtained without applying the signal correction. However, for samples causing excessive cell death, the correction did not allow to obtain accurate results. For example, the recovery for a sample with 0.50 µM of Hg^{2+} and DMSO 25%$_{v/v}$ was 81% with signal correction (Table 5.1). In this case, a biosensor viability threshold was set for samples having cytotoxicity ≥ 20% (obtained with DMSO confrontations ≥ 10%$_{v/v}$). DMSO 10%$_{v/v}$ caused a signal decrease of 55% for the *E. coli*-paper and 44% for the β-gal paper.
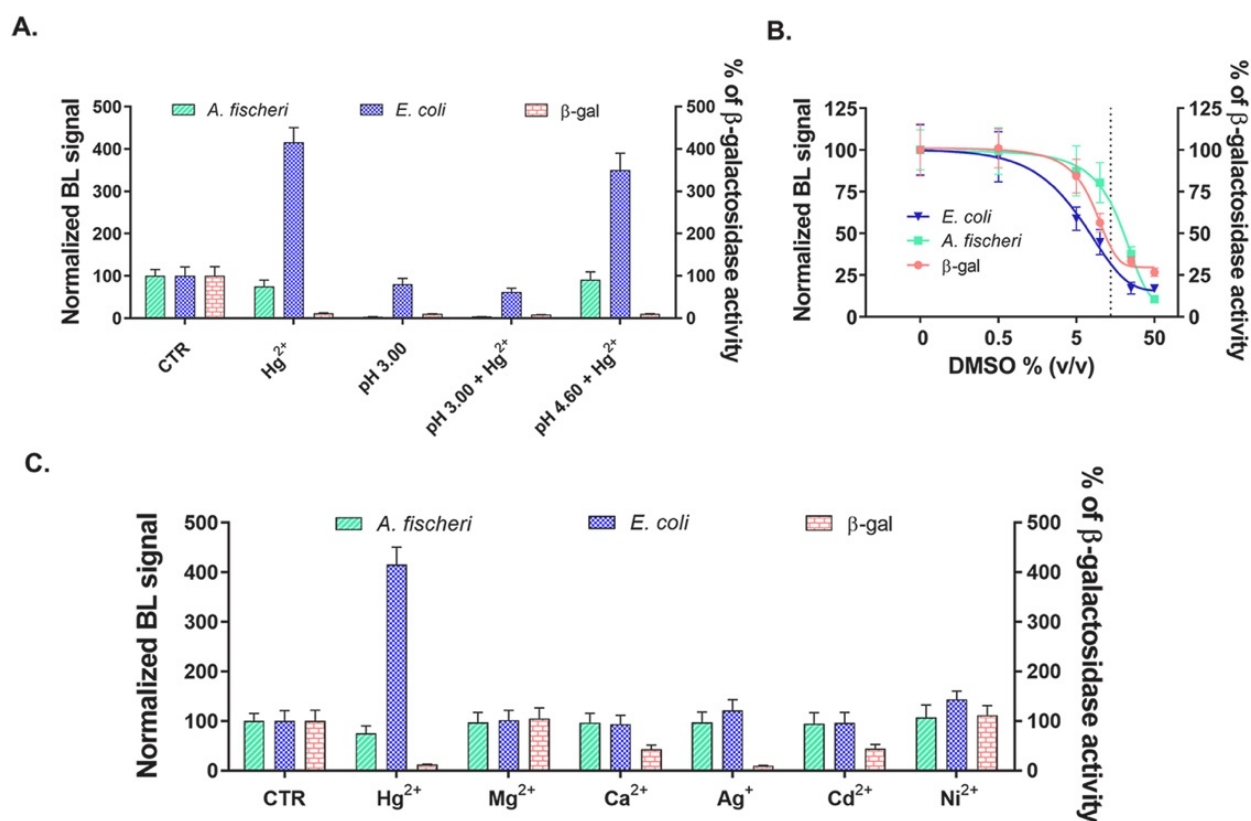
Fig. 5.9: *Mercury(II) detection with the three-leaf biosensor, interference and selectivity studies. A) Biosensor response to simulated complex samples with Hg^{2+} and pH-induced cytotoxicity effect; B) Biosensor inhibition induced by increasing cytotoxicity effect of varying DMSO concentrations with Hg^{2+} 0.50 µM; C) Biosensor response to different interferents (1.00 µM).*

5.3.8 Specificity studies

The three-leaf biosensor specificity was evaluated with various interferents measured at a concentration of 1.00 µM (Figs. 5.9 and 5.10). Control well signals were normalized as 100% of signal for all the sensing papers. In the presence of 1 mM Hg^{2+}, used as the positive control, an induction of 400% for *E. coli* mercury-sensitive paper and an inhibition of 88% for β-gal paper was reached. No interference was detected for both sensing papers in the presence of highly concentrated Mg^{2+} (101% and 104% for the *E. coli* mercury sensitive paper and the β-gal paper). A different behavior was observed in the presence of Ca^{2+} no induction was reported with the *E. coli* mercury-sensitive paper, while a 43% inhibition was reported with the β-gal paper. A similar behavior was found with Cd^{2+} which caused a 44% inhibition of β-gal while no signal increase was reported for the *E. coli* mercury-sensitive paper. In contrast, 1.00 µM Ni^{2+} showed no inhibition of β-gal activity, in agreement with previous reports (Hossain and Brennan, 2011), and a low induction of *E. coli* mercury-sensitive paper (143%). At the same concentration, Ag$^+$ showed a low level of induction

(121%) for *E. coli* mercury-sensitive paper and an almost complete inhibition (91%) for β-GA β-gal paper. The inhibition of Ag^+ and Cd^{2+} is consistent with previous reports (Hossain and Brennan, 2011) and, while Ag^+ is not a commonly encountered water contaminant, the presence of Cd^{2+} in drinking water and rivers, even at low concentrations, is toxic to all living organisms, with a maximum limit in groundwater of 3.00 μg/L (WHO, 2004). Excluding mercury, none of the metals at the tested concentration (1.00 μM) showed significant cytotoxic effects; the highest cytotoxicity effects were obtained with Cd^{2+} with a 6% of signal decrease (Fig. 5.10).
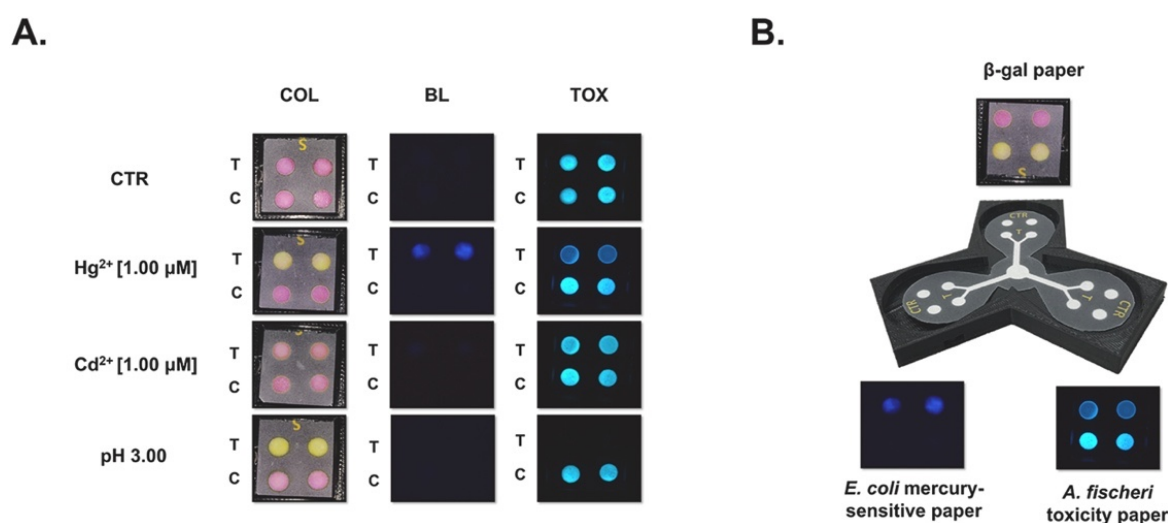

Fig. 5.10: *Selectivity studies. A) Pictures of the three-leaf biosensor responses to different compounds and with different simulated complex samples; B) Images showing the results of the three-leaf biosensor for Hg^{2+} detection.*

5.3.9 Recovery studies

Recovery studies were performed to demonstrate the applicability of the three-leaf paper biosensor for mercury(II) detection in water samples and in simulated toxic samples. Water samples were spiked with different mercury concentrations in the presence of a toxic compound (DMSO). In the absence of toxicity ($0\%_{v/v}$ DMSO) both the colorimetric and BL sensing papers provided a good recovery for all the tested concentrations (Table 5.1). With $10\%_{v/v}$ and $25\%_{v/v}$ DMSO concentrations a toxicity of 20% and 50% was observed with the *A. fischeri* toxicity paper and a different behavior was observed for the *E. coli* mercury-sensitive paper and the β-gal paper. In the presence of $2.5\%_{v/v}$ DMSO and 0.25 μM of Hg^{2+} (toxicity lower than 10%) a recovery of 112% was obtained by applying the *A. fischeri* signal correction. In contrast, at higher toxicity, such as with 25% DMSO a complete inhibition of β-gal was observed. This inhibition, without the inclusion of a toxicity sensor paper in the

same device, could cause an erroneous interpretation with a false positive output. Therefore, this approach could be extended to all biosensors relying on living cells or enzymes to avoid artefact results.

DMSO (%$_{v/v}$)	HgCl$_2$ (µM)	BL detection			COL detection		
		Found - Tox corrected (µM)	Recovery (%)	RDS (%)	Found (µM)	Recovery (%)	RDS (%)
0	5.00x10^{-3}	5.36x10^{-3} ± 5.89x10^{-4}	107± 12	11	*n.d.*	*n.d.*	*n.d.*
	0.10	0.11 ± 0.01	111 ± 10	9	0.10 ± 8.00x10^{-3}	101 ± 8	8
	0.25	0.22 ± 0.02	88 ± 8	9	0.27 ± 0.03	110 ± 13	12
	1.00	1.14 ± 0.09	114 ± 9	8	0.98 ± 0.08	98 ± 8	8
2.5	5.00x10^{-3}	5.84x10^{-3} ± 6.31x10^{-4}	117 ± 13	11	*n.d.*	*n.d.*	*n.d.*
	0.10	0.15 ± 0.02	150 ± 20	13	0.13 ± 9.00x10^{-3}	128 ± 9	7
	0.25	0.28 ± 0.03	112 ± 12	11	0.30 ± 0.03	121 ± 13	10
	1.00	1.08 ± 0.09	108 ± 9	8	1.01 ± 0.08	101 ± 8	8
10	5.00x10^{-3}	8.30x10^{-3} ± 7.20x10^{-4}	1650 ± 143	8	*n.d.*	*n.d.*	*n.d.*
	0.10	0.13 ± 7.74x10^{-3}	133 ± 8	6	0.92 ± 0.07	924 ± 70	7
	1.00	0.92 ± 0.11	91 ± 11	12	1.05 ± 0.09	105 ± 9	9
25	5.00x10^{-3}	*n.d.*	*n.d.*	*n.d.*	*n.d.*	*n.d.*	*n.d.*
	0.25	0.20 ± 0.03	81 ± 11	13	1.08 ± 0.10	431 ± 40	9
	1.00	0.74 ± 0.09	73 ± 9	12	1.11 ± 0.08	111 ± 8	7

Table 5.1: *Recovery of mercury (II) in lake water (n = 3). n.d.: not detectable*

5.3.10 Biosensor's stability evaluation

The reproducibility of the immobilization procedures was evaluated using the constitutive BL signal of *A. fischeri* immobilized according to the procedure described in the experimental section with agarose (7.5%$_{w/v}$) and trehalose (10%$_{w/v}$). We obtained, by immobilizing approximately 8×10^7 cells/well an average BL signal of 1.35×10^6 RLU and a CV% of 18%

(30 wells). An increased BL signal (1.2 fold higher) of freshly immobilized bacteria was observed for bacteria immobilized in calcium alginate compared to those immobilized into agarose gel. However, no significant signal changes were reported after 7 days storage for the two immobilization methods. Instead, a significant increase of BL signal was observed for bacteria immobilized in either agarose or calcium alginate supplemented with trehalose (10%$_{w/v}$) and milk (10%$_{v/v}$). The addition of trehalose (10%$_{w/v}$) resulted in BL signal 2.7 and 2.9 fold higher (at time 0) for bacteria immobilized in calcium alginate and in agarose, respectively; the addition of milk caused 2.9 and 2.2 fold increase of BL signal for calcium alginate and agarose, respectively. Unexpectedly, no significant viability improvement was observed after storage with both supplements. The *A. fischeri* toxicity paper supplemented with agarose 0.75%w/v remained responsive for 7 days, at 4°C, sealed in plastic bag, with a maximum signal decrease of 25% and CV% of 19%. As for the *A. fischeri* paper the same stability was evaluated for the *E. coli* mercury-sensitive paper. Concerning the β-gal paper, the stability was evaluated up to 2 months by lyophilizing 5 μL of 1 U/mL β-galactosidase with 20 %$_{v/v}$ of R18 medium directly on the paper. The β-gal paper was sealed in plastic bags and stored at 4°C. The enzymatic activity of the β-gal paper after 24, 48, 72 h and 1 week was 100%, 103%, 98% and 106% respectively. After 4 weeks the enzymatic activity was 94% while after 5 weeks a 45% decrease in the enzymatic activity was observed. After 2 months the enzymatic activity was equal to 24% of the initial one.

5.4 Conclusions

We developed a new biosensor integrating two different biorecognition elements, responding to the same analyte, mercury(II), and a toxicity control in the same device to improve the robustness and ac- curacy of mercury(II) detection in complex samples, such as samples with a certain level of toxicity. The integration of microbial biosensors and enzymes combined with exploitation of different optical detection modes, i.e., BL and colorimetric detection, allowed us to develop a biosensor with higher robustness and did not affect neither the complexity of the biosensor design nor the workflow of assay procedure. In fact, the inclusion of β-gal, having a response time within 15 min, provides a very quick response about presence of potential health threats well in advance to the light signal emitted by the mercury-sensitive whole-cell biosensor, which requires 1 h of incubation with the sample. Moreover, the lack of specificity of β-gal, which is certainly a drawback in standard laboratory-based analytical techniques, turns out to be useful to provide a first level "warning" about the possible presence of other toxic heavy metals such as cadmium. In

addition, thanks to the inclusion of a pre-made substrate-paper containing chromogenic and BL substrates the device does not require additional steps such as substrate addition, simplifying the assay procedure and enabling its use by non-skilled personnel. Owing to its analytical performance we envisage possible applications of the developed biosensor to monitor drinking water, surface waters or industrial waters as a rapid and low-cost screening tool in the field before more accurate and expensive analysis are performed.

5.5 Acknowledgements

5.6 References

Bae, J.W., Seo, H.B., Belkin, S., Gu, M.B., 2020. Anal. Bioanal. Chem. 412, 3373–3381.

Bergua, J.F., A ́lvarez-Diduk, R., Hu, L., Hassan, A.H., Merkoçi, A., 2021. J. Hazard Mater. 406, 124434.

Calabretta, M.M., A ́lvarez-Diduk, R., Michelini, E., Roda, A., Merkoçi, A., 2020. Biosens. Bioelectron. 150, 111902.

Calabretta, M.M., Montali, L., Lopreside, A., Fragapane, F., Iacoangeli, F., Roda, A., Bocci, V., D'Elia, M., Michelini, E., 2021. Anal. Chem. 93 (20), 7388–7393.

Camanzi, L., Bolelli, L., Maiolini, E., Girotti, S., Matteuzzi, D., 2011. Environ. Toxicol. Chem. 30, 801–805.

Cevenini, L., Lopreside, A., Calabretta, M.M., D'Elia, M., Simoni, P., Michelini, E., Roda, A., 2018. Anal. Bioanal. Chem. 410, 1237–1246. EFSA Scientific Committee, 2015. EFSA journal 13 (1), 3982.

European Commission, 2012. Report from the Commission to the European Parliament and the Council on the Implementation of the Water Framework Directive (2000/ 60/EC) River Basin Management Plans.

European Environment Agency, 2018. Mercury in Europe's Environment: A Priority for European and Global Action. Publications Office of the European Union.

Gu, M.B., Mitchell, R.J., Kim, B.C., 2004. Biomanufact, pp. 269–305.

Gu, Z., Zhao, M., Sheng, Y., Bentolila, L.A., Tang, Y., 2011. Anal. Chem. 83, 2324–2329.

Guo, M., Wang, J., Du, R., Liu, Y., Chi, J., He, X., Huang, K., Luo, Y., Xu, W., 2020. Biosens. Bioelectron. 150, 111899.

Hall, M.P., Kincaid, V.A., Jost, E.A., Smith, T.P., Hurst, R., Forsyth, S.K., Fitzgerald, C., Ressler, V.T., Zimmermann, K., Lazar, D., Wood, M.G., Wood, K.V., Kirkland, T.A., Encell, L.P., Machleidt, T., Dart, M.L., 2021. Anal. Chem. 93, 5177–5184.

Hossain, S.M., Brennan, J.D., 2011. Anal. Chem. 83, 8772–8778.

Jung, I., Seo, H.B., Lee, J.E., Kim, B.C., Gu, M.B., 2014. Analyst 139, 4696–4701.

Lee, J.H., Mitchell, R.J., Kim, B.C., Cullen, D.C., Gu, M.B., 2005. Biosens. Bioelectron. 21 (3),500–507.

Lemm, J.U., Venohr, M., Globevnik, L., Stefanidis, K., Panagopoulos, Y., van Gils, J., Posthuma, L., Kristensen, P., Feld, C.K., Mahnkopf, J., Hering, D., Birk, S., 2021. Global Change Biol. 27 (9), 1962–1975.

Leopold, K., Foulkes, M., Worsfold, P., 2010. Anal. Chim. Acta 663 (2), 127–138.

Li, L., Zhang, L., Zhao, Y., Chen, Z., 2018. Microchim. Acta. 185, 235.

Liu, J., Morales-Narv́aez, E., Orozco, J., Vicent, T., Zhong, G., Merkoçi, A., 2018. Nano Res.11(1),114–125.

Lobsiger, N., Venetz, J.E., Gregorini, M., Christen, M., Christen, B., Stark, W.J., 2019. Biosens.Bioelectron. 146, 111710.

Lopreside, A., Calabretta, M.M., Montali, L., Ferri, M., Tassoni, A., Branchini, B.R., Southworth, T., D'Elia, M., Roda, A., Michelini, E., 2019a. Anal. Bioanal. Chem. 411 (19), 4937–4949.

Lopreside, A., Wan, X., Michelini, E., Roda, A., Wang, B., 2019b. Anal. Chem. 91, 15284–15292.

Ma, Z., Liu, J., Sallach, J.B., Hu, X., Gao, Y., 2020. Biosens. Bioelectron. 168, 112528.

Mirasoli, M., Feliciano, J., Michelini, E., Daunert, S., Roda, A., 2002. Anal. Chem. 74, 5948–5953.

Montali, L., Calabretta, M.M., Lopreside, A., D'Elia, M., Guardigli, M., Michelini, E., 2020. Biosens. Bioelectron. 162, 112232.

Roda, A., Roda, B., Cevenini, L., Michelini, E., Mezzanotte, L., Reschiglian, P., Hakkila, K., Virta, M., 2011. Anal. Bioanal. Chem. 401, 201–211.

Sahin, S., Caglayan, M.O., Üstündag, Z., 2020. Talanta 220, 121437.

Sajed, S., Arefi, F., Kolahdouz, M., Sadeghi, M.A., 2019. Sensor. Actuator. B Chem. 298, 126942.

Selifonova, O., Burlage, R., Barkay, T., 1993. Appl. Environ. Microbiol. 59, 3083–3090.

Shemer, B., Shpigel, E., Hazan, C., Kabessa, Y., Agranat, A.J., Belkin, S., 2020. Microb. Biotechnol. 14, 251–261.

Stocker, J., Balluch, D., Gsell, M., Harms, H., Feliciano, J., Daunert, S., Malik, K.A., Van der Meer, J.R., 2003. Environ. Sci. Technol. 37, 4743–4750.

U.S. EPA, 2009. National Primary Drinking Water Regulations. https://www.epa.gov/ground-water-and-drinking-water/national-primary-drinking-water-regulations.

Van der Meer, J.R., Belkin, S., 2010. Nat. Rev. Microbiol. 8, 511–522.

Wan, X., Volpetti, F., Petrova, E., French, C., Maerkl, S.J., Wang, B., 2019. Nat. Chem. Biol. 15, 540–548.

Wang, B., Barahona, M., Buck, M., 2013. Biosens. Bioelectron. 40, 368–376.

WHO, 2004. Cadmium in Drinking-Water: Background Document for Development of WHO Guidelines for Drinking-Water Quality. World Health Organization, Geneva. WHO, 2011. Guidelines for Drinking Water Quality, fourth ed. World Health Organization, Geneva http://whqlibdoc.who.int/publications/2011/9789241548151_eng.pdf.

Zhong, Y.Q., Ning, T.J., Cheng, L., Xiong, W., Wei, G.B., Liao, F.S., Ma, G.Q., Hong, N., Cui, H.F., Fan, H., 2021. Talanta 23, 121709.

6

A Genetically Encoded Bioluminescence Intracellular Nanosensor for Androgen Receptor Activation Monitoring in 3D Cell Models

6.1 Introduction

The availability of reliable tools for the rapid detection of protein–protein interactions (PPI) has become necessary for identifying biologically active compounds, especially in the early phases of drug discovery (Misawa et al., 2010; Shin et al., 2020). Among the different methods that are available, split proteins have provided an elegant way to detect and image PPI in real time (Biewenga et al., 2020). A reporter protein can be split into two fragments that can spontaneously reassemble, without covalent linking, to reconstitute the functional protein. Therefore, the cDNAs encoding for the two fragments can be genetically fused to produce two genes encoding for the target proteins under investigation; these genetically encoded sensors can be inserted into living cells and, after interaction of the two target proteins, functional reassembly of the split protein will occur (Lang et al., 2019; Cevenini et al., 2015).

A pivotal work, describing the exploitation of split reporters in protein-fragment complementation assays (PCA) for targeting PPI, was reported by Johnsson and Varshavsky with a split ubiquitin (Johnsson and Varshavsky, 1994). Since then, several reporter proteins have been used in PCA, such as the Green Fluorescent Protein (GFP) and its variants (Romei and Boxer, 2019), B-galactosidase (Rossi et al., 1997), and different luciferases (Luker et al., 2004; Paulmurugan and Gambhir, 2007; Oladzad et al., 2020). One of the main limitations of split reporters is that they rely on nonspecific reassembly of the fragments in the absence of an interaction between the target proteins and on irreversible protein complementation. To circumvent these issues, Dixon et al. developed a new complementation reporter, called NanoLuc Binary Technology (NanoBiT), starting from the engineered luciferase NanoLuc derived from a deep-sea luminous shrimp. NanoLuc luciferase is characterized by an enhanced bioluminescence, making it an excellent reporter for cell-based assays (England et al., 2016). NanoBiT has two subunits: A large one (LgBiT) and a small peptide one (SmBiT), of 18 and 1.3 kDa, respectively, characterized as having a very low affinity. Notably, the reassembly is reversible, thus enabling both protein association and dissociation to be monitored (Biewenga et al., 2020). NanoBiT has been successfully applied to monitor PPI and detect intracellular calcium levels (Nguyen et al., 2020), endosome disruption (Kilchrist et al., 2020), and circulating microRNAs with such a high sensitivity that it could be implemented in smartphone-based assays (Zhou et al., 2021). In another configuration, split reporter proteins provide a single-molecule probe to monitor ligand-induced conformational

changes in a single molecular backbone (Kim et al., 2007; Kim et al., 2009; Paulmurugan and Gambhir, 2006). An elegant modular sensor was developed by Ni et al., based on competitive intramolecular complementation of split NanoLuc luciferase, allowing tuning of the sensor's dynamic range (Ni et al., 2019). Folding sensors relying on human estrogen receptor ligand-binding domain (hER-LBD) fusion proteins leading to split Renilla/firefly luciferase reporter complementation were particularly successful in detecting estrogens and antiestrogens both in cell cultures and for the in vivo imaging of ligand- induced intramolecular folding in living mice (Paulmurugan and Gambhir, 2006). Analogously, the human androgen receptor binding domain (hAR-LBD) was sandwiched between a dissected click beetle luciferase (Kim et al., 2007). The androgen receptor is a ligand-activated nuclear transcription factor that is responsible for mediating the intracellular action of androgens (Van Royen et al., 2007). It is involved in the maintenance and function of male reproductive organs and plays a key role in prostate cancer and other pathologies. Since its role is exerted via homodimerization and interactions with cofactors, PCA was proposed for screening adverse chemicals acting on the androgen receptor and new therapeutic targets (Kim et al., 2007).

All these assays are generally performed either in vitro using purified chimeric proteins or with conventional two-dimensional (2D) cell cultures. Although these cell models are still considered the "gold standard", a growing body of evidence suggests that they fail to replicate the in vivo complexity and actual cellular architecture comprising the extracellular matrix (ECM) microenvironment and cell–cell interactions (Brancato et al., 2020). 3D cell culture systems overcome many of the limitations of traditional 2D cell culture systems, more closely mimicking the complex phenotypic heterogeneity that chemical gradients produce during cell growth. In fact, 3D cellular systems reproduce cell–cell and cell– matrix interactions, intra- and inter-cellular signaling networks, and diffusion/transport conditions, which are important for differentiation, proliferation, and various cellular functions. We previously demonstrated the suitability of using bioluminescence (BL) as a detection technique for reporter assays developed in 3D cell models from human cell lines (Calabretta et al., 2020).

We hereby report an intracellular nanosensor for androgenic activity detection relying on the human androgen receptor (hAR) fused to NanoBiT that can be employed in 2D and 3D cell models (Fig. 6.1). Human Embryonic Kidney (HEK-293) cells were transiently transfected with vectors expressing the two chimeric proteins LgBiT-hAR and hAR-SmBiT

under the control of a constitutive promoter. This genetically encoded sensor also represents a new tool for real time imaging of the activation state of the androgen receptor, thus being suitable for analyzing molecules with androgenic activity, including new drugs or endocrine disrupting chemicals.
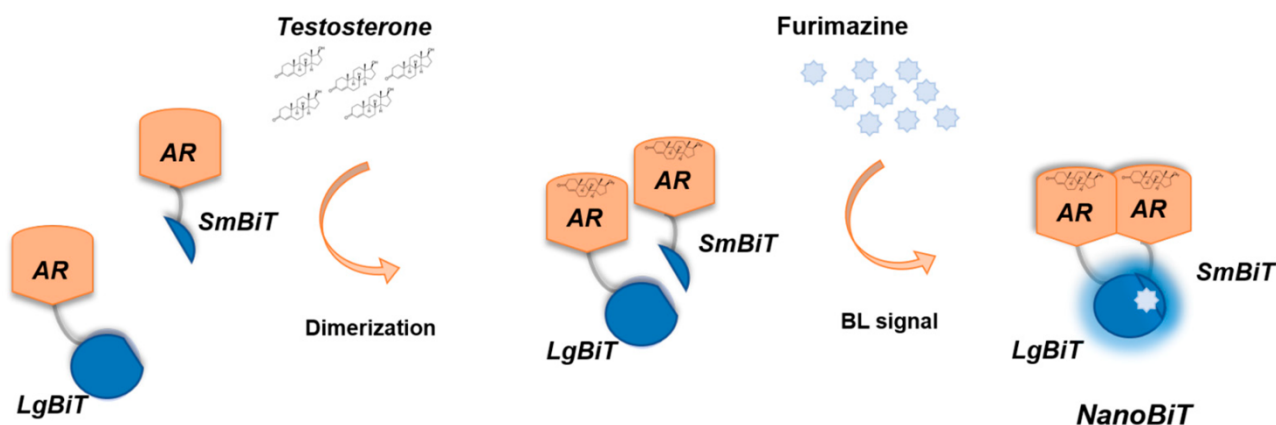

Fig. 6.1: *Schematic representation of the genetically encoded nanosensor principle. A large NanoLuc Binary Technology (NanoBiT) subunit (LgBiT) and small NanoBiT subunit (SmBiT) are genetically fused to the human androgen receptor (hAR), in the presence of testosterone, used as a model ligand with androgenic activity. Dimerization of hAR causes the reconstitution of NanoBiT luciferase, which in turn will emit light after the addition of the furimazine substrate.*

6.2 Materials and Methods

6.2.1 Reagents and Plasmids

Human embryonic kidney HEK293 cells were obtained from the American Type Culture Collection (ATCC, Manassas, VA, USA), and penicillin, streptomycin, and all cell culture reagents were obtained from Carlo Erba Reagents (Cornaredo, Milano, Italy). Enzymes for PCR and the cloning procedure (FastDigest, FastDigest Green Buffer, FastAP Thermosensitive Alkaline Phosphatase, T4 DNA ligase and Phusion high-fidelity DNA polymerase) were obtained from ThermoFisher Scientific (Waltham, MA, USA). The reporter vectors pGL3-SV40-LgBiT-hAR and pGL3-SV40-hAR-SmBiT were obtained by standard molecular cloning procedures. The PureYieldTM Plasmid Miniprep System kit, gel, and PCR extraction kit were obtained from Promega (Promega, Madison, WI, USA). The Nano-Glo Live Cell Assay System substrate and FuGENE HD transfection reagent were obtained from Promega (Promega, Madison, WI, USA). The 96-well microspace round-bottom cell culture plates were obtained from Elplasia (Kuraray, Japan). Testosterone and all other chemicals were purchased from Sigma-Aldrich (St. Louis, MO, USA).

6.2.2 Plasmids Construction

Standard molecular biology techniques were used to construct plasmids driving the constitutive expression of chimeric proteins hAR-SmBiT and LgBiT-hAR under different promoters. The hAR-SmBiT and LgBiT-hAR sequences were kindly provided by Promega (Promega, Madison, WI, USA). The herpes simplex virus (HSV) thymidine kinase (TK) promoter and early promoter of the simian virus 40 (SV40) were selected for constitutive expression in mammalian cells using pGL3 (SV40) and pTK vectors. hAR-SmBiT and LgBiT-hAR sequences were amplified by a polymerase chain reaction (PCR) and cloned using NheI and SalI fast digestion enzymes. The developed mammalian expression vectors were called pTK-hAR-SmBiT, pTK-LgBiT-hAR, pGL3 (SV40)-hAR-SmBiT, and pGL3 (SV40)-LgBiT-hAR. All vector sequences were confirmed by restriction analysis and sequencing (Fig. 6.2).
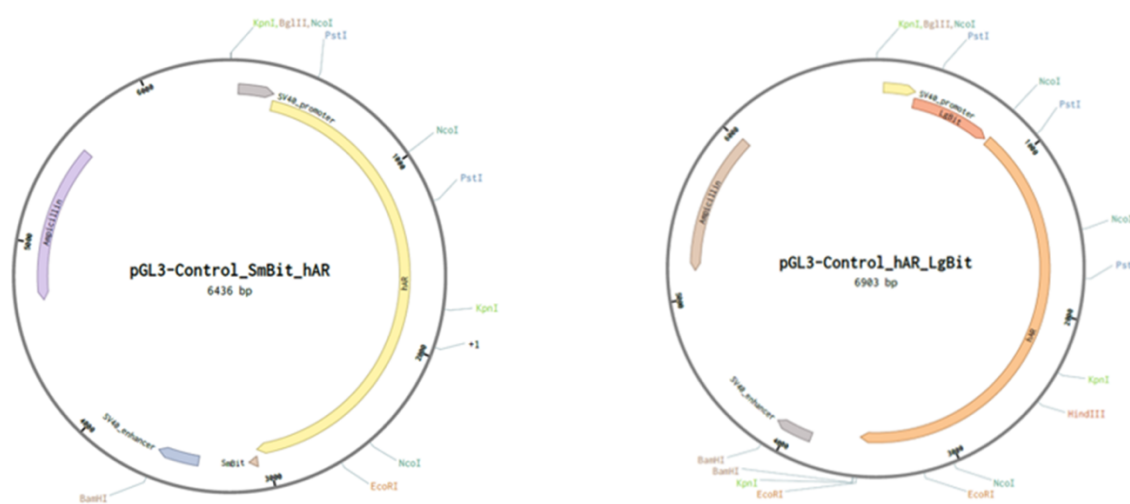

Fig. 6.2: *Representative plasmid maps for the vectors pGL3-Control-SV40-hAR-SmBiT and pGL3-Control-SV40-LgBiT-hAR.*

6.2.3 Comparison of TK and SV40 Promoters

To evaluate the expression of chimeric proteins hAR-SmBiT and LgBiT-hAR under the regulation of different promoters (TK and SV40) and to define the optimal co-transfection conditions and incubation times, HEK293 cells, cultured using Dulbecco's Modified Eagle's Medium (DMEM) supplemented with 10% (v/v) FBS, 2 mM L-glutamine, 50 U/mL penicillin, and 50 μg/mL streptomycin, were plated in flat-bottom clear 24-well plates at a density of 8.0×10^4 cells/well with 500 μL of complete growth medium and incubated under standard conditions for 24 h (37°C, 5% CO_2). After overnight incubation, medium was removed from

the cells, washed with PBS 0.1 M pH 7.2, and replaced with DMEM fresh medium containing 10% (v/v) FBS charcoal stripped, 2 mM L-glutamine, 50 U/mL penicillin, and 50 μg/mL streptomycin. Following this, HEK293 cells were transiently co-transfected with 0.25 μg pTK-hAR-SmBiT and 0.25 μg pTK-LgBiT-hAR, using the FUGENE® HD standard protocol with a ratio of 3:1. In parallel, HEK293 were co-transfected with 0.25 μg of the pGL3-SV40-LgBiT-hAR construct and 0.25 μg of pGL3-SV40-hAr-SmBiT using the FUGENE® HD standard method with a ratio of 3:1.

BL measurements were carried out after 24 and 48 h post-transfection. In particular, HEK293 cells were washed with PBS 0.1 M pH 7.2, detached with Trypsin 1X, and centrifugated for 5 min at 1200 rpm. After resuspension with PBS 0.1 M pH 7.2, an 87.5 μL volume of cell suspension ($5.0×10^4$ cells) was seeded in a 96-well black microplate. The basal signal was measured for 1 min using Tecan Microplate Reader Spark® (Tecan Trading AG, Switzerland) and the basal BL activity was measured for 3 min after the addition of 25 μL/well of 5× Nano-Glo® Live Cell Assay System substrate. Finally, cells were treated with 12.5 μL of testosterone solution (final concentration of 100 nM) prepared in ethanol solution 1% (v/v) or with 12.5 μL of ethanol solution 1% (v/v) as a control. BL measurements were performed in real time with Tecan Microplate Reader Spark®, acquiring BL signals for 100 min.

6.2.4 2D Cell Culture, Transfection, and PPI Assay

The HEK293 cell line was cultured using DMEM supplemented with 10% (v/v) FBS, 2 mM L-glutamine, 50 U/mL penicillin, and 50 μg/mL streptomycin. The day before transfection, cells were plated in flat-bottom clear 24-well plates at a density of $8.0×10^4$ cells/well with 500 μL of complete growth medium and incubated under standard conditions for 24 h (37°C, 5% CO_2). After overnight incubation, medium was removed from the cells, washed with PBS 0.1 M pH 7.2, and replaced with DMEM fresh medium containing 10% (v/v) FBS charcoal stripped, 2 mM L-glutamine, 50 U/mL penicillin, and 50 μg/mL streptomycin. Afterwards, HEK293 cells were transiently co-transfected with 0.25 μg of the pGL3-SV40-LgBiT-hAR construct and 0.25 μg of pGL3-SV40-hAR-SmBiT using the FUGENE®HD standard method with a ratio of 3:1. At 48 h post-transfection, HEK293 cells were washed with PBS 0.1 M pH 7.2, detached with Trypsin 1X, centrifugated for 5 min at 1200 rpm, and resuspended with PBS 0.1 M pH 7.2. A volume of 87.5 μL of cell suspension containing $5.0×10^4$ cells was seeded per well in a 96-well black microplate. The basal signal was measured for 1 min by Tecan Microplate Reader Spark® and the basal BL activity was measured for 3 min after the

addition of 25 µL/well of 5× Nano-Glo® Live Cell Assay System substrate. Finally, cells were treated in triplicate with 12.5 µL of testosterone solutions (concentration range from 0.001 to 100 nM) prepared in ethanol solution 1% (v/v) or with 12.5 µL of ethanol solution 1% (v/v) as a control. BL measurements were performed in real time with Tecan Microplate Reader Spark®, acquiring BL signals for 100 min. The correct BL signal was obtained by subtracting the basal signal of each well from its BL signal, while the testosterone dose-response curve was generated using GraphPad Prism software normalized to the BL signal of the control. All measurements were performed in triplicate and repeated at least three times. The detection limit is defined as the testosterone concentration that corresponds to the blank plus three times the standard deviation (s.d.).

The half maximal effective concentration (EC50), which is the concentration of testosterone which produces 50% of the maximum possible response, was calculated using the following equation: Y = Bottom + (Top-Bottom)/(1 + 10^((LogEC50-X) * Hillslope)), where X is the logarithmic concentration of testosterone, Y is the response, and Y starts at the Bottom and goes to the Top with a sigmoid shape. Data were analyzed using GraphPad Prism software.

6.2.5 3D Cell Culture, Transfection, and PPI Assay

For PPI luminescence readout in 3D cell culture models, co-transfection was carried out in a 24-well clear flat-bottom plate with the same procedure reported for the 2D cell-based assay. At 24 h post-transfection, cells were washed with PBS 0.1 M pH 7.2, detached with Trypsin 1X, centrifugated for 5 min at 1200 rpm, and resuspended with fresh medium added with 10% (v/v) FBS charcoal stripped. Before cell seeding in 96-well microspace round-bottom cell culture plates (ElplasiaTM Kuraray, Tokyo, Japan), 100 µL of complete culture medium was added to each well, followed by 200 µL of cell suspension containing 3.0×10^4 cells per well. Spheroid formation was obtained by incubating the plate at 37°C and 5% CO_2.

Brightfield images of HEK293 spheroids were used to calculate the sphericity factor (φ) employing ImageJ version 1.51d software to define each spheroid's perimeter (P) and projected area (A):

$$\varphi = \frac{\pi x \sqrt{(\frac{4A}{\pi})}}{P} \qquad (1)$$

6.2.6 2D Live Cell Imaging

HEK293 cells, grown in 2D flat-bottom clear 24-well plates for 24 h, were washed with 200 µL of PBS 0.1 M pH 7.2 and the medium was replaced with DMEM supplemented with 10% (v/v) FBS charcoal stripped, 2 mM L-glutamine, 50 U/mL penicillin, and 50 µg/mL streptomycin. Then, cells were co-transfected with 0.25 µg pGL3-SV40-LgBiT-hAR and 0.25 µg of pGL3-SV40-hAR-SmBiT constructs using an FUGENE® HD/DNA ratio of 3:1 and incubated for 48 h at 37°C with 5% CO_2. Before each imaging session, cell culture medium was gently removed and replaced with 200 µL PBS 0.1 M pH 7.2 and BL imaging was performed using an Olympus CL40 inverted microscope connected to an electron multiplying charge-coupled device (EMCCD) camera (ImagEM-X2, Hamamtsu). Images of the 2D cell culture were obtained by acquiring the BL signal with a 20× objective using an integration time of 5 min, at a gain set to 500, and after 30 min, adding 60 µL/well of 5× Nano-Glo® Live Cell Assay System substrate signal and 40 µL of testosterone solution (100 nM final concentration) or 40 µL of ethanol solution 1% (v/v) as a control. All experiments were performed in triplicate and repeated at least three times.

6.3 Results

6.3.1 Characterization of the NanoBiT Reporter Expressed in 2D and 3D Cell Models

To preliminarily investigate the suitability of complementation of split NanoLuc luciferase in 2D and 3D cell models, bioluminescence measurements were performed in nonlysing conditions using HEK293 co-transfected with pGL3-SV40-LgBiT-hAR and pGL3-SV40-hAR-SmBiT constructs and treated with testosterone at a final concentration of 100 nM. The binding of testosterone to hAR activates a series of conformational changes leading to homodimerization and complementation of the split NanoLuc luciferase. We first characterized NanoBiT re-assembly in HEK293 grown as a monolayer and in HEK293 spheroids with an average diameter of 130 ± 20 µm. This size was selected because it has been shown to be suitable for maintaining an adequate cell viability with a negligible necrotic core, of less than 2% of cells (Langan et al., 2016; Anada et al., 2012; Cevenini et al., 2017). Since all BL systems require molecular oxygen, the availability of oxygen is a crucial factor in BL measurements. This is not an issue when cells are grown as a monolayer; however, it must be taken into consideration with 3D cell models. Therefore, spheroids with a maximum diameter of 150–200 µm were used. Emission spectra and kinetics were

measured to highlight issues that could circumvent BL detection in 3D cultures, such as substrate and oxygen availability issues at the core of spheroids. As expected, the emission spectrum of reconstituted NanoBiT did not significantly change when compared with that obtained with HEK293 monolayer cultures (Fig. 6.3a). The maximum emission wavelength was 460 nm in 2D cultures and 458 nm in 3D cultures, with a minor broadening effect reported in the 3D format, with a bandwidth at half-maximal intensity of 53 nm vs. 75 nm obtained in 2D cultures.
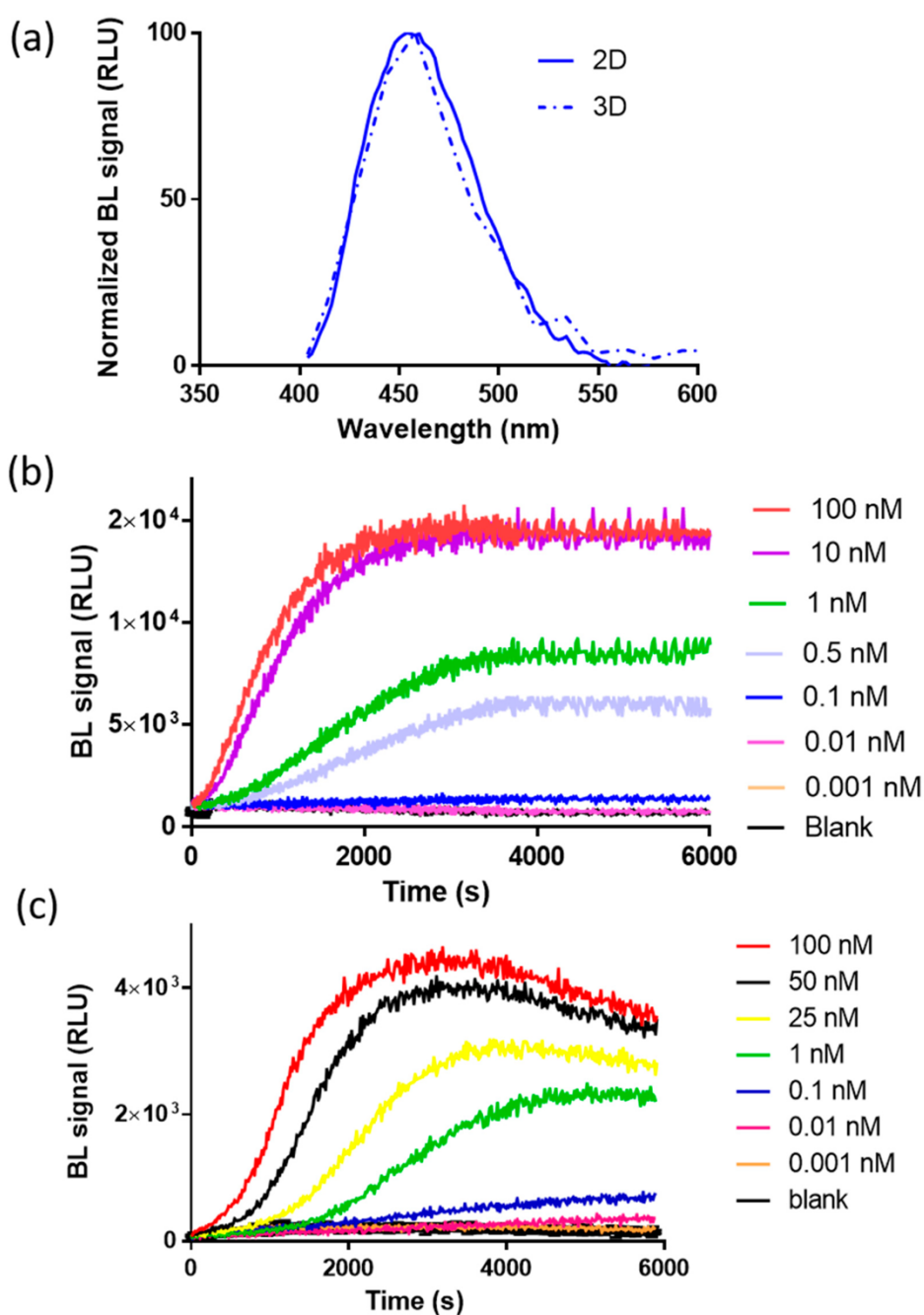
Fig 6.3: *Characterization of the bioluminescence (BL) nanosensor signal in 2D and 3D cells. (a) Normalized emission spectra of reconstituted NanoBiT in spheroids (dotted line) and in 2D cell cultures (solid line) after the addition of 100 nM of testosterone (final concentration). Emission spectra were obtained in nonlysing conditions using the Nano-Glo® Live Cell Assay System substrate; (b) emission kinetics of reconstituted NanoBiT in the 2D cell culture obtained in nonlysing condition after the addition of testosterone solutions (concentration range of 0.001–100 nM); (c) emission kinetics of reconstituted NanoBiT in HEK293 spheroids obtained in nonlysing condition after the addition of testosterone (concentration range of 0.001–100 nM).*

BL emission kinetics in 2D and 3D cell cultures were obtained by co-transfecting 2D and 3D HEK293 cell models with plasmids, driving the expression of LgBiT-hAR and hAR-SmBiT under the regulation of the SV40 promoter, after the addition of testosterone (concentration range from 0.001 to 100 nM), showing a glow-type emission with a maximum BL signal obtained at approximately 30 min after substrate addition in the 2D cell culture (Fig. 6.3b); the maximum signal was obtained at different times, depending on the testosterone concentration, ranging from 50 to 65 min in 3D cell culture models (Fig. 6.3c). We identified an optimal acquisition time window between 40 and 60 and 50 and 65 min for 2D and 3D cell models, respectively. To fully confirm the reconstitution of NanoBiT after testosterone addition, BL imaging of HEK293 cell (8.0×10^4 cells per well) monolayers co-transfected with plasmids driving the expression of LgBiT-hAR and hAR-SmBiT was performed (Fig. 6.4a). Cells were grown as a monolayer and 48 h post-transfection, were imaged using a 20× objective to identify single cells and allowing, by BL imaging, the direct visualization of AR dimerization in living cells at a subcellular level. Due to the lower BL intensities and blurry signals in 3D cell models, BL imaging performed in HEK293 spheroids did not provide additional information (data not shown).
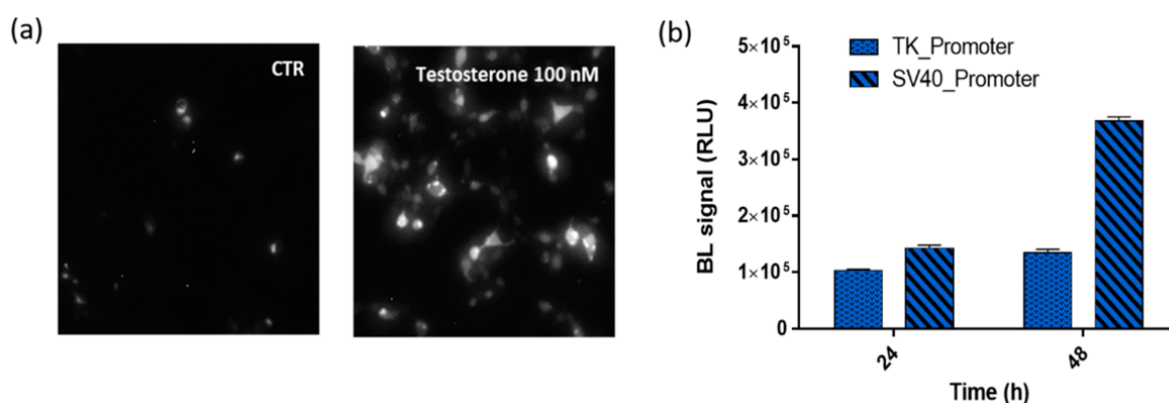

Fig. 6.4: *BL nanosensor expression. (a) BL imaging of the Human Embryonic Kidney (HEK293) monolayer culture (20× objective, 5-min acquisition) co-transfected with pGL3-SV40-LgBiT-hAR and pGL3-SV40-hAR-SmBiT and treated, 48 h post-transfection, with 100 nM testosterone solution or*

6.3.2 Comparison of Chimeric Protein Expression under TK and SV40 Promoters

Preliminary co-transfection studies were carried out to identify the optimal transfection conditions and to optimize the transfection efficiency with suitable amounts of LgBiT-hAR and hAR-SmBiT chimeric proteins. Different combinations were tested and using 50% of pGL3-SV40-LgBiT-hAR and 50% of pGL3-SV40-hAR-SmBiT provided the strongest signals and widest dynamic range. We investigated the suitability of using a strong SV40 and weak TK promoter and different post-transfection incubation times were evaluated (24 and 48 h).

The comparison of the BL emissions obtained from the two chimeric proteins LgBiT-hAR and hAR-SmBiT under the regulation of the TK and SV40 promoters is shown in Fig. 6.4b, where, at 24 and 48 h post-transfection, the TK/SV40 ratio is 0.75 and 0.38, respectively. Moreover, by comparing the same promoter at different post-transfection incubation times, the TK and SV40 promoters show a 48/24 h ratio of 1.4 and 2.66, respectively. These results confirmed that the brightest BL signal was obtained when using plasmids in which the two chimeric proteins LgBiT-hAR and hAR-SmBiT were under the regulation of the SV40 promoter.
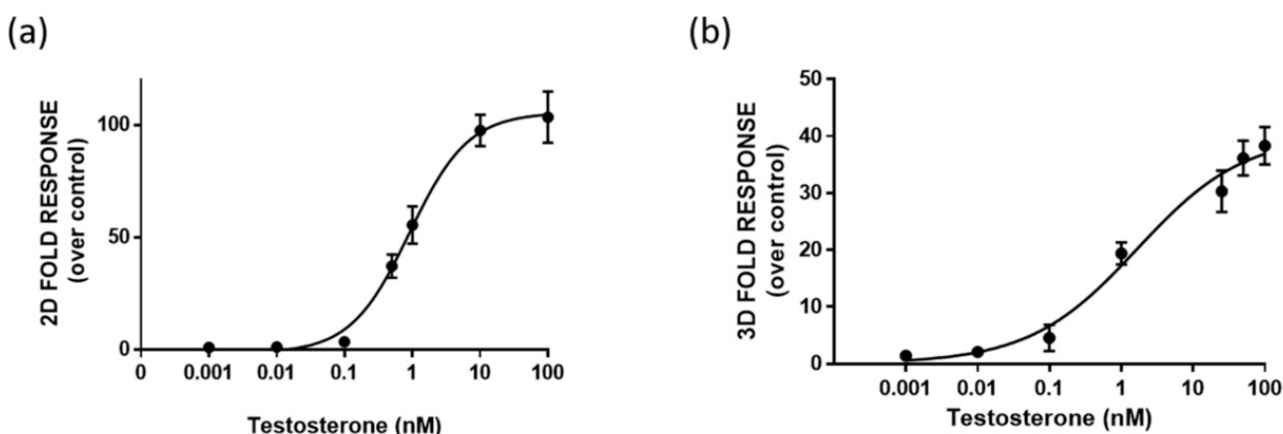

Fig. 6.5: *Dose-response curve for testosterone obtained in 2D cell culture (a) and 3D cell culture models (b). HEK293 cells were co-transfected with LgBiT-hAR and hAR-SmBiT under the regulation of the SV40 promoter and treated at 48 h with testosterone. BL measurements were obtained after the addition of Nano-Glo® Live Cell Assay System substrate. The results are expressed as the fold response over basal control activity. Data are the mean ± s.d. of at least three independent experiments, each performed in triplicate.*

6.3.3 3D Bioluminescent Assay for Androgen Receptor Activation Monitoring

One-day-old HEK293 spheroids, previously co-transfected in the 2D monolayer with plasmids driving the expression of LgBiT-hAR and hAR-SmBiT under the regulation of the SV40 promoter, were treated with different concentrations of testosterone (concentration range of 0.001–100 nM). HEK293 spheroids with a uniform size and shape exhibited BL emission that increased with the testosterone concentration in a dose-dependent matter. We chose to treat 1-day-old already-formed aggregates with a mean diameter of 130 ± 20 μM, in order to visualize the cell response after treatment, based on NanoBiT re-assembly in the presence of testosterone. Dose-response curves for testosterone and the calculated half maximal effective concentrations (EC50) were obtained with both 2D cell cultures and spheroids, obtaining EC50 values of 0.86 ± 0.02 and 1.7 ± 0.3 nM, respectively (Fig. 6.5a,b). A lower limit of detection (LOD) of 4 pM, calculated as the concentration that corresponds to the blank plus three times the standard deviation, was obtained in 3D spheroids in comparison to that obtained with 2D cells (40 pM). Moreover, dose-response curves for testosterone were obtained in HEK293 spheroids by analyzing BL signals at 30, 60, and 90 min (Fig. 6.6). LODs of 1.2 nM, 4 pM, and 1 pM were obtained at 30, 60, and 90 min, respectively. EC50 values were 36 ± 2, 1.7 ± 0.3, and 0.6 ± 0.1 nM, calculated at 30, 60, and 90 min, respectively. The light signal was proportional to the concentration of testosterone at 60 and 90 min, showing a linear range from 0.007 to 100 and 0.008 to 25 nM, respectively. The response was reproducible with an intra-assay variability of 18% and an inter-assay variability of 25%. This variability could be associated with transient transfections and it could be reduced by employing stable transfection (Campana et al., 2016).
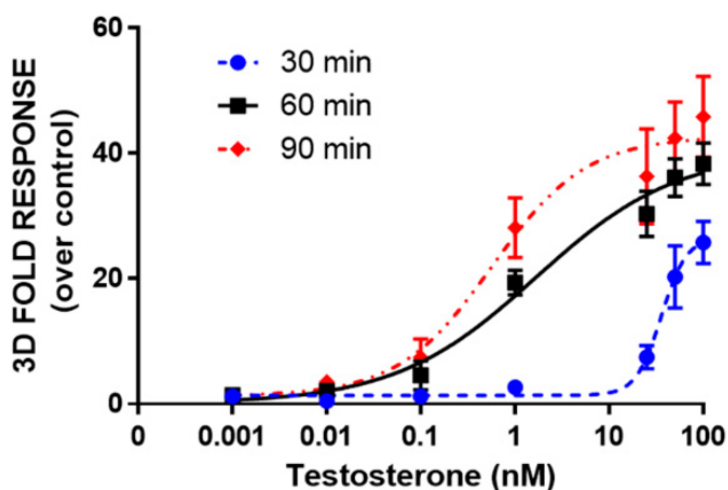
Fig. 6.6: *Dose-response curve for testosterone obtained in 3D cell culture models. HEK293 cells were co-transfected with LgBiT-hAR and hAR-SmBiT under the regulation of the SV40 promoter and treated at 48 h post-transfection with testosterone (concentration range of 0.001–100 nM). BL measurements were obtained after the addition of Nano-Glo® Live Cell Assay System substrate and analyzed the BL signals at 30, 60, and 90 min. Data are the mean ± s.d. of at least three independent experiments, each performed in triplicate.*

6.4 Discussion

A novel intracellular nanosensor was developed based on the complementation of split NanoLuc luciferase. Thanks to the NanoBiT high BL signal, low self-assembly affinity, and high signal to noise ratio, the expression of fusion proteins can be kept at physiological levels, thus providing an efficient tool for quantitatively investigating PPI under physiological conditions (Dixon et al., 2016). We developed an assay to monitor homodimerization of the human androgen receptor in real time and in 3D cell models using the NanoBiT split-luciferase system. The androgen receptor is an important therapeutic target that plays a pivotal role in mediating several diseases, including prostate cancer and male infertility. Therefore, the availability of methods for identifying new compounds with androgenic activity is of vital importance. Most of the assays and biosensors previously reported by us and others rely on reporter gene technology, exploiting BL and fluorescent reporters under the control of the androgen response element (ARE) in mammalian and yeast cells (Michelini et al., 2008; Bovee et al., 2009). Although these assays are generally very sensitive, they do not provide an accurate picture of intracellular dynamics. Conversely, PCA enables the spatiotemporal dynamics of receptor activation to be investigated. Generally, all these assays are performed with conventional 2D cell cultures and are considered an important pillar of the drug discovery process. Sometimes, these tests provide misleading and nonpredictive data on in vivo responses.

To overcome many of the limitations of traditional 2D cell culture systems, the 3D cellular system was selected to reproduce cell–cell and cell–matrix interactions, intra- and inter-cellular signalling networks, and diffusion/transport conditions, which are important for differentiation, proliferation, and various cellular functions.

We chose the HEK293 cell line for transient co-transfection with plasmids driving the expression of similar expression levels of LgBiT-hAR and hAR-SmBiT under the regulation of the SV40 promoter, which allowed the strongest signals and widest dynamic range (Fig.

6.4b). The SV40 promoter was selected to increase chimeric receptor expression and the ratio of recombinant constructs with respect to endogenous receptors. This reduces competition for dimerization with native androgen receptors, which are present at very low levels in HEK293 cells (Hu et al., 2014). NanoBiT reconstitution was fully confirmed by BL imaging in the HEK293 monolayer with the direct visualization of hAR dimerization in living cells at a subcellular level (Fig. 6.4).

To investigate the suitability of the novel intracellular nanosensor in 3D cell models, firstly, we characterized NanoBiT re-assembly in HEK293 grown as monolayer and in HEK293 spheroids with an average diameter of 130 ± 20 μM. The spheroid size selected is able to maintain an adequate cell viability with a negligible necrotic core, of less than 2% of cells (Langan et al., 2016; Anada et al., 2012; Cevenini et al., 2017) and to obtain a sufficient oxygen availability, which is essential for BL measurements. After the addition of testosterone, both 2D and 3D culture systems showed similar emission spectra and glow-type emission kinetics, with maximum BL signals at 30 and from 50 to 65 min, respectively (Fig. 6.3b,c). This is partially due to the bioavailability of testosterone and the longer time required to penetrate the spheroid in depth, so the major contribution of BL emission will derive from external cell layers. Interestingly, a decline in the BL signal was observed after approximately one hour in 3D models, probably due to substrate inactivation. In addition, oxygen availability represents a critical factor of the cell microenvironment; as previously reported, firefly luciferin-luciferase systems exposed to hypoxic conditions (near 0% O_2) resulted in a 3.4-fold reduction of total photon flux when compared to normoxia (21% O_2). This decrease derives from the requirement of molecular oxygen for the oxidation of firefly luciferin. Moreover, in an ATP-dependent luciferase- catalyzed reaction, this decrease was also related to a reduction in the intracellular ATP content under hypoxia (Lambrechts et al. 2014). For this reason, ATP-independent luciferases, such as NanoLuc, could be more advantageous than firefly luciferases for applications in 3D cell models.

To evaluate the feasibility of using 3D bioluminescence spheroids of HEK293 for improving the predictivity of the method (Pinto et al., 2020), we developed a 3D cell-based assay to monitor homodimerization of the human androgen receptor in real time using the NanoBiT split-luciferase system. To the best of our knowledge, no PCA assays have been reported in spheroids or 3D cell models. Therefore, such implementation is also highly valuable for other targets and sensor formats. Compared to a PCA reported by Kim et al., relying on the intramolecular complementation of split click beetle luciferase with an LOD for testosterone

of, ~10^{-5} M (Kim et al., 2007), both the assays in 2D and 3D cells provided a higher sensitivity, with LODs of 40 and 4 pM, respectively. The lower LOD obtained with 3D cell models can be partially explained by the formation of spheroid structures in which cells grow in layers, similar to the in vivo condition, thus replicating not only the cellular topology, but also gene expression, metabolism, and signaling.

Moreover, the LOD obtained for the 3D cell culture system is one order of magnitude lower than that previously reported in yeast reporter assays for androgenic compounds (Michelini et al., 2008) and two orders of magnitude lower than mammalian cell-based assays (Campana et al., 2016), which require longer incubation times (18 h). Considering its low limit of detection and rapidity, the developed assay could be considered a valuable alternative for the predictive screening of androgenic compounds.

The analytical performance of this 3D assay supports its use for clinical applications, i.e., to monitor total blood androgenic activity during testosterone replacement therapy (Hassan and Barkin, 2016; Matsumoto and Bremner, 2004). Physiological total serum testosterone levels range from 280 to 1100 ng/dL (corresponding to 9.71–38.17 nM) for adult males; these concentrations are fully covered by the working range of the reported method. As previously demonstrated (Ekström et al., 2013; Piper et al., 2020), bioassays relying on androgen receptor activation may be employed as sensitive tools to detect andro- genic activity in clinical samples (e.g., plasma and urine). Moreover, these assays have the potential to detect the presence of unknown androgenic substances and identify samples that need to undergo confirmatory analysis. This possibility opens new applications for antidoping screenings.

6.5 Conclusions

We developed a new intracellular nanosensor that exploits intermolecular NanoLuc complementation for the fast and sensitive detection of androgenic-like compounds. Two chimeric proteins with a split bioluminescent reporter (SmBit and LgBit) fused with an hAR receptor were expressed in HEK293 cells. The feasibility of monitoring receptor dimerization in real time was also demonstrated with bioluminescence single cell imaging. To assess the suitability of this nanosensor in 3D models, HEK293 spheroids were engineered to express the two chimeric constructs and an adequate analytical performance was achieved. After further characterization, this nanosensor could find application not only in drug screening, but also for the rapid detection of androgen-like chemicals, for example, for monitoring

endocrine disrupting compounds in food and environmental samples. To expand the applicability of the sensor, future work will involve an investigation of anti-androgenic molecules' effect on the nanosensor and the analysis of complex matrices.

6.6 Acknowledgements

6.7 References

Anada, T.; Fukuda, J.; Sai, Y.; Suzuki, O. 2012, *Biomaterials. 33*, 8430–8441.

Biewenga, L.; Rosier, B.J.H.M.; Merkx, M. 2020, *Biochem. Soc. Trans. 48*, 2643–2655.

Bovee, T.H.F.; Bor, G.; Heskamp, H.H.; Lasaroms, J.J.; Sanders, M.B.; Nielen, M.W.F. 2009, *Anal. Chim. Acta. 637*, 225–234.

Brancato, V.; Oliveira, J.M.; Correlo, V.M.; Reis, R.L.; Kundu, S.C. 2020, *Biomaterials. 232*, 119744.

Calabretta, M.M.; Montali, L.; Lopreside, A.; Michelini, E.; Roda, A. In *Bioluminescent Imaging*; Humana: New York, NY, USA, 2020; Volume 2081, pp. 3–14.

Campana, C.; Rege, J.; Turcu, A.F.; Pezzi, V.; Gomez-Sanchez, C.E.; Robins, D.M.; Rainey, W.E. 2016, *J. Steroid Biochem. Mol. Biol. 156*, 17–22.

Cevenini, L.; Calabretta, M.M.; Calabria, D.; Roda, A.; Michelini, E. In *Bioluminescence: Fundamentals and Applications in Biotechnology*; Thouand, G., Marks, R., Eds.; Springer: Cham, Switzerland, 2015; Volume 154, pp. 3–17.

Cevenini, L.; Calabretta, M.M.; Lopreside, A.; Branchini, B.R.; Southworth, T.L.; Michelini, E.; Roda, A. 2017, *Photochem. Photobiol. 93*, 531–535.

Dixon, A.S.; Schwinn, M.K.; Hall, M.P.; Zimmerman, K.; Otto, P.; Lubben, T.H.; Butler, B.L.; Binkowski, B.F.; Machleidt, T.; Kirkland, T.A.; et al. 2016, *ACS Chem. Biol. 11*, 400–408.

Ekström, L.; Cevenini, L.; Michelini, E.; Schulze, J.; Ethörngren, J.-O.; Belanger, A.; Guillemette, C.; Egarle, M.; Roda, A.; Rane, A. 2013, *Eur. J. Clin. Investig. 43*, 248–255.

England, C.G.; Ehlerding, E.B.; Cai, W. 2016, *Bioconjug. Chem. 27*, 1175–1187.

Hassan, J.; Barkin, J. 2016, *Can. J. Urol. 23*, 20–30.

Hu, D.G.; Hickey, T.E.; Irvine, C.; Wijayakumara, D.D.; Lu, L.; Tilley, W.D.; Selth, L.A.; Mackenzie, P.I. 2014, *Horm. Cancer 5*, 61–71.

Johnsson, N.; Varshavsky, A. 1994, *Proc. Natl. Acad. Sci. USA 91*, 10340–10344.

Kilchrist, K.V.; Tierney, J.W.; Duvall, C.L. 2020, *ACS Sens. 5*, 1929–1936.

Kim, S.B.; Otani, Y.; Umezawa, Y.; Tao, H. 2007, *Anal. Chem. 79*, 4820–4826.

Kim, S.B.; Sato, M.; Tao, H. 2009, *Anal. Chem. 81*, 67–74.

Lambrechts, D.; Roeffaers, M.B.J.; Goossens, K.; Hofkens, J.; Van De Putte, T.; Schrooten, J.; Van Oosterwyck, H. 2014, *PLoS ONE 9*, e97572.

Lang, Y.; Li, Z.; Li, H. 2019, *Curr. Protoc. Toxicol. 82*, e90.

Langan, L.M.; Dodd, N.J.; Owen, S.F.; Purcell, W.M.; Jackson, S.K.; Jha, A.N. 2016, *PLoS ONE 11*, e0149492.

Luker, K.E.; Smith, M.C.P.; Luker, G.D.; Gammon, S.T.; Piwnica-Worms, H.; Piwnica-Worms, D. 2004, *Proc. Natl. Acad. Sci. USA 101*, 12288–12293.

Matsumoto, A.M.; Bremner, W.J. 2004, *J. Clin. Endocrinol. Metab. 89*, 520–524.

Michelini, E.; Cevenini, L.; Mezzanotte, L.; Leskinen, P.; Virta, M.; Karp, M.; Roda, A. 2008, *Nat. Protoc. 3*, 1895–1902.

Misawa, N.; Kafi, A.K.; Hattori, M.; Miura, K.; Masuda, K.; Ozawa, T. 2010, *Anal. Chem. 82*, 2552–2560.

Nguyen, L.P.; Nguyen, H.T.; Yong, H.J.; Reyes-Alcaraz, A.; Lee, Y.N.; Park, H.K.; Na, Y.H.; Lee, C.S.; Ham, B.J.; Seong, J.Y.; et al. 2020, *Mol. Cells 43*, 909–920.

Ni, Y.; Arts, R.; Merkx, M. 2019, *ACS Sens. 4*, 20–25.

Oladzad, A.; Nikkhah, M.; Hosseinkhani, S. 2020, *Sensors 20*, 1782.

Paulmurugan, R.; Gambhir, S.S. 2006, *Proc. Natl. Acad. Sci. USA 103*, 15883–15888.

Paulmurugan, R.; Gambhir, S.S. 2007, *Anal. Chem. 79*, 2346–2453.

Pinto, B.; Henriques, A.C.; Silva, P.M.A.; Bousbaa, H. 2020, *Pharmaceutics 12*, 1186.

Piper, T.; Heimbach, S.; Adamczewski, M.; Thevis, M. 2021, *Drug Test. Anal. 13(5), 916-928.*

Romei, M.G.; Boxer, S.G. 2019, *Annu. Rev. Biophys. 48*, 19–44.

Rossi, F.; Charlton, C.A.; Blau, H.M. 1997, *Proc. Natl. Acad. Sci. USA 94*, 8405–8410.

Shin, W.H.; Kumazawa, K.; Imai, K.; Hirokawa, T.; Kihara, D. 2020, *Adv. Appl. Bioinform. Chem. 13*, 11–25.

Van Royen, M.E.; Cunha, S.M.; Brink, M.C.; Mattern, K.A.; Nigg, A.L.; Dubbink, H.J.; Verschure, P.J.; Trapman, J.; Houtsmuller, A.B. 2007, *J. Cell Biol. 177*, 63–72.

Zhou, L.; Zhang, L.; Yang, L.; Ni, W.; Li, Y.; Wu, Y. 2021, *Biosens. Bioelectron. 173*, 112824.

7

Conclusions and future perspectives

In conclusion, during my PhD several biosensors for point-of-need rapid monitoring of hazardous chemicals for human health and for the environment have been developed and optimized. These biosensors could be suitable for real-time food safety and quality assessment, drug screening, environmental monitoring and point-of-care applications. Compared to other analytical tools, biosensors do not require sample treatment steps, sophisticated equipment or skilled personnel. Indeed, thanks to the specificity of the biological recognition element, an analyte of interest, or a class of analytes, can be selectively detected in complex matrices (i.e. wastewater, body fluids). Moreover, whole-cell biosensors offer unique features as they provide information about the bioavailable fraction and synergic effects, being able to detect also unknown compounds. Several optical detections (colorimetric, chemiluminescent and bioluminescent detection) and biorecognition elements (enzymes, purified proteins, bacteria and mammalian cells) have been exploited in order to select the best candidate for our purpose. Different immobilization methods and 3D printing technology have been also investigated to integrate the new developed biosensors into portable analytical platforms. Several user-friendly portable light detectors, like smartphone, CCD and Silicon PhotoMultiplier, have been also investigated for real setting application. Optimizing different parameters and experimental conditions, including incubation times, immobilization methods and others, the analytical performance of biosensors, in terms of dynamic range, limit of detection and response time, have been improved providing fast and sensitive enzymatic and whole-cell biosensors. Moreover, combining different biorecognition elements (i.e. enzyme and whole cell) and thanks to an orthogonal detection exploiting bioluminescence and colorimetry, very robust and standard biosensors have been developed, capable of limiting the presence of false positives and interferers.

As future perspective, in order to develop a more stable and robust biosensor, stability of biorecognition elements immobilized on paper has to be improved. To provide a more predictive and comprehensive information about sample toxic effects on humans and animal wildlife, a combination of the developed cell biosensors based on different biorecognition principles could be developed. To increase the multiplexing, different optical detection principles could be coupled, and also different bioluminescent reporter proteins could be implemented and detected with spectral resolution in the same cartridge. Each color could be associated with a target bioactivity, i.e., general toxicity, inflammation, or to the detection of a target analyte. To this end, numerous challenges will have to be faced, such as the identification of innovative strategies for cell immobilization to keep biosensors alive and

responsive for long periods of time, and the improvement of light emitted by the cells to enable detection with portable light detectors, while keeping adequate sensitivity, comparable with that obtained with benchtop detectors. For achieving more valuable information, e.g., in terms of reliability of data, in particular in relation to toxicity and bioactivity, many 3D cell models will be developed providing an environment that faithfully mimics the in vivo physiological conditions. For all these reasons, future work will be directed to optimize the shelf-life of cell cartridges i.e. direct growth of cell-biosensor on 3D-scaffolds inside the 3D-printed cartridges and the immobilization of cells into suitable biocompatible matrices to improve cell viability during cell storage and reduce the time-to response signal. Moreover, the use of alternative new culture medium for mammalian cells will be also explored to preserve the cells responsiveness in uncontrolled experimental conditions. At the end, to obtain a better reproducibility, the production systems of sensing papers must be optimized. To obtain commercially available biosensors, the proposed 3D printed prototypes will have to be improved to enter the market in the near future.

Acknowledgments